Inaugural dissertation
for
obtaining the doctoral degree
of the
Combined Faculty of Mathematics, Engineering and Natural Sciences
of the
Ruprecht - Karls - University
Heidelberg

Presented by

Katharina Lindner, M.Sc.

born in: Munich, Germany

Oral examination: 27.07.2023

Identification and validation of neoepitope-specific T cell receptors for glioma immunotherapy

Referees: Prof. Dr. Michael Platten
Prof. Dr. Thomas Höfer

Statutory Declaration/Eidesstattliche Versicherung

Eidesstattliche Versicherung gemäß § 8 der Promotionsordnung der Gesamtfakultät für Mathematik, Ingenieur- und Naturwissenschaften der Universität Heidelberg

1. Bei der eingereichten Dissertation mit dem Titel

Identification and validation of neoepitope-specific T cell receptors for glioma immunotherapy

handelt es sich um meine eigenständig erbrachte Leistung.

2. Ich habe nur die angegebenen Quellen und Hilfsmittel benutzt und mich keiner unzulässigen Hilfe Dritter bedient. Insbesondere habe ich wörtlich oder sinngemäß aus anderen Werken übernommene Inhalte als solche kenntlich gemacht.

3. Die Arbeit oder Teile davon habe ich bislang nicht an einer Hochschule des In- oder Auslands als Bestandteil einer Prüfungs- oder Qualifikationsleistung vorgelegt.

4. Die Richtigkeit der vorstehenden Erklärungen bestätige ich.

5. Die Bedeutung der eidesstattlichen Versicherung und die strafrechtlichen Folgen einer unrichtigen oder unvollständigen eidesstattlichen Versicherung sind mir bekannt.

Ich versichere an Eides statt, dass ich nach bestem Wissen die reine Wahrheit erklärt und nichts verschwiegen habe.

....

Ort und Datum Unterschrift

Acknowledgements

This thesis would not have been possible without the support of many people. First of all, I would like to express my gratitude to Michael Platten for giving me the opportunity to join his laboratory and for his trust, optimism and support of my work throughout the years. I always appreciated how well you are informed about the latest progress of projects in the lab, while at the same time being fully up-to-date with the most recent literature, allowing you to give helpful advice in lab meetings.

A special thanks goes to my primary supervisor Isabel Poschke, who interacted with me on a daily basis and was always available for questions or discussions, even during her maternity leave. I am very grateful for your supervision, dedication and expertise, and learned a lot from you. Thank you for proof-reading my thesis.

Moreover, I would like to thank Georg Stoecklin and Thomas Höfer for their helpful input during my TAC meetings. Thanks also to Oliver Fackler and Chong Sun who, together with Thomas Höfer, agreed to form my examination committee.

I was very lucky to be part of two wonderful labs, the Immune Monitoring Unit (IMU) at the NCT, and the laboratory in the DKFZ main building, both being part of the D170 unit. My base for day-to-day work was the IMU, and I could not be more grateful to each and every member of the team for creating an amazing work environment, for their support, and the fun we had and still have. Because of all of you I always enjoy coming to the lab. I would also like to extend my thanks to Mariana, who unfortunately already retired two years ago and is no longer actively working at the IMU, but helped me a lot by teaching basic techniques like ELISpot at the beginning of my thesis and suggested many excellent and well-established protocols from the Beckhove lab to me, which were used in this thesis. As you also preferred working later in the evenings we spend a lot of time together, which I enjoyed due to your warm and caring nature. You are still missed and if you ever find any spare time we would love to have you back in the lab!

Also, thanks to each and every member of the laboratory in the main building. While I could unfortunately not be around on a daily basis I always felt well included in the lab and enjoyed spending time with you. I am grateful for interacting a lot with the immunogenomics team, led by Edward Green. It is inspiring to see how many novel creative ideas you have, which made the TCR pipelines evolve to a great extend over the years. Despite not being my primary supervisor, you spent a lot of time in giving me guidance and allowed me to use the tools which you developed, without which this thesis would not have been possible at all. Thanks also to Gordon for his tremendous support in TCR cloning, to Kyle for his support with bioinformatic analysis and supporting me after late-night FACS sorts with single cell sequencing to speed up the whole process, to Tamara for exchanging ideas on TCR testing, to Alice for always being extremely supportive in all matters, and all of you for being great colleagues and people. Also, thanks to Lukas Bunse for organizing patient samples and for his helpful input for the IDH1 project, which was originally started by him and Theresa Bunse. I would also like to thank all core facilities involved in this project highlighting the flow cytometry and single cell sequencing core facility, collaboration partners, the Helmholtz Graduate School for funding me for three years, as well as the patients and their families for donating tissue and blood which made this research possible.

Finally, and most importantly, I want to thank the people most close to me. Both of my parents, my brothers and their wives, who are at the same time part of my circle of friends, for always believing in me, supporting me throughout the years and for keeping my spirits high. I am deeply grateful to Pascal for his continuous loving support, for motivating me while at the same time reminding me to take breaks, and for making sure that I go to bed at a reasonable time to catch enough sleep. I am very thankful to have each and every one of you in my life.

Abstract

Immunotherapy is a promising tool for cancer treatment and there is great interest to implement T cell-based therapies in patient care. Development of T cell-based therapies has focused on highly immunogenic tumors. Due to their low-mutational load and limited immune infiltration, gliomas are considered difficult targets for immune intervention and thus remained understudied, despite the urgent need to define new therapeutic options for these aggressive brain tumors.

This thesis aimed at (I) identification and characterization of T cell responses elicited upon vaccination of glioma patients against the recurrent driver mutation R132H in isocitrate dehydrogenase 1 (IDH1), (II) identifying tumor-reactive T cell receptors (TCRs) targeting tumor-private antigens and (III) antigen-agnostic TCR identification in non-vaccinated patients with the overall aim to define a gene expression signature characteristic for tumor-reactive T cells.

The IDH1R132H oncogenic driver mutation is found in about 70% of WHO grade 2 and 3 gliomas. Its homogenous exclusive expression in tumor tissue makes it an attractive target for immunotherapy, and vaccinations with an IDH1R132H encoding long peptide were shown to efficiently mediate tumor shrinkage in pre-clinical mouse models. The vaccine was proven to be immunogenic in primary WHO grade 3 and 4 IDH1-mutant astrocytomas in the completed NOA16 phase I clinical trial, and also shows immunogenicity in the ongoing NOA21 phase I clinical trial, where combination of the vaccine with the PD-L1 inhibitor avelumab is tested in patients with IDH1 mutant recurrent gliomas.

To gain a deeper understanding of the T cell response following vaccination, I established “epitope specific expansion cultures” (ESPEC) with “subsequent identification of TCRs” (SUIT) to pre-select TCRs for testing their reactivity. Based on ESPEC, a total of 120 CD4-derived TCRs from seven patients were selected for cloning and functional validation in in vitro co-culture assays, of which 106 were shown to be reactive. IDH1R132H-reactive clones were found to be enriched intratumorally as compared to concurrently sampled blood of vaccinated patients. 49 identified IDH1R132H-reactive TCRs showed in vitro reactivity against wildtype IDH1 if the peptide was used at supraphysiological concentrations, but not at lower peptide concentrations as shown for a selection of TCRs. Analysis of HLA restrictions indicates promiscuous binding of the IDH1R132H peptide to HLA-DR alleles, which is in accordance with the high immunogenicity of the vaccine in an HLA-diverse patient population.

Contrary to what was reported so far, I also observed CD8+ T cell responses against IDH1R132H in two of three tested patients. Mass spectrometry confirmed presentation of short IDH1R132H peptides on HLA-B*07:05 and HLA-B*35:01, with these HLA alleles being representative for 12.3% of the German population taking HLA supertype families into account. Using ESPEC-SUIT, one CD8-derived TCR reactive against IDH1R132H was identified. The TCR was found to infiltrate the tumor, making up 0.24% of the T cell repertoire and being positive for granulysin, which could be an indication of cytotoxic function. Extending the screening for reactive CD8-derived TCRs to further patients is planned to gain deeper insights into the vaccine-induced immune response.

ESPEC-SUIT was also used to identify TCRs reactive to patient-individual antigens. Private neoepitopes, both from SNVs and fusion events, were predicted based on whole exome and RNA sequencing data of the tumor, and used to stimulate autologous PBMCs. ESPEC cultures were performed with individual peptides or in peptide pools to screen for reactive TCRs against 18-189 peptides per patient. For a colon carcinoma patient (POC-001), 25 of 28 screened TCRs were reactive, covering reactivities against 14 of 18 predicted neoantigens. For patient POC-004 with liposarcoma (12 mutations included for testing) and patient POC-005 with metastatic melanoma (50 mutations included for testing), several hundred expanded TCRs have been identified and await functional validation. While POC-001 and POC-004 were vaccinated with long peptides representative for a selection of mutanome encoded antigens prior to ESPEC, patient POC-005 did not receive such vaccination, but T cells were found to be

expanded in post-ESPEC cultures for three short peptides and 32 long peptides, underlining the sensitivity of the ESPEC approach.

To further understand the role of anti-tumor T cell immunity in brain tumors, tumor infiltrating lymphocytes (TILs) of non-vaccinated patients were used for single cell sequencing with the overall aim to identify a gene signature that can distinguish between tumor-reactive clones and non-reactive bystander clones for future antigen-agnostic identification of reactive TCRs. While gene signatures based on published markers identified no TCRs in primary brain tumors, a total of 46 reactive TCRs were identified when screening the top 83 TIL clonotypes from a melanoma brain metastasis tumor sample. On basis of this data, Chin Leng Tan (DKFZ Heidelberg, Germany) is working on establishing a gene signature, which could be used for antigen-agnostic discovery of reactive TCRs.

Collectively, this thesis presents two strategies on how putatively tumor-reactive TCRs can be selected and validated on a larger scale. Screening for IDH1R132H-reactive TCRs allowed to gain deeper insights into the peripheral and intratumoral immune response elicited upon vaccination with the IDH1R132H peptide vaccine in brain tumor patients. The antigen-targeted approach was shown to be highly efficient for selecting reactive TCRs, which could potentially help to implement TCR-transgenic T cell therapies in patient care.

Zusammenfassung

Immuntherapien sind ein vielversprechendes Werkzeug zur Behandlung von Krebs und es gibt ein großes Interesse, T-Zell-basierte Therapien in der medizinischen Krankenversorgung zu implementieren. Die Entwicklung T-Zell-basierter Therapien hat sich bislang auf stark immunogene Tumore fokussiert. Aufgrund ihrer geringen Mutationslast und der limitierten Immuninfiltration werden Gliome als schwieriges Ziel für Immuninterventionen angesehen und wurden daher bislang von der Wissenschaft vernachlässigt, obwohl es einen dringenden Handlungsbedarf gibt, neue, therapeutische Optionen für diese aggressive Form Gehirntumore zu definieren.

Diese Doktorarbeit zielt darauf ab, (I) T-Zell Antworten, die durch die Impfung von Gliompatienten gegen die wiederholt auftretende Verstärker-Mutation R132H in der Isocitrat Dehydrogenase 1 (IDH1) hervorgerufen wurden, zu identifizieren und charakterisieren, (II) Tumor-reaktive T-Zellrezeptoren (TZRs), die auf private Tumorantigene abzielen zu identifizieren und (III) Antigen-agnostisch TZRs in nicht geimpften Patienten zu identifizieren, um darüber für tumorreaktive T-Zellen charakteristische Genexpressionssignaturen zu definieren.

Die onkogene IDH1R132H Verstärker-Mutation ist in etwa 70% der WHO-Grad 2 und 3 Gliome präsent. Aufgrund ihrer homogenen und exklusiven Expression in Tumorgewebe ist sie ein attraktives Ziel für Immuntherapien. Es wurde gezeigt, dass die Impfung mit einen für IDH1R132H kodierenden langen Peptid zu einer effizienten Reduktion von Tumormasse in präklinischen Mausmodellen geführt hat. Anhand der abgeschlossenen Phase 1 klinischen Studie NOA16 wurde die Immunogenität des Impfstoffes in primären WHO Grad 3 und 4 IDH1-mutierten Astrozytomen nachgewiesen. Der Impfstoff zeigt auch in der aktuell laufenden Phase 1 klinischen Studie NOA21 Immunogenität, wo dessen Kombination mit dem PD-L1 Inhibitor Avelumab in Patienten mit IDH1 mutierten rezidivierenden Gliomen getestet wird.

Um ein besseres Verständnis der T-Zellantwort nach Impfungen zu erlangen habe ich „Epitop-spezifische Expansionskulturen“ (ESPEC) mit „anschließender Identifizierung von TZRs“ zur Vorauswahl von TZRs für anschließende Tests von deren Reaktivität etabliert. Basierend auf ESPEC wurden insgesamt 120 TZRs von CD4+ Klonen von sieben Patienten ausgewählt, von denen 106 nach der Klonierung und funktionellen Validierung in in vitro Ko-Kultur Versuchen Reaktivität aufwiesen. IDH1R132H-reaktive Klone wurden bei einem direkten Vergleich von zum gleichen Zeitpunkt entnommenem Blut und Tumorgewebe von geimpften Patienten mit einer Anreicherung im Tumor gefunden. 49 der identifizierten IDH1R132H-reaktiven TZRs waren in vitro gegen das IDH1 wildtyp Peptid reaktiv, wenn dieses in supraphysiologischen Konzentrationen eingesetzt wurde, aber nicht bei niedrigeren Peptidkonzentrationen, was anhand einer Auswahl an TZRs gezeigt wird. Analysen der HLA-Restriktion deuten an, dass das IDH1R132H Peptid promiskuitiv an HLA-DR Allele binden kann, was im Einklang zu Beobachtungen zur hohen Immunogenität des Impfstoffes in einer HLA-diversen Patientenpopulation steht.

Entgegen vorheriger Berichte konnte ich auch eine CD8+ T-Zellantwort gegen IDH1R132H in zwei von drei getesteten Patienten beobachten. Massenspektrometrie hat die Präsentation von kurzen IDH1R132H Peptiden auf HLA-B*07:05 und HLA-B*35:01 bestätigt, wobei diese zwei HLA Allele unter Berücksichtigung von HLA-Supertypen repräsentativ für 12.3% der deutschen Bevölkerung sind. Mithilfe von ESPEC-SUIT wurde ein von CD8+ Zellen abstammender TZR mit Reaktivität gegen IDH1R132H gefunden. Der TZR infiltriert den Tumor, wo er 0.24% des T-Zellrepertoires ausmacht und positiv für den Marker Granulysin ist, was als Indiz für Zytotoxität gesehen werden kann. Das Ausweiten des Screens auf eine größere Patientenpopulation zur Identifikation weiterer TZRs von CD8+ Klonen ist geplant, um einen tieferen Einblick in die impfinduzierte Immunantwort zu erlangen.

ESPEC-SUIT wurde auch verwendet, um gegen patientenindividuelle Antigene TZRs zu identifizieren. Aus Einzelnukleotid-Polymorphismen und Gen-Fusionen hervorgegangene private Neoepitope wurden anhand von Exom- und RNA-Sequenzierungen von Tumorgeweben vorhergesagt und verwendet, um damit autologe PBMCs zu stimulieren. ESPEC-Kulturen wurden entweder mit einzelnen Peptiden oder mit mehreren Peptiden auf einmal stimuliert, um reaktive TZRs gegen zwischen 18 bis 189 Peptide pro Patient zu screenen. Bei einem Patienten mit Kolonkarzinom (POC-001) waren 25 von 28 gescreenten TZRs reaktiv, was Reaktivitäten gegen 14 von 18 vorhergesagten Neoantigenen abdeckt. Bei Patient POC-004 (Liposarkom, 12 Mutationen wurden analysiert) und Patient POC-005 (metastasierendes Melanom, 50 Mutationen wurden analysiert) wurden mehrere hundert expandierte TZRs beobachtet, die nun auf ihre funktionelle Validierung warten. Während POC-001 und POC-004 mit langen Peptiden geimpft wurden, welche repräsentativ für einen Teil deren Mutanom-kodierten Antigene vor ESPEC sind, hat Patient POC-005 keine solche Impfung erhalten, wobei dennoch nach ESPEC expandierte T-Zellen in Kulturen mit drei kurzen Peptiden oder mit 32 langen Peptiden vorgefunden wurden, was die Sensitivität des ESPEC Ansatzes unterstreicht.

Um die Rolle der anti-Tumor T-Zell Immunität in Hirntumoren besser zu verstehen, wurden außerdem Tumor-infiltrierende Lymphozyten (TILs) von nicht-geimpften Patienten für Einzelzellsequenzierungen verwendet. Dabei war die allgemeine Zielsetzung die Identifizierung einer Gensignatur, die eine Unterscheidung zwischen Tumor-reaktiven und nicht-reaktiven Klonen erlaubt und somit in Zukunft ohne Kenntnis des Antigens die Identifizierung von reaktiven TZRs ermöglichen soll. Während mit einer Gensignatur, die auf Basis von publizierten Markers erstellt wurde, zunächst keine reaktiven TZRs in primären Hirntumoren gefunden wurden, wurden insgesamt 46 reaktive TZRs entdeckt, als die 83 intratumoral am stärksten expandierten TIL Klontypen einer Melanom-Hirnmetastase auf Reaktivität getestet wurden. Auf Basis dieser Daten wird von Chin Leng Tan (DKFZ Heidelberg, Deutschland) eine Genexpressionssignatur zur Vorhersage von reaktiven T-Zellen entwickelt.

Zusammengefasst zeigt diese Doktorarbeit zwei Strategien auf, um Tumor-reaktive TZRs im großen Maßstab auszuwählen und zu validieren. Das Screening von IDH1R132H-reaktiven TZRs hat es ermöglicht tiefere Einblicke in die durch den IDH1R132H Peptidimpfstoff hervorgerufene periphere und intratumorale Immunantwort von Hirntumorpatienten zu erlangen. Darüber hinaus wurde gezeigt, dass der auf ein spezielles Antigen ausgerichtete Ansatz eine hocheffiziente Methoden ist, um reaktive TZRs auszuwählen, was das Potential birgt, über diese Methode geeignete TZRs für zukünftigen TZR-transgenen T-Zell-Therapien auszuwählen.

List of Publications

Publications related to this thesis:

Bunse, L., A. K. Rupp, I. Poschke, T. Bunse, **K. Lindner**, A. Wick, J. Blobner, M. Misch, G. Tabatabai, M. Glas, O. Schnell, J. Gempt, M. Denk, G. Reifenberger, M. Bendszus, P. Wuchter, J. P. Steinbach, W. Wick, and M. Platten. 2022. 'AMPLIFY-NEOVAC: a randomized, 3-arm multicenter phase I trial to assess safety, tolerability and immunogenicity of IDH1-vac combined with an immune checkpoint inhibitor targeting programmed death-ligand 1 in isocitrate dehydrogenase 1 mutant gliomas', Neurol Res Pract, 4: 20.

Publications not related to this thesis:

Poschke, I. C., J. C. Hassel, A. Rodriguez-Ehrenfried, **K. A. M. Lindner**, I. Heras-Murillo, L. M. Appel, J. Lehmann, T. Lovgren, S. L. Wickstrom, C. Lauenstein, J. Roth, A. K. Konig, Jbag Haanen, J. van den Berg, R. Kiessling, F. Bergmann, M. Flossdorf, O. Strobel, and R. Offringa. 2020. 'The Outcome of Ex Vivo TIL Expansion Is Highly Influenced by Spatial Heterogeneity of the Tumor T-Cell Repertoire and Differences in Intrinsic In Vitro Growth Capacity between T-Cell Clones', Clin Cancer Res, 26: 4289-301.

Friedrich, M., N. Kehl, N. Engelke, J. Kraus, **K. Lindner**, P. Munch, I. Mildenberger, C. Groden, A. Gass, N. Etminan, M. Fatar, A. von Deimling, D. Reuss, M. Platten, and L. Bunse. 2021. 'Intrathecal activation of CD8(+) memory T cells in IgG4-related disease of the brain parenchyma', EMBO Mol Med, 13: e13953.

Lu, K. H., J. Michel, M. Kilian, K. Aslan, H. Qi, N. Kehl, S. Jung, K. Sanghvi, **K. Lindner**, X. W. Zhang, E. W. Green, I. Poschke, M. Ratliff, T. Bunse, F. Sahm, A. von Deimling, W. Wick, M. Platten, and L. Bunse. 2022. 'T cell receptor dynamic and transcriptional determinants of T cell expansion in glioma-infiltrating T cells', Neurooncol Adv, 4: vdac140.

Kilian, M., R. Sheinin, C. L. Tan, M. Friedrich, C. Kramer, A. Kaminitz, K. Sanghvi, **K. Lindner**, Y. C. Chih, F. Cichon, B. Richter, S. Jung, K. Jahne, M. Ratliff, R. M. Prins, N. Etminan, A. von Deimling, W. Wick, A. Madi, L. Bunse, and M. Platten. 2023. 'MHC class II-restricted antigen presentation is required to prevent dysfunction of cytotoxic T cells by blood-borne myeloids in brain tumors', Cancer Cell, 41: 235-51 e9.

T. Boschert, K. Kromer, T. Lerner, **K. Lindner**, G. Haltenhof, C. L. Tan, K. Jähne, I. Poschke, L. Bunse, N. Grassl, I. Mildenberger, K. Sahm, M. Platten, J. M. Lindner, and E. W Green. 2023. 'Neoepitope-specific vaccination of a patient with diffuse midline glioma targeting H3K27M induces polyclonal B and T cell responses across diverse HLA alleles', bioRxiv: 2023.04.28.538672.

In preparation (may be subject to change):

K. Lindner, …, M. Platten* and I. Poschke* (*shared). 'Efficient discovery of MHCI and MHCII-restricted tumor-reactive TCRs by ESPEC-SUIT (epitope specific expansion cultures with subsequent identification of TCRs) '

K. Lindner, …, M. Platten. 'A warehouse of IDH1R132H-reactive TCRs.'

C. L. Tan, **K. Lindner**, T. Boschert, Z. Meng, A. Rodriguez Ehrenfried, A. De Roia, G. Haltenhof, L. Bunse, R. P. Harbottle, M. Ratliff, R. Offringa, I. Poschke, M. Platten and E. W. Green. 'predicTCR – a classifier for rapid ML-guided identification of tumor-reactive T cell receptors from tumor-infiltrating T cells across cancer'

T. R. Wagner, N. Kehl, S. Steiger, M. Kilian, K. Foster, T. Boschert, G. Hernandez, J. G. Abelin, **K. Lindner**, L. S. Sester, J. H. Frenking, B. Schönfelder, S. Schumacher, E. W. Green, P. Schmidt, L. Bunse, B. Chain, C. Müller-Tidow, H. Goldschmidt, N. Weinhold, S. A. Carr, K. Yong, K. Rippe, M. S. Raab, M. Platten, S. B. Eichmüller, M. J. Friedrich. 'Molecular signatures of T cells targeting multiple myeloma'

Contents

List of Abbreviations

2-HG	2-Hydroxyglutarate
α-KG	alpha-Ketoglutarate
AML	Acute myeloid leukemia
APC	Antigen presenting cell
Arg	Arginine
AVE	Avelumab
BBB	Blood-brain barrier
BCR	B cell receptor
B-LCL	B-lymphoblastoid cell line
CD40LG	CD40 ligand
CDKN2A/B	Cyclin dependent kinase inhibitor 2A/B
CMV	Cytomegalovirus
CNS	Central nervous system
CRISPR	Clustered regularly interspaced short palindromic repeats
CSF	Cerebrospinal fluid
CSP	Cell surface protein
CXCL	C-X-C motif chemokine
DC	Dendritic cell
DCM	Dead cell marker
DMSO	Dimethyl sulfoxide
DNA	Deoxyribonucleic acid
EBV	Epstein-Barr virus
EGFR	Epidermal growth factor receptor
ELISpot	Enzyme-Linked-Immuno-Spot
EOT	End of treatment
ESPEC	Epitope-specific expansion cultures
FACS	Fluorescence activated cell sorting
FCS	Fetal calf serum
FFPE	Formalin-fixed paraffin-embedded
FKBP8	FKBP prolyl isomerase 8
FLAIR	Fluid-attenuated inversion recovery
GBM	Glioblastoma multiforme
GEX	Gene expression
GM-CSF	Granulocyte-macrophage colony-stimulating factor

GNLY	Granulysin
gRNA	Guide RNA
Gy	Gray
GZMA	Granzyme A
GZMB	Granzyme B
GZMK	Granzyme K
HEN	Hen egg lysozyme
His	Histidine
HLA	Human leukocyte antigen
ICI	Immune checkpoint inhibitor
IDH1	Isocitrate dehydrogenase 1
IDO	Indolamine 2,3-dioxygenase
IFNγ	Interferon gamma
IL-2	Interleukin 2
IL7R	Interleukin 7 receptor
IVT	In vitro transcription
KDM	Lysine-specific demethylase
LINC00892	Long intergenic non-protein coding RNA 892
MAGE-A3	Melanom-antigen A3
MART1	Melanoma antigen recognized by T-cells 1
MANAFEST	Mutation-associated neoantigen functional expansion of specific T cells
MBP	Myelin basic protein
MCE	Mixed cellulose esters
MHC	Major histocompatibility complex
Min	Minutes
Mio	Million
mL	Milliliter
ML	Machine learning
MOG	Myelin oligodendrocyte glycoprotein
MRI	Magnetic resonance imaging
MS	Mass spectrometry
NADPH	Nicotinamide adenine dinucleotide phosphate
NK	Natural killer cell
NKG7	Natural killer cell granule protein 7
NMPD	National marrow donor program
NOA	Neuroonkologische Arbeitsgemeinschaft
NSCLC	Non-small cell lung cancer

PBMC	Peripheral mononuclear cells
PBS	Phosphate buffered saline
PCC	Pigeon cytochrome *c*
PCR	Polymerase chain reaction
PD-1	Programmed death 1
PDAC	Pancreatic ductal adenocarcinoma
PD-L1	Programmed death-ligand 1
PDX	Patient-derived xenograft
PGE2	Prostaglandin E2
PMA	Phorbol-12-myristat-13-acetat
pMHC	Peptide – MHC complex
PRF1	Perforin
PsPD	Pseudoprogression
PVDF	Polyvinylidene fluoride
QC	Quality control
Rec.	Recurrent
REP	Rapid expansion protocol
RNA	Ribonucleic acid
RNAseq	RNA sequencing
ROS	Reactive oxygen species
RT	Room temperature
SD	Standard deviation
SEB	Staphylococcal enterotoxin B
SMAR	Scaffold/matrix attachment region
SNV	Single nucleotide variant
SUIT	Subsequent identification of TCRs
SYDE1	Synapse defective Rho GTPase homolog 1
TAM	Tumor-associated macrophages
TCR	T cell receptor
TCR-POC	TCR proof-of-concept
TERT	Telomerase reverse transcriptase
TET	Ten-eleven translocation methyl cytosine dioxygenase
T-FINDER	T cell functional identification and (Neo)-antigen discovery of epitopes and receptors
TGFβ	Transforming growth factor β
T_H	T helper cell
TIL	Tumor infiltrating lymphocyte (here referring to T cells only)

TLS	Tertiary lymphoid structures
TME	Tumor microenvironment
TMG	Tandem minigene
TNFα	Tumor necrosis factor alpha
TNFSF14	TNF superfamily member 14
T_{reg}	Regulatory T cell
V	Visit
VAC	Peptide vaccination with IDH1R132H
V(D)J	Variability, Diversity, and Joining gene segments
w/o	Without
WDR12	WD repeat domain 12
WES	Whole exome sequencing
WHO	World Health Organisation
WT1	Wilms tumor 1

List of Figures

List of Supplementary Figures

List of Tables

List of Supplementary Tables

1. Introduction

1.1 Glioma classification

Gliomas are primary brain tumors of the central nervous system (CNS) and are named according to their cell population of origin, glial cells (Louis et al. 2021; Weller et al. 2015; Yang et al. 2022). The latest edition of the world health organization (WHO) Classification of Tumors of the Central Nervous System (WHO CNS6) differentiates between diffuse gliomas and circumscribed gliomas as based on histological analysis as well as analysis of molecular biomarkers (Yang et al. 2022; Weller et al. 2021). Circumscribed gliomas are benign, requiring only complete surgical resection for cure, whereas diffuse gliomas are more aggressive and cannot be cured by surgery alone (Yang et al. 2022).

While the old edition of the WHO classification system (WHO CNS5) from 2016 was largely based on histological analysis and only partly on molecular biomarkers, WHO CNS6 relies even stronger on molecular analysis of the tumor sample, as depicted in **Figure 1** (Horbinski et al. 2022).

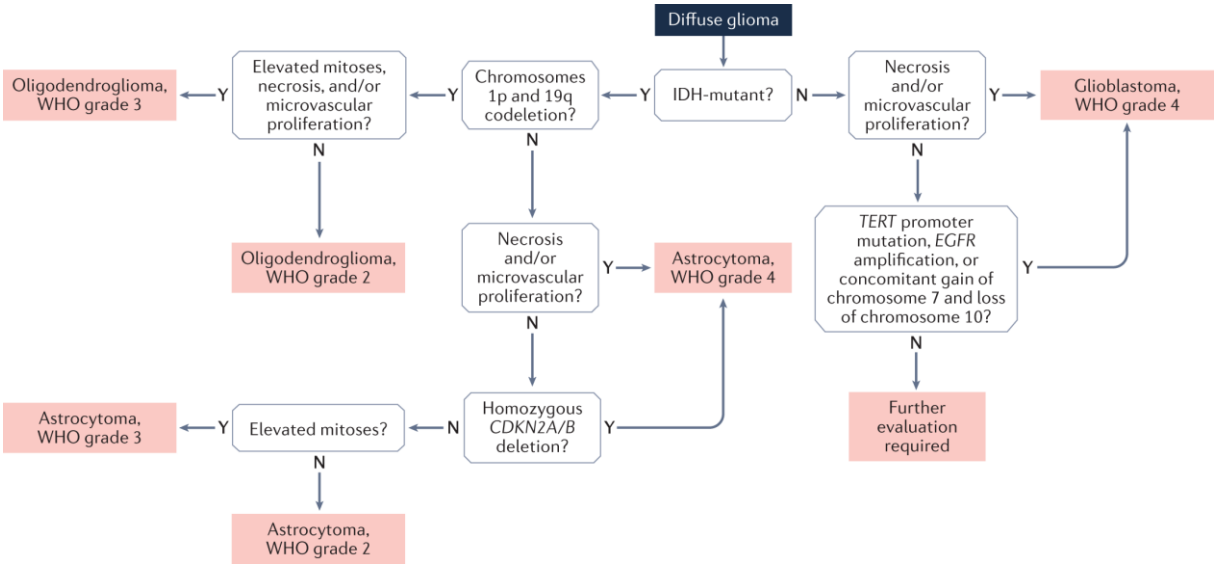

Figure 1. Classification of diffuse gliomas according to the WHO CNS6 classification system. Tumors are classified according to molecular characteristics, such as IDH1 mutational status, co-deletion of 1p/19q, homozygous deletion of CDKN2A/B, mutation of the TERT promoter, gene amplification of EGFR, gain of chromosome 7 and loss of chromosome 10, as well as mutations ins histone H3.3. Figure and information from "Horbinski, C., T. Berger, R. J. Packer, and P. Y. Wen. 2022. 'Clinical implications of the 2021 edition of the WHO classification of central nervous system tumours', *Nat Rev Neurol*, 18: 515-29.". Abbreviations: IDH= isocitrate dehydrogenase, CDKN2A/B= Cyclin Dependent Kinase Inhibitor 2A/B, TERT= Telomerase Reverse Transcriptase, EGFR= Epidermal Growth Factor Receptor.

Early diagnosis of glioma is difficult, as, unlike other tumors such as breast cancer, there are no screening campaigns in place which could allow to detect glioma timely after onset by using for example neuroimaging. The incidence for glioma is relatively low with only around 6 cases per 100,000 individuals per year worldwide (Weller et al. 2021). Gliomas are usually diagnosed after patients experience symptoms such as epileptic seizures, cognitive disorders, focal deficits, headache or fatigue (Weller et al. 2021; Posti et al. 2015). Gliomas are then diagnosed through magnetic resonance imaging (MRI) as well as electroencephalography in case of epileptic seizures (Ellingson, Wen, and Cloughesy 2017; Weller et al. 2021). If feasible, tumors are removed through surgery and tissue subsequently undergoes molecular as well as histological analysis to allow planning further treatment (Weller et al. 2021). In case of a dismal condition of the patient or suboptimal intracranial tumor location, stereotactic biopsies are performed to allow for a guided treatment decision (Weller et al. 2021). Many

patients undergo radiation therapy and receive alkylating chemotherapy in form of temozolomide as standard of care (Horbinski et al. 2022). In general, treatment of brain tumors is difficult, as for example the blood-brain barrier (BBB) can limit access of therapeutic molecules to the brain (Aldape et al. 2019).

Patients with IDH1-mutant gliomas have a superior medium survival as compared to patients with IDH1-wildtype gliomas: based on data from 2009, when WHO CNS5 was used to classify tumors and not WHO CNS6 depicted in **Figure 1**, median survival in IDH1-mutant patients was 31 months and 65 months in glioblastoma and anaplastic astrocytoma, respectively. For IDH1-wildtype patients, median survival was shorter with 15 months and 20 months (Yan et al. 2009).

1.2 Brain tumor immunity and immunotherapy

For a long time, the CNS was regarded as immune privileged site as based on tissue-grafting experiments performed in the 1940s, where heterotopic tissue implanted into the brain did not elicit immunity and was not rejected (Medawar 1948). The notion of the brain as an immune privileged site has since then been disproven.

For example, lymphatic drainage of soluble antigens from the brain to the deep cervical lymph nodes via the arachnoid sheath of olfactory nerves (Bradbury and Westrop 1983) or lymphatic vessels in the meninges (Sampson et al. 2020), as well as the glial-lymphatic (glymphatic) pathway were discovered (Jessen et al. 2015; Sampson et al. 2020). The glymphatic system functions as both garbage disposal and nutrient-distribution system, with perivascular channels formed by astroglia cells allowing for constant flow of fluid containing waste products and nutrients through the brain parenchyma and interstitium towards cerebrospinal fluid (CSF). Only in 2015, lymphatic vessels in the meninges were discovered (Louveau et al. 2015; Aspelund et al. 2015).

However, the immune system functions different in the brain as compared to elsewhere in the body, as for example immunity in healthy brain is suppressed to prevent neurotoxicity, and since the BBB serves as a barrier for many molecules from the periphery (Wischnewski et al. 2023; Sampson et al. 2020; Jessen et al. 2015). It has to be noted that immune responses generated in the periphery are able to enter the brain through the leptomeninges and to perform immunosurveillance (Schlager et al. 2016; Owens, Bechmann, and Engelhardt 2008), which is in accordance to aforementioned early findings from Peter Medawar, who observed immunity against heterotopic tissue if it was first implanted in the periphery and then in the brain (Medawar 1948).

The overall number of TILs and other effector cells is low in CNS tumors, with T cells frequently showing signs of exhaustion (Sevenich 2019). Brain tumors were shown to have a strongly immunosuppressive tumor microenvironment (TME), with tumor-associated macrophages (TAMs) inhibiting T cell function and further secreting cytokines that interfere with immunity and can moreover even promote proliferation of tumor cells (Aldape et al. 2019). On top of that, glioblastoma cells can recruit regulatory T cells (T_{reg}) through production of high amounts of indolamine 2,3-dioxygenase (IDO) (Wainwright et al. 2012). Production of IDO also causes depletion of tryptophan, thereby inhibiting T cell proliferation (Uyttenhove et al. 2003).

New therapies are aiming at improving the TME by making it more immunogenic, using for example IDO inhibitors, targeting immunosuppressive cytokines such as transforming growth factor β (TGFβ) with blocking antibodies, or directly targeting TAMs to create a more immunogenic TME (Sampson et al. 2020). Immune checkpoint inhibitors (ICI) frequently fail in brain tumor therapy, which is most likely due to the low mutational load (Chalmers et al. 2017) resulting in little number of antigenic targets which could be potentially detected by T cells. Patients with hypermutated brain tumors show superior

response to ICI as compared to patients that are not hypermutated (Aslan et al. 2020; Sampson et al. 2020).

Besides ICB therapy, therapeutic vaccinations studies with either antigen-loaded dendritic cells (DCs), or peptides targeting epidermal growth factor receptor variant III (EGFRvIII), survivin, wilms tumor 1 (WT1), patient-individual neoantigens, or IDH1R132H show promising results (Aldape et al. 2019), with IDH1 being further discussed in the following.

1.3 IDH1

Isocitrate dehydrogenases (IDH) are enzymes that catalyze the conversion of isocitrate to alpha-ketoglutarate (α-KG) through oxidative decarboxylation (Han et al. 2020; Al-Khallaf 2017). In total, three isoforms of IDH enzymes are known, with the isoform IDH1 being found in both the cytoplasm and peroxisomes, IDH2 and IDH3 are enzymes located within the mitochondrial matrix. IDH1 and IDH2 proteins homodimerize and change their confirmation to a closed structure upon binding to isocitrate, whereas IDH3 is a heterotrimer made up of two alpha subunits, one beta and one gamma subunit (Al-Khallaf 2017).

Mutations in IDH are associated with several cancer entities, such as glioma, but also fractions of patients with acute myeloid leukemia (AML, 16%), thyroid carcinoma (16%), chondrosarcoma (56%) and intrahepatic cholangiocarcinoma (23%) (Schumacher, Bunse, Wick, et al. 2014; Han et al. 2020; Yang et al. 2012). More than 80% of glioma WHO grade 2/3 cases and 73% of WHO grade 4 secondary GBMs carry IDH1 mutations (Han et al. 2020).

With a prevalence of 70%, the most frequent IDH1 mutation in gliomas is the R132H mutation (arginine (Arg, R) exchange to histidine (His, H) at position 132), which is located in the catalytic pocket of the enzyme (Schumacher, Bunse, Wick, et al. 2014; Yang et al. 2012). The replacement of the highly positively charged Arg by a His with low polarity hinders the formation of hydrogen bonds with isocitrate, but increases its affinity to NADPH, which is required to convert α-KG to 2-HG. As most tumors are heterozygous for IDH1-wildtype and IDH1R132H, a larger fraction of the IDH1 protein dimers are made up of one wildtype and one mutant IDH1 protein. The wildtype protein uses the NADP+ co-factor to convert isocitrate to α-KG, thereby producing NADPH, which is then used by the mutated IDH1 protein to convert α-KG to 2-HG. The resulting accumulation of 2-HG causes DNA hypermethylation and histone methylation by acting as a competitive inhibitor for the DNA-demethylase TET (Ten-eleven translocation methyl cytosine dioxygenase) and histone-demethylases KDM (lysine-specific demethylase) (Han et al. 2020). Decreased amounts of NADPH leads to accumulation of reactive oxygen species (ROS) and associated oxidative damage. Moreover, elevated levels of 2-HG also inhibit DNA repair enzymes.

Overall, IDH1 mutations are known as driver mutations in glioma, as they usually occur early in tumorigenesis, causing genetic instability and therefore malignant transformation (Schumacher, Bunse, Wick, et al. 2014; Cohen, Holmen, and Colman 2013). This is also reflected by the finding that only 3.7% of primary GBMs express mutated IDH1, whereas almost three quarters of WHO grade IV secondary GMBs are IDH1 mutant (Han et al. 2020). Patients with IDH-mutated gliomas show a prolonged median survival as compared to IDH-wildtype glioma patients, which might be due to their increased sensitivity to radiotherapy and chemotherapy (Han et al. 2020). However, IDH-mutated gliomas have a higher chance of accumulating further mutations and to develop a hypermutation phenotype, which is associated with shorter survival (Han et al. 2020).

Its homogenous expression within the tumor makes IDH1R132H an attractive target for glioma therapy (Schumacher, Bunse, Wick, et al. 2014). Approaches to target IDH1R132H are for example the use of

small molecule inhibitors such as olutasidenib (FT-2102), which was FDA-approved for relapsed or refractory AML in patients with IDH1R132H mutation in December 2022, or ivosidenib (AG-120), or vorasidenib, (AG-881), also FDA-approved for AML treatment (Han et al. 2020; Kayki-Mutlu et al. 2023; de la Fuente et al. 2023). Olutasidenib can penetrate the blood-brain barrier, underlining its potential for use in glioma therapy, which is currently evaluated in a phase Ib/II clinical trial with IDH1R132H-mutated glioma (ClinicalTrials.gov, NCT03684811) (de la Fuente et al. 2023).

Mutated IDH was also shown to have a major effect on the immunological tumor microenvironment by suppressing cytotoxic T cells, NK cells and other tumor-infiltrating lymphocytes (Han et al. 2020), as well as inhibiting T cell recruitment through downregulation of cytokines such as C-X-C motif chemokine 10 (CXCL10) (Sampson et al. 2020). Elevated levels of 2-HG epigenetically silence PD-1 and PD-L1, however, elevated levels of 2-HG do also suppress TCR signaling and recruitment of CD8+ T cells to the tumor, thereby inhibiting the antitumor T cell immunity (Han et al. 2020). Using an IDH1-mutant inhibitor along with anti-PD-1 immunotherapeutic antibodies was shown to increase intratumoral proliferation of CD4+ T cells and to prolong survival in patients with IDH1-mutant tumors (Han et al. 2020).

Moreover, peptide vaccines for generating an immune response against the IDH1R132H neoantigen were developed, which was shown to be presented on MHC class II molecules and which induced a CD4+ T helper cell (T_H1) response (Schumacher, Bunse, Pusch, et al. 2014). Overall targeting of IDH1R132H by vaccination is a promising approach, as the epitope is only expressed in cancer cells and since the TME of low-grade gliomas is less immunosuppressive, with longer survival times as compared to GBM allowing for more time to generate a vaccination-induced meaningful immune response (Pellegatta et al. 2015). The long IDH1R132H peptide vaccine is currently further evaluated in clinical trials.

1.4 IDH1R132H-vaccination trials

The IDH1R132H driver mutation is an attractive target for anti-tumor T cell-based immunotherapy due to its homogenous expression within glioma tissues, thereby reducing the risk for immune escape upon targeting the tumor with an anti-IDH1R132H T cell immune response, and slow proliferation of tumor cells (Schumacher, Bunse, Pusch, et al. 2014; Schumacher, Bunse, Wick, et al. 2014). Moreover, the mutation is not expressed in healthy tissue, reducing the risk of possible side effects (Schumacher, Bunse, Wick, et al. 2014).

Pre-clinical studies showed that a long IDH1R132H (p123-142) peptide-vaccine is able to induce a CD4+ T helper type 1 (T_H1) cell response as well as mutation-specific antibodies in A2.DR1 mice (Schumacher, Bunse, Pusch, et al. 2014). These mice were modified to express human MHC class I and II alleles, namely HLA-A*02:01, as well as HLA-DRA*01:01 and HLA-DRB*01:01, and were subcutaneously injected with IDH1R132H sarcomas. Using CD4 depletion experiments as well as DRB1-blocking antibodies showed that the anti-tumor immune response observed in these mice appeared to be mediated through CD4+ T cells, and not through CD8+ T cells. Neither binding predictions nor binding assays indicated that HLA-A*02:01 is indeed able to present a processed IDH1R132H peptide. However, CD8-mediated anti-IDH1R132H responses were observed in a study in which not human but the murine GL261 tumor cell line was implanted intracranially in mice that did not express humanized MHC alleles, which were then vaccinated with short and long IDH1R132H peptides, with the short peptide vaccine eliciting a CD8 response and causing tumor shrinkage (Pellegatta et al. 2015).

Spontaneous antibody and CD4+ T_H1 responses against IDH1R132H were observed in few patients with IDH1-mutant diffuse gliomas (Schumacher, Bunse, Pusch, et al. 2014). Seeing that whole-tumor cell vaccinations of mice with IDH1-mutant sarcomas induced an anti-IDH1R132H immune response

(Schumacher, Bunse, Pusch, et al. 2014) could suggest that in vivo immune responses in patients could potentially be induced by apoptotic tumor cells (Brossart 2020).

Based on pre-clinical data in A2.DR1 mice, the NOA16 trial (NOA: Neurooncology Working Group of the German Cancer Society; ClinicalTrials.gov identifier NCT02454634) was initiated in 2015, in which 33 patients carrying IDH1R132H-mutant WHO grade III and IV astrocytomas were treated with the long IDH1R132H peptide vaccine (Platten et al. 2021). The successful multi-center first-in-human phase I trial proved safety as well as immunogenicity of the vaccine, with 93.3% of the HLA-diverse patient population responding to vaccination. Immunogenicity analysis was possible in 30 patients, with T cell responses observed in 26 patients and B cell responses observed in 28 patients. Pseudoprogression (PsPD), a contrast enhancement observed after three to six months after patients received treatment in form of radiation therapy and temozolomide and/or immunotherapy in T2- Fluid-attenuated inversion recovery (FLAIR) magnetic resonance imaging (MRI), which is caused by strong infiltration with immune cells and difficult to distinguish from true progression (Ma et al. 2019; Bunse et al. 2022), was more frequently observed as compared to a molecularly matched control group and only in patients in which T cell responses were detected (Platten et al. 2021). The vaccine increased progression-free as well as death-free survival in patients in which vaccine-induced T cell responses on basis of IFNγ ELISpots were observed, whereas patients without such immune response progressed. After a maximum treatment of 23 weeks, with most patients receiving 8 vaccination doses and a median follow-up time of 47 months, 26 of 32 patients were still alive (one patient participating in the trial did not receive the vaccine due to fever).

Peripheral T cells responding to the vaccine were classified as T_H1 and T_H17 subtypes, and no cytotoxic CD8+ T cells were found as based on flow cytometric analysis. However, strong evidence for CD8+ T cell response as reflected by TNFα/IFNγ double positive CD8+ T cells found within a TIL single cell sequencing dataset were observed.

Based on the success of the NOA16 trial, the peptide vaccine is currently being tested in combination with the programmed death-ligand 1 (PD-L1)-targeting immune checkpoint inhibitor avelumab in a randomized three-arm phase I clinical trial, called NOA21 (AMPLIFY-NEOVAC, ClinicalTrials.gov identifier NCT03893903) (Bunse et al. 2022). The vaccine is emulsified in Montanide and administered subcutaneously with topical application of imiquimod to boost the associated immune response. The trial aims at demonstrating safety, tolerability and immunogenicity of the IDH1R132H peptide vaccine alone or in combination with the PD-L1 inhibitor avelumab. Application of immune checkpoint inhibitors alongside vaccination against cancer epitopes were reported to have synergistic effects (Vreeland et al. 2016).

NOA21 is planned as a “window-of-opportunity” trial, meaning that patients with recurrent resectable IDH1-mutant tumors after receiving standard-of-care are recruited, allowing for analysis of on-trial tumor tissue which is resected at visit 7 after three doses of vaccination (**Figure 2**). Tumor tissue allows to gain deeper insights into the mode of action of the IDH1R132H peptide vaccine with or without combination with avelumab, for which single cell analysis of multiple intratumoral immune cell populations, such as T cells, B cells, NK cells and myeloid cells, as well as spatial transcriptomics are planned. Besides tumor tissue, multiple blood samples and stool samples are obtained throughout treatment to be able to perform immune monitoring of the T and B cell response elicited upon vaccination and to relate treatment outcome to the gut microbiome. Composition of the latter has a strong influence on clinical outcome of ICI treatment in cancer therapy (Lee et al. 2022).

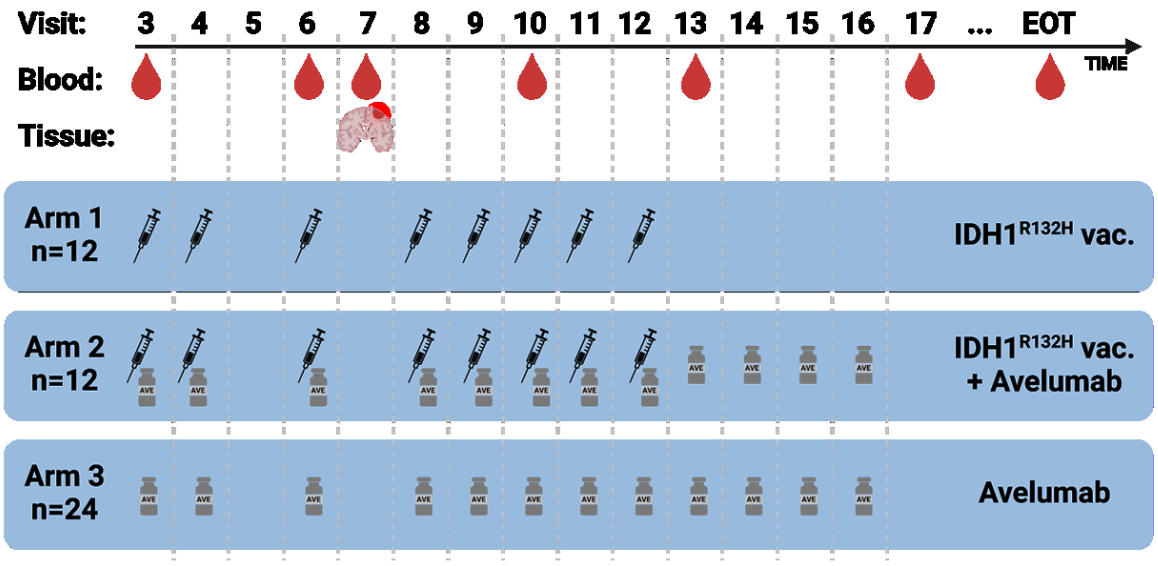

Figure 2. Treatment scheme of the NOA21 clinical trial. A total of 48 patients will be recruited, of which 12 will receive only the IDH1R132H peptide vaccine, 12 will receive the vaccine in combination with avelumab, and 24 will receive only avelumab. Concurrently sampled blood allows for monitoring of the peripheral immune response, and a tissue sample allows for flow cytometric and single-cell based analysis of the intratumoral immune response. Not depicted are MRI assessments at V5, V7, V10, V13 and V16, as well as feces sampling. Visits 3-7 take place at bi-weekly or weekly intervals, and visits 8-17 at monthly intervals. In arms 2 and 3, avelumab is administered at every visit after surgery until progression (Bunse et al. 2022).

1.5 TCR engineered therapy

Immunotherapy and T cell-based therapies are gaining more and more interest for anti-tumor therapy. Pioneering work for melanoma treatment led by Steven Rosenberg showed that ex vivo expansion and subsequent re-infusion of autologous TILs from melanoma patients can lead to a sustained anti-tumor response and successfully cure patients, with objective response rates observed in 49-72% of patients (Rosenberg and Dudley 2009). This approach, called adoptive T cell transfer, could also be applied to many other cancer entities for which outgrowth of reactive TILs in in vitro expansion assays was observed, such as renal cell carcinoma (Andersen et al. 2018), breast cancer (Lee et al. 2017), non-small cell lung cancer (NSCLC) (Ben-Avi et al. 2018) or cervical cancer (Stevanovic et al. 2015). One downside of this approach is that relevant tumor-reactive clones, which are frequently exhausted, might be lost from the expansion culture, thereby limiting therapeutic efficacy (Poschke et al. 2020). Applicability of TIL therapy for primary brain tumors and brain metastases was investigated and showed that adoptively transferred TILs trafficked into the CNS, but also showed limited response rates in patients (Mehta et al. 2018).

As an alternative and more targeted approach, patients can be treated with TCR-engineered T cell therapy, where peripheral T cells obtained from a leukapheresis are engineered to express a TCR with reactivity against a target-of-interest before infusion into a lymphodepleted patient (Shafer, Kelly, and Hoyos 2022; Tsimberidou et al. 2021). T cells are often engineered to co-express a so-called suicide switch which can be activated in vivo in case T cell responses cause for example a life threatening cytokine release syndrome, thereby abrogating the ongoing T cell response and increasing safety of this approach (June 2007).

TCR-transgenic therapies using “non-autologous” TCRs can pose a certain risk for cross-reactivity against healthy autologous tissue, with severe consequences as observed for TCR-transgenic therapies of malignant melanoma against Melanom-Antigen A3 (MAGE-A3), which caused severe neurotoxicity

in three of nine patients and was fatal for two (Morgan et al. 2006; Morgan et al. 2013). Using autologous TCRs for therapy is a good alternative, as T cell clones that are able to expand in vivo must undergo thymic selection, where T cell responses with potential auto-reactivity are eliminated (Khan and Ghazanfar 2018). Moreover, non-autologous TCRs require patients to express both a specific HLA allele as for example HLA-A*02:01 as well as the target mutation which is being recognized by the TCR available for therapy, which limits its broad applicability (Tsimberidou et al. 2021). For glioma therapy, transgenic T cell therapy was so far only tested in the murine system, were tumor shrinkage and long-term cures were observed upon injection of TCR-transgenic T cells against the mImp3 antigen expressed by the murine GL261 cell line, which was intracranially injected (Schaettler et al. 2023).

One difficulty that could be faced when applying TCR transgenic therapy against brain tumors in the clinic is the low mutational load of these tumors, which can limit the number of potential immunogenic epitopes available for therapy, as well as the highly immunosuppressive TME (Kilian et al. 2021). Promising data from chimeric antigen receptor (CAR) T cells tested for brain tumor treatment in the clinic, targeting amongst others the disialoganglioside GD2 (Majzner et al. 2022) and EGFRvIII (O'Rourke et al. 2017), show that it is principally possible to apply transgenic T cell therapies for glioma therapy and that engineered T cells can indeed infiltrate into the tumor.

2. Materials and Methods

2.1 Patient material

Blood from healthy donors was obtained from the IKTZ (Institut für Klinische Transfusionsmedizin und Zelltherapie) in Heidelberg. Patient blood and tissue was obtained from the university hospitals in Mannheim, Heidelberg, Tübingen and Essen. All patients gave informed written consent prior to sample collection, which conforms to the principles set out in the WMA Declaration of Helsinki. Work was approved by the institutional research ethics committees (reference numbers 2017-005F-MA (NOA21 trial), 2019-643N (brain tumor patients including patient BT21), 2021-689 (IDH1R132H-vaccinated patients not included in NOA16 and NOA21 trial), S-207/2005 (TCR-POC patients)).

FFPE tissue was provided from the neuropathologies of the university of Heidelberg and university of Essen.

2.2 Isolation of peripheral blood mononuclear cells (PBMCs)

PBMCs were isolated by density-gradient centrifugation. 15.5 mL of Ficoll-Paque Plus density gradient media (Cytiva, 17144003) were loaded into 50 mL Leucosep tubes (Greiner Bio-One, 227288) and spun down. After adding 3 mL of phosphate buffered saline (PBS; Sigma, D8537-500ML) per tube, 25 mL of heparinized blood were pipetted on top. Tubes were then filled up to a total volume of 45 mL using PBS. Density gradient centrifugation was performed at 2000 revolutions per minute (rpm) for 20 minutes (min) at room temperature (RT) (acceleration 4, deceleration 3). The interphase containing PBMCs was harvested using a Pasteur pipette and transferred into a fresh 50 mL Falcon tube. Cells were washed twice with PBS (centrifugation at 400 g, 10 min, RT), counted using trypan blue (0.4% stock diluted in a 1:2 ratio with PBS; Sigma, T8154) and turk's solution (Merck, 109277), and cryopreserved until further analysis.

2.3 Cryopreservation of cells

Cells were cryopreserved after determining total cell numbers using trypan blue and, in case erythrocytes were present and needed to be excluded from counting, using turk's solution. PBMCs or expanded PBMCs were ideally frozen at a density of 2-3*10^7 cells per cryovial to achieve optimal cell viability. In short, cells were resuspended in appropriate amounts of freezing media A (60% X-Vivo20 + 40% FCS) at room temperature. 500 µL of cell suspension were added per cryovial. Afterwards, the same amount of freezing media B (80% FCS + 20% DMSO) were added to minimize time of exposure to DMSO. Cell suspensions were resuspended twice, and cryovials were immediately transferred into a controlled rate freezing device (biocision, CoolCell BCS-405) and placed at -80°C. Cells were transferred to a liquid nitrogen tank for long-term storage at -140°C either the next day or within a maximum of 7 days to ensure high cell viability.

2.4 Thawing of cells

PBMCs, expanded PBMCs and cell lines were thawed by submerging cryovials into a 37°C water bath while preventing contact of the cryovial lid with water and without swirling. Cryovials were removed from the water bath as soon as only a 2 mm clump of ice was left within the vial, sprayed with ethanol, and transferred under a tissue culture hood. Cells were slowly pipetted into 10 mL of pre-warmed media (RPMI1640 (Sigma, R8758-500ML) for JURKAT cell lines, tumor cell lines and tumor single cell suspensions; X-Vivo15 or X-Vivo20 (both Lonza, BE02-060Q and 04-448Q) for PBMCs, expanded PBMCs or TILs) in a 50 mL Falcon tube using a Pasteur pipette. If (expanded) PBMCs, tumor single cell suspensions or TILs were thawed, 50 IU/mL benzonase (speed BioSystems, YCP1200-500KU) were

supplemented to the media to prevent cell clumping. Cells were spun ((expanded) PBMCs or TILs: 400 g, 10 min, RT; All other cell lines: 350xg, 5 min, RT), gently resuspended in fresh media, counted, and either plated in the appropriate media or immediately used for downstream assays.

2.5 Processing of tumor tissue

Freshly resected tumor tissue was transported on ice while fully submerged in PBS, RPMI or X-Vivo15 media, and immediately processed to ensure high sample quality. Representative pieces of tissue were removed for embedding into Tissue-Tek O.C.T. compound (Sakura, 4583) for later histological analysis. Histology of NOA21 tissues was performed on snap frozen tissue. At least 3x tissue pieces with at least 3 x 3 x 3 mm in size were snap frozen in liquid nitrogen, which were also used for whole exome sequencing (WES) and RNA sequencing (RNAseq). If tissue samples were sufficient in size, larger pieces (1 cm^3) were snap frozen for mass spectrometry (MS)-based immunopeptidomics analysis. All snap frozen tissue pieces were stored at -80°C until further analysis.

The remaining tissue was dissected into small pieces (2 x 2 x 2 mm in size) and a 24-well plate with one tumor piece per well in 1 mL TIL expansion media was set up for ex vivo expansion of tumor infiltrating lymphocytes (TILs). The next day, 500 µL of media was removed per well and 500 µL of fresh TIL expansion media supplemented with 6000 IU/mL IL-2 (Novartis, Proleukin S) was slowly added without disturbing cells to avoid perturbation of cell clusters. If cells proliferated strongly and formed very dense clumps of cells, TIL cultures were resuspended by pipetting up and down to destroy cell clusters and split in a 1:2 ratio using TIL expansion media supplemented with 6000 IU/mL IL-2. After two weeks of cultivation, TILs were harvested and either underwent further expansion using the rapid expansion protocol (REP) or were cryopreserved.

The remaining tissue was gently mashed through a 100 µm cell strainer using the back side of a syringe plunger and filtrated through a 70 µm cell strainer. Myelin was removed using myelin removal beads II (Miltenyi, 130-096-733) according to the manufacturers protocol. Single cell suspensions were cryopreserved.

A small fraction of the tumor single cell suspension was used to set up tumor cell lines by transferring cells into tumor growth media in T25 flasks (Greiner, 690195). If cells started to proliferate and were sufficiently dense, they were detached using Accutase (Thermo Fisher Scientific, A1110501) and propagated.

2.6 Flow cytometry

Cells were washed with PBS before transferring them into U-bottom 96-well plates (TPP, 92097) for staining prior to flow cytometry of fluorescence associated cell sorting (FACS). The centrifugation speed during all steps of the staining protocol was 400 g, 4 min, 4°C and samples were protected from light to avoid fluorophore bleaching.

To allow for discrimination of viable and dead cells, cells were stained with 50 µL fixable viability dye (AF700, eBioscience) diluted 1:1000 in PBS for 10 min at RT and washed with 150 µL FACS buffer (PBS containing 0.5% BSA (Sigma-Aldrich, A3294-50g) and 2 mM EDTA (Genaxxon Bioscience, C4263.0100)). If required, Fc-receptors were blocked using 50 µL of human Fc block reagent (BD Biosciences, 564220) 1:20 diluted in FACS buffer. For tumor single cell suspensions, 10% human serum in PBS was used for Fc receptor blocking. Cells were incubated for 10 min at RT, washed with 100 µL FACS buffer, and then stained at 4°C with fluorescently labelled antibodies in a total volume of 50 µL for 20 min. If only cell surface staining was of interest, cells were subsequently washed twice using 150 µL FACS buffer, resuspended in 200 µL FACS buffer and stored on ice until acquisition on a FACSLyric (BD Biosciences)

or until they were sorted using an FACSAria Fusion I or II (BD Biosciences) device. Cell populations were sorted into tubes coated for >15 min with 5% BSA in H_2O containing a small volume of 0.04% BSA in PBS using a 100 µm nozzle.

If intracellular staining was of interest, cells were resuspended in 100 µL of Cytofix solution and incubated for 20 min on ice, before washing them twice with Cytoperm (both Cytofix and Cytoperm from BD Biosciences, 554714) solution that was diluted at a 1:10 ratio in H_2O. If Epstein-Barr virus (EBV)-containing lymphoblastoid B cell lines (B-LCLs) were stained, incubation time in paraformaldehyde-containing Cytofix was extended to a total of 30 min to ensure complete inactivation of viral particles. Cells were then stained with fluorophore-coupled antibodies for intracellular staining, which were added to 1:10 diluted Cytoperm for a total volume of 50 µL. After 30 min of incubation in ice, cells were washed twice with 150 µL of 1:10 diluted Cytoperm solution, resuspended in 200 µL of FACS buffer, and acquired on a FACSLyric device.

Flow cytometry data was analyzed using FlowJo software (FlowJo LLC).

2.7 Single-cell sequencing of TILs

For single-cell sequencing of tumor single cell suspensions, cryovials were thawed as described before, and resuspended in PBS for counting with trypan blue and turk's solution. Cells were stained for FACS sorting using the fixable viability dye AF700 (eBioscience) for live/dead discrimination, 10% human serum for Fc receptor blocking, and fluorescently labelled antibodies for cell surface staining (CD235a (clone HI264, APC, BioLegend), CD11b (clone ICRF44, BB515, BD), CD45 (clone 2D1, APC-H7, BD), and CD3 (clone HIT3A, BV510, BD)). If applicable, barcoded antibodies were added to the panel to allow for cell hashing and multiplexing, or to allow gathering information on cell surface proteins using CITE-seq antibodies (**Table 3**). To enrich for CD3+ cells, cells were gated on viable singlets that were negative for the erythrocyte marker 235a, negative for CD11b but positive for CD45 and CD3 (**Supplementary figure 1**).

After FACS sorting, cells were centrifuged at 350xg, 10 min, 4°C. Supernatant was not completely removed to allow for resuspension of cells in residual volume (around 40 µL) and to prevent loss of cells. Cells were counted using 8 µL of trypan blue and 2 µL of cell suspension, and subsequently loaded for 5' single cell sequencing (10X Genomics, kit versions v1, v1.1 or v2) according to the manufacturers protocols. V(D)J, gene expression (GEX) or cell surface protein (CSP) libraries were generated and sequenced using the NovaSeq 6000 or HiSeq4000 platforms (Illumina). Fastq files were processed using 10x Genomics' Cellranger software platform v6.1.2 (Zheng et al. 2017), h5 matrices were imported using R >4.1 (RStudio Team, 2021. *RStudio: Integrated Development Environment for R*, Boston, MA. Available at: http://www.rstudio.com/) and analysis was performed using the Seurat package v4 (Hao et al. 2021).

2.8 Isolation of DNA from blood and (FFPE) tissue

DNA from PBMCs, cell lines, B-LCLs and tissue was isolated using the DNeasy Blood and Tissue kit (Qiagen, 69504) according to the manufacturers protocol, and DNA from whole blood samples was isolated using the QIAamp DNA blood maxi kit (Qiagen, 51192). To isolate DNA from FFPE tissue, the QIAamp DNA FFPE tissue kit (Qiagen, 56404) was used. If necessary, DNA was concentrated using a vacuum centrifuge (Thermo Scientific, DNA120 SpeedVac). DNA concentrations were quantified using a Nanodrop (Thermo Scientific) or a Qubit (Thermo Scientific). Integrity of DNA was monitored using a TapeStation (Agilent).

2.9 Isolation of RNA from tissue

RNA was isolated from brain tissue using the RNeasy Lipid Tissue Mini kit (Qiagen, 74804) along with the TissueLyser II (Qiagen). RNA concentrations were measured using a Nanodrop (Thermo Scientific) or a Qubit (Thermo Scientific). The RNA integrity number (RIN) was determined using a TapeStation (Agilent).

2.10 ESPEC-SUIT

PBMCs were thawed as described earlier, resuspended in X-Vivo20 and cell numbers were counted using trypan blue. Cell numbers were set to 4-8*10^6 cells per mL with 5 mL of cell suspension per 50 mL Falcon Tube and rested overnight in a 37°C CO_2 incubator with slightly twisted open lid. The next day, cells were spun down (400 g, 10 min, RT) and resuspended in fresh X-Vivo20 media supplemented with 2% AB serum (Sigma Aldrich, H4522-100ML). Cell numbers after resting were determined using trypan blue and cells were diluted to a concentration of 2*10^6 cells per mL. Half of the available cells were set aside, diluted to 1*10^6 cells per mL, and 500 µL were plated per well of a 24-well plate. Of the remaining cells, 250 µL were plated per well into a second 24-well plate, but pulsed with 250 µL of X-Vivo20 supplemented with 2% AB serum containing (I) the peptide-of-interest, (II) the wildtype counterpart to the peptide-of-interest, (III) a control peptide (such as MOG), (IV) no peptide. Peptides were usually added to achieve a final amount of 2 µg per well (**Table 6**). Both plates were placed in a 37°C CO_2 incubator and after four hours, cells from the plate without peptide were resuspended and transferred to the plate containing peptide pulsed cells to achieve a final density of 1*10^6 cells per well. Finally, cells were placed back into the 37°C CO_2 incubator.

On days 4, 7, 9 and 11, half of the medium per well was removed and fresh X-Vivo20 containing 2% AB medium and supplemented with 100 IU/mL IL-2, 50 ng/mL IL-7 (Milteyni, 130-095-362) and 50 ng/mL IL-15 (Milteyni, 130-095-764) were added to the culture. Cells were split in a 1:2 ratio if required. On day 14, cells of each expansion condition were harvested, spun down (400 g, 10 min, RT), resuspended in X-Vivo20 supplemented with 2% AB serum but without cytokines, and rested overnight in 50 mL Falcon tubes with slightly twisted open lids. A maximum number of 4*10^7 cells were kept in 5 mL per tube.

The next day, cells were subjected to a quality control IFNγ ELISpot to verify the peptide-specific expansion per culture, as described in chapter 2.22. Cells were spun down (400 g, 10 min, RT), resuspended in X-Vivo20 without AB serum, counted with trypan blue, and set to the desired cell concentration. Depending on the antigen-of-interest and whether patients received vaccinations against the epitope-of-interest or not, 25,000 – 250,000 cells were plated per well in triplicates, or in duplicates in case the total number of cells available was not sufficient. A mixture of phorbol-12-myristat-13-acetat (PMA; 20 ng/mL, Sigma Aldrich, P8139—1MG) and ionomycin (1 µg/mL, Sigma Aldrich, 407950-1) was used as a positive control. After 44 hours of re-stimulation, ELISpots were stopped and analyzed. In parallel to ELISpot analysis, a minimum number of 1*10^6 cells were cryopreserved and later subjected to single cell V(D)J sequencing to determine the correct alpha beta pairing per TCR for cloning. To do so, cells were thawed, counted using trypan blue, and loaded for 5' single cell sequencing using the platform of 10X Genomics (kit versions v1, v1.1 or v2) according to the manufacturers protocols.

In addition, cell pellets were cryopreserved at -80°C and later subjected to TCRβ deep sequencing analysis (chapter 2.21) to be able to select interesting TCRs for cloning, if peptide-specific expansion was observed in ELISpot. Optionally, populations of interest were enriched prior to TCRβ deep sequencing analysis. Such populations could be either CD4+, CD8+, or TNFα+ cells after TNFα secretion assay (Miltenyi, 130-091-268), which can be enriched by FACS sorting on the Aria Fusion cell sorter

(Becton Dickinson), or by magnetic bead-based enrichment (Miltenyi; CD4+ cells: 130-042-401; CD8+ cells: 130-096-495). For FACS sorting, CD3 (clone HIT3A, BV510, BD), CD4 (clone SK3=Leu3a, BV786, BD) and CD8a (clone RPA-T8, PerCP-Cy5.5, Invitrogen) were used for staining.

Clones with strong expansion as compared to the baseline PBMC sample and with low expansion in the no peptide control were selected for cloning and testing. The FEST algorithm (Danilova et al. 2018) was used to select candidate TCRs for TCR cloning and testing.

2.11 Rapid expansion protocol (REP)

The rapid expansion protocol (REP) was used to expand T cells. If PBMC-derived T cells were expanded, REP media without fungizone, gentamicin and penicillin/streptomycin was used, whereas full media was used if TILs were expanded.

In short, PBMCs from three independent donors were thawed and irradiated at 40 Gray (Gy) using a Gammacell 1000 (AECL) irradiation device to serve as feeder cells. $1*10^7$ cells from each donor were pooled together, cells were spun down (400 g, 10 min, RT), resuspended in REP media and plated into a standing T25 flask. Either (I) 100,000 TILs, or (II) 100,000 CD4/CD8 magnetic bead-based enriched T cells (Miltenyi; CD4+ cells: 130-042-401; CD8+ cells: 130-096-495), or (III) 150,000 PBMCs were added to feeder cells for expansion. 666 µg of OKT-3 antibody (Life technologies, 16-0037-85) were added to the culture. The flask was filled up to reach a total volume of 20 mL. The next day, 5 mL of X-Vivo15 supplemented with 2% AB serum containing 7,500 IU IL-2 were slowly added to the culture to prevent whirl up of cells.

Three days later, 12.5 mL of media were removed and 12.5 mL of X-Vivo15 supplemented with 2% AB serum containing 600 IU/mL IL-2 was slowly added to the culture by pipetting on the back of the flask. If required at a later timepoint, cells were split in a 1:2 ratio by resuspending the culture, transferring 12.5 mL of cell suspension into a second standing T25 flask, and adding 12.5 mL of X-Vivo15 supplemented with 2% AB and 600 IU/mL IL-2 to both flasks.

2.12 HLA-typing

At least 100 µL of DNA with a concentration of at least 20 ng/µL was isolated from blood as described before and submitted for high-resolution HLA-typing (DKMS Germany).

2.13 Generation of B-LCLs

B-LCLs are B cells that were immortalized after infection with EBV and which can be used as autologous antigen presenting cells (APCs) in co-culture assays. EBV was obtained by harvesting supernatant of the B95-8 cell line, originating from EBV-transformed lymphocytes of a female cotton-top tamarin (Desgranges et al. 1979), which was a kind gift from the laboratory of Prof. Dr. Hedda Wardemann (DKFZ Heidelberg, Germany). In short, B95-8 cells were propagated by seeding $10*10^6$ cells in 20 mL of B95-8 growth media in a T150 flask. After three days, when media turned yellow while most cells were still adherent, supernatant was carefully and completely removed while avoiding detachment of cells and filtrated through 45 µM polyvinylidene fluoride (PVDF) filters (Merck, SLHV033RS) using 20 mL syringes (Terumo, SS+20L1). Supernatant was aliquoted using 1.5 mL per 2 mL protein low bind tube (Eppendorf, 022431102) and frozen at -80°C. Wearing of personal protection such as eye protection and a mask are mandatory for EBV-related work due to its classification as risk group 2.

To immortalize B cells, PBMCs of a donor-of-interest were thawed, counted using trypan blue, and rested overnight in a 37°C CO_2 incubator in 5 mL of X-Vivo20 in a 50 mL Falcon tube with slightly twisted open lid to allow for air circulation. The next day, B cells were isolated using the B Cell Isolation Kit II, human (Miltenyi, 130-091-151), resuspended in B-LCL growth media, counted using trypan blue, and diluted to a concentration of $0.3125*10^6$ cells per mL in 12 mL total volume. EBV supernatant was carefully thawed and 3 mL were added to the B cells, as well as 75 µL of 6 µg/µL Transferrin (Sigma, T4132-100mg) and 15 µL of 2.5 µg/µL CpG-ODN2006 (Invivogen, tlrl-2006). After thoroughly mixing the cell suspension, 200 µL of cell suspension were plated per well of a round-bottom 96-well plate, with outer wells being filled with PBS to minimize evaporation effects. If less B cells were available following B cell isolation, the protocol was scaled down accordingly.

Clonal expansion of B-LCLs was monitored in the following weeks and cells were transferred into larger culture volumes upon proliferation.

2.14 CRISPR-Cas knockouts in B-LCLs

To abolish expression of DRA-, DP- and DQ-MHC II alleles in B-LCLs, the respective loci were targeted with CRISPR-Cas, using crRNA previously functionally validated by others (Lee et al. 2020). The protocol for electroporation of B-LCLs with CRISPR constructs was inspired by (Jiang et al. 2018) and a protocol of the manufacturer IDT.

In short, B-LCLs were split one day prior to electroporation to increase cell viability and proliferation. The next day, guide RNA (gRNA) was formed by mixing 2.2 µL of 200 µM Alt-R CRISPR-Cas9 crRNA (IDT, custom designed; crRNA DRA-58 (gRNA seq.: TGAGGACGTTTACGACTGCA), crRNA DPA-13 (gRNA seq.: GAGACTCAGCAGGAAAGCCA); crRNA DQA-40 (gRNA seq.: GAAGAAGGAATGATCACTCT)), 2.2 µL of 200 µM Alt-R CRISPR-Cas9 tracrRNA (IDT, 1072532) and 5.6 µL of IDTE buffer (IDT, 11010202). The mixture was heated at 95°C for 5 min before placing it at RT to slowly cool down. In the meantime, Alt-R Cas9 enzyme (IDT, 1081061) (62 µM stock) was diluted to a concentration of 36 µM using TE buffer and carefully mixed. 0.5 µL of guide RNA and 0.5 µL of 36 µM Alt-R Cas9 enzyme were mixed and incubated at RT for 10-20 min.

B-LCLs were counted in trypan blue and cells were washed once (350xg, 5 min, RT) in a 15 mL Falcon tube using PBS. Per electroporation, $0.5*10^6$ cells were required, the following protocol refers to the electroporation of only one condition, but can be scaled up accordingly. Before electroporation, cells were centrifuged at 100xg for 10 min at RT, PBS was completely removed, and the pellet was carefully resuspended in 18.5 µL of buffer SF (Lonza, kit V4XC-2032, nucleofector solution was supplemented in a 1:4.5 ratio with supplement buffer according to the manufacturer's protocol). Cells were transferred into one well of a 16-well Nucleocuvette strip and electroporated using the EN-138 program of the Lonza 4D nucleofector device. Immediately after electroporation, 180 µL of RPMI plus 20% foetal bovine serum (FBS) were added to the well and cells were left at RT to allow cellular pores to close, thereby reducing the negative effects of mechanic stress on cell viability related to pipetting. After 10 minutes, cells were carefully resuspended once and transferred into one well of a 48-well plate containing pre-warmed RPMI plus 20% FBS, which was equilibrated in a 37°C CO_2 incubator for at least 30 min.

Cells were placed back into an incubator and cultivated for at least five days. If required due to strong cell proliferation, cells were transferred into larger volumes. Successful knockdown of MHC II alleles was verified after 5-7 days using flow cytometry. Cells were stained with fixable viability dye (AF700, eBioscience), and fluorescently labelled antibodies for cell surface staining (HLA-DR (clone L243, PerCP-eF710, Thermo Fisher), HLA-DQ (clone Tu169, BV421, BD), and HLA-DP (clone B7/21, PE, BD)). A fraction of B-LCLs with CRISPR-knockouts was cryopreserved for future assays.

2.15 Generation of dendritic cells

PBMCs were thawed in X-Vivo20 media as described before and cell numbers were determined using trypan blue. CD14+ monocytes were positively selected using magnetic bead-based enrichment (Miltenyi, 130-050-201) and counted. Cell density was set to $1*10^6$ cells per mL in X-Vivo 20 supplemented with 500 IU/mL IL-4 (Miltenyi, 130-093-921) and 560 IU/mL granulocyte-macrophage colony-stimulating factor (GM-CSF; PeproTech, 300-03-100), and 3 mL were plated per well of a 6-well plate.

If T cells were of interest for downstream assays such as ELISpot, column flow through was collected and plated in X-Vivo15 supplemented with 100 IU/mL IL-2 as well as 60 IU/mL IL-4, and placed in a 37°C CO_2 incubator for a maximum of one week.

To cultivate monocytes, half of the media was carefully removed and replaced by fresh X-Vivo20 supplemented with 1000 IU/mL IL-4 and 1120 IU/mL GM-CSF two and four days after enrichment. Immature DCs were harvested by collecting the media containing floating cells, and by adding ice cold 0.9 mM EDTA in PBS. After incubation for at least 10 min on ice, detaching cells were carefully washed off and used in downstream assays.

If mature DCs were required, 1000 IU/mL TNFα (PeproTech, 300-01A-100), 10 ng/mL IL-1β (PeproTech, 200-01B-10), IL-6 (PeproTech, 200-06-20) and 1000 ng/mL prostaglandin E2 (PGE2; Sigma Aldrich, P0409-1MG) were added to the culture for 24h and cells were harvested as described for immature DCs.

2.16 TCR cloning into SMAR

The protocol for Golden Gate assembly of TCR fragments in pSMARTer v5 plasmids, the pSMARTer v5 plasmid and the inhouse JSONanalyser software package for design of fragments encoding for TCR alpha- and beta-chains from single cell sequencing data of 10X Genomics were all developed by Edward Green (DKFZ Heidelberg, Germany). In short, DNA oligos encoding for alpha and beta TCR chains were ordered from TWIST Bioscience. A Golden Gate reaction was set up by combining 10 ng of alpha chain fragment, 10 ng of beta chain fragment, 75 ng of pSMARTer v5 plasmid, 0.5 µL BsaI-HF v2 Golden Gate enzyme (NEB, E1601S) and 0.5 µL T4 ligase buffer in a total volume of 5 µL. The reaction was run for 30 cycles (1 min at 37°C, 1 min at 16°C) with a final step for 5 min at 55°C. 2 µL of product was transformed into NEB 5alpha competent E. coli (NEB, C2987H), either commercially available or competent bacteria expanded using the Mix & Go! E. coli Transformation Kit (Zymo, T3001). Bacteria were plated on LB agar plates (25 g/L LB media powder (Applichem, A0954), 14 g/L agarose (Roth, 2267.4) containing 100 µg/mL ampicillin (Roth, K029.2) and single colonies were picked the next day to inoculate 5 mL of LB media (25 g/L LB media powder in H_2O) containing 100 µg/mL ampicillin. Glycerol stocks were prepared by mixing 500 µL of 80% glycerol (Fisher Chemical, G/0650/08) in H_2O and 500 µL bacteria suspension and frozen at -80°C. DNA or bacteria were submitted for sequence verification at Eurofins or at Microsynth using the primers pSMARTer_EF1a_seqF_v2 and pSMARTer_apoB_seqR_v2.

2.17 In vitro transcription (IVT)

In vitro transcription (IVT) was used to produce TCR-expressing RNA plasmids for electroporation into expanded PBMCs and TCR testing.

If TCR-encoding pSMARTer v5 plasmids were used as a template, TCR sequences were amplified using a polymerase chain reaction (PCR), with primers designed to add a T7 promoter to the TCR-encoding sequence. Briefly, 10 ng of pSMARTer v5-TCR DNA diluted in 20 µL H_2O, 2.5 µL of 10^{-4} M primer

MmTRAC_co mRNA rev, 2.5 µL of 10^{-4} M primer T7 EF1a F, 25 µL of CloneAmp HiFi PCR Premix (Takara, 639298) were mixed and incubated in a T100 thermal cycler (Bio-Rad). A PCR was set up with initial denaturation of the DNA template at 98°C for 30 seconds (sec), followed by 30x cycles of denaturation (98°C, 5 sec), annealing (55°C, 5 sec) and extension (72°C, 12 sec). A final single elongation step at 72°C for 15 sec was added before cleaning up using the PCR product using the DNA Clean & Concentrator-25 kit (Zymo, D4033) and measuring DNA concentrations using a Nanodrop (Thermo Scientific). 1 µg of DNA was used to set up an IVT with capping and poly-A-tailing using the T7 mScript Standard mRNA Production System (CELLSCRIPT, C-MSC100625) according to the manufacturer's instructions, but using 1h incubation time for the Standard mScript T7 IVT reaction instead of only 30 min. RNA concentrations were determined using a Nanodrop (Thermo Scientific).

All IDH1 TCRs presented in this thesis were prepared using TCR-encoding pSMARTer v5 plasmids as a template. Cloning and IVT were kindly supported by Gordon Haltenhof (DKFZ Heidelberg, Germany).

2.18 Oligo-based production of TCR-encoding RNA

A high throughput and cost-efficient method for the preparation of TCR-encoding RNA was developed and established by Edward Green and Tamara Boschert (DKFZ Heidelberg, Germany). Preparation of TCR-encoding RNA of patient BT21 was performed by Gordon Haltenhof (DKFZ Heidelberg, Germany). A pool of DNA oligos with a length of 250 bp was ordered from TWIST Biosciences for Golden Gate assembly. Specific primer sequences were added to the 3' and 5' ends of these oligos to allow for demultiplexing and assembly of DNA oligos using a high-fidelity PCR.

PCRs were set up using 1 µL oligo library (0.1 ng/µL stock), 5 µL of forward and reverse primer each (0.8 µM stock) and 10 µL of 2x Kapa HiFi HS master mix (Roche, KK2600). The PCR reaction was run on a MasterCycler X50 (Eppendorf) with initial denaturation of the DNA template at 95°C for 3 min, followed by 3x touchdown cycles with denaturation (98°C, 20 sec), annealing (68°C, 40 sec, Δ -1°C/cycle) and extension (72°C, 15 sec). After another 30 cycles with denaturation (98°C, 20 sec), annealing (65°C, 40 sec) and extension (72°C, 15 sec), a final single elongation step at 72°C (60 sec) was performed. The resulting DNA product was cleaned up under size selected using AMPure beads (Beckman Coulter, A63881) at a 1:1 ratio to retain fragments with >200 bp size. DNA concentrations were determined using a Nanodrop (Thermo Scientific).

The resulting product was used to assemble alpha and beta TCR chains separately using a Golden Gate assembly reaction. A total of 40 ng demultiplexed oligo, 20 ng of T7 alpha (or T7 beta) encoding plasmid, 20 ng of TRAC (or TRBC) expression plasmid were combined in a 10 µL BsaI-HF Golden Gate reaction and cycled 30 times (1 min at 37°C, 1 min at 16°C). 0.5 µL of the Golden Gate reaction, 1 µL of primer_F, 1 µL of primer_R, 5 µL of CloneAmp HiFi PCR Premix and 2.5 µL of H_2O were mixed and a PCR reaction with denaturation of the DNA template at 98°C for 30 seconds (sec), followed by 30x cycles of denaturation (98°C, 5 sec), annealing (62°C, 5 sec) and extension (72°C, 10 sec) and a subsequent final elongation step (72°C, 10 sec) was run on a MasterCycler X50 (Eppendorf).

DNA was cleaned up by adding 10 µL of H_2O and AMPure beads at RT at a 1:1.8 ratio to clean up DNA fragments with 1-1.2 kb in size. DNA and beads were mixed and incubated for 5 minutes, before placing the solution on a magnet. Supernatant was removed, beads were washed twice with 200 µL of 80% ethanol and beads were dried for 2 min at RT. Fragments were eluted in 10 µL of water, and 4 µL were sent for sequence verification of TCR alpha- and beta-chains at Microsynth using the primer_R. IVT was performed as described before.

2.19 Electroporation and co-culture assays with JURKAT reporter cell lines

The JURKAT-reporter cell lines JURKAT-TPR-CD8ab (TPR: triple parameter reporter) and JURKAT-NF-κB were obtained from the laboratory of Peter Steinberger. They were generated by infection of the CD4 positive JURKAT E6.1 cell line with self-inactivating retrovirus, making them express fluorescent proteins after TCR activation (Jutz et al. 2017; Jutz et al. 2016). The JURKAT-TPR-CD8ab cell line were transduced to express CD8, and to inducible expresses CFP, eGFP and mCherry after TCR activation due to stimulation of the response elements NF-κB, NFAT and AP-1, respectively (Jutz et al. 2016; Rosskopf et al. 2018). The JURKAT-TPR-CD8ab cell line can be used to test either CD4+ or CD8+ derived TCRs. The JURKAT-NF-κB eGFP cell line turns eGFP positive upon TCR stimulation due to induction of the NF-κB response element and is not co-transduced with CD8 (Jutz et al. 2017).

To electroporate JURKAT-reporter cell lines with TCR-expressing DNA or RNA, cells were split one day before electroporation to stimulate proliferation and ensure high cell viability. The next day, a 48-well plate was filled with 1 mL of media (RPMI supplemented with 10% FCS) per well and placed in a 37°C CO_2 incubator. JURKAT cells were counted using trypan blue and the required number of cells was transferred into 50 mL Falcon tubes, spun down (350xg, 10 min, RT) and washed once with TexMACS media (Miltenyi, 130-097-196) in a 15 mL Falcon tube. Cells were spun down (100xg, 10 min, RT), $2*10^6$ cells were resuspended in 20 µL SE nucleofector solution (Lonza, V4SC-1096) supplemented according to the manufacturer's protocol per electroporation condition, and transferred into 16-well Nucleocuvette strips containing either 2 µg of TCR-encoding pSMARTer v5 DNA or 2 µg of TCR-encoding RNA. Cells were electroporated using the CL-120 nucleofection program of the Lonza 4D nucleofector device and subsequently left at RT to allow pores to close. After 10 min, 180 µL of pre-warmed media from the 48-well plate are added per well, and cells were carefully transferred into the corresponding wells of the same plate, before placing it back to a 37°C CO_2 incubator.

After 18-24 h (RNA-based electroporation) or 42-48 h (DNA-based electroporation), cells were harvested and counted using trypan blue. mTCRβ expression was quantified by flow cytometry after staining with fixable viability dye (AF700, eBioscience) and mTCR-beta (clone H57-597, PE, BioLegend). After confirming TCR expression, a total of 150,000 JURKAT cells was co-cultured with 15,000 DCs or 50,000 B-LCLs, which were previously pulsed with peptide for 1-24 hours. After 18 hours of co-culture, fluorescence was measured using the SpectraMax plate reader (Molecular devices), or using the FACS Lyric (Becton Dickinson) after staining with fixable viability dye (AF700, eBioscience) and CD69 (clone FN50, APC, BD) fluorescent antibody.

2.20 Electroporation and co-culture assays with expanded PBMCs

A 48-well plate was filled with 1 mL of media (TexMACS supplemented with 2% AB serum) per well and placed in a 37°C CO_2 incubator. Expanded PBMCs from autologous or non-autologous donors were either thawed and rested overnight in X-Vivo15 supplemented with 2% AB serum, or used freshly without intermediate cryopreservation after REP-based expansion. If TCRs derived from either only CD4+ or CD8+ clones were to be tested, CD4+ or CD8+ magnetic bead-based enriched T cells were used to set up the REP.

Cells were washed once using TexMACS or RPMI media, counted in trypan blue, and the required number of cells was spun down (100xg, 10 min, RT). $2*10^6$ cells were required per electroporation condition, the following protocol refers to the electroporation of only one condition, but can be upscaled accordingly. Cells were resuspended in 20 µL of supplemented buffer P3 solution (supplemented according to the manufacturer's protocol; Lonza, V4XP-3032) per $2*10^6$ cells and were transferred into one well of a 16-well Nucleocuvette strip containing 750 ng of TCR-encoding RNA per well. The EO-115 nucleofection program of the Lonza 4D Nucleofector was used for transfection and

cells were subsequently left at room temperature for 10 min. After 10 min, 180 µL of pre-warmed media from the previously prepared 48-well plate were added per well of the Nucleocuvette strip, and 200 µL of cell suspension were carefully transferred back into the corresponding wells of the 48-well plate. Electroporated cells were transferred into a 37°C CO_2 incubator.

After 18-24 h, cells were harvested in tubes containing benzonase for a final concentration of 50 IU/mL to prevent cell clumping. Cells were spun down, resuspended in X-Vivo15 supplemented with 2% HAS (Human Albumin 20% salzarm, Behring, CH.-B.: P100245582), cell numbers were determined using trypan blue, and cell concentrations were set to $1.5*10^6$ cells per mL. After confirming mTCRβ expression through flow cytometry (viability dye (AF700, eBioscience), CD4 (clone SK3=Leu3a, BV786, BD), CD8a (clone RPA-T8, PerCP-Cy5.5, BD), mTCR-beta (clone H57-597, PE, BioLegend)), 100 µL of cells were plated in the appropriate wells of a 96-well U-bottom plate.

To test the reactivity of each transduced TCR, co-cultures were performed with three different types of APCs, depending on the target-of-interest: (I) 75,000 cells of a tumor cell line treated with 300 IU/mL IFNγ for 48 h, (II) 15,000 peptide-pulsed DCs, or (III) 15,000 peptide-pulsed B-LCLs. Co-cultures were set up in a total volume of 200 µL per well in X-Vivo15 supplemented with 2% HSA. Anti-CD3/CD28 T Cell TransAct beads (1.5 µL/well; Miltenyi, 130-111-160) served as positive controls for each tested TCR. Wells without APCs, with APCs that were not pulsed with peptide, or DCs or B-LCLs pulsed with irrelevant peptides such as myelin oligodendrocyte glycoprotein (MOG) or with wildtype peptides of the neoepitope-of-interest were used as negative controls.

On top of that, TCRs with previously confirmed reactivity were used in parallel co-culture assays, such as a Flu TCR restricted to Flu peptide (PKYVKQNTLKLAT) presented on MHC II alleles DRB1*01:01 und DRB1*04:01, or the DMF5 TCR reactive against MART1 peptide (ELAGIGILTV) presented on MHC I allele HLA-A*02:01. In co-culture assays with tumor cell lines, the MART1+ HLA-A*02:01+ melanoma-derived tumor cell line MeWo served as a positive control.

After setting up the co-culture assay, 5 µL of CD107a (clone H4A3, APC-H7, BD) were added to each well, cultures were mixed by pipetting up and down, and the plate was spun for 1 min at 10 g to ensure immediate contact between expanded PBMCs and APCs. Upon stimulation, granules mediate the release of cytokines and CD107a which is located inside the membrane of granules is transiently being presented as the cell surface, FACS antibodies can bind the protein, and both are together being internalized into the cytoplasm (Betts and Koup 2004). Cells were transferred into a 37°C CO_2 incubator. After 1h, 10 µL of 1:44 pre-diluted GolgiStop (BD, 554724) and 10 µL of 1:44 pre-diluted GolgiPlug (BD, 555029) were added per well, cultures were resuspended by pipetting up and down, the plate was spun for 1 min at 10 g and placed back into a 37°C CO_2 incubator. GolgiStop and GolgiPlug both inhibit protein transport, thereby preventing TNFα from secretion. After four additional hours of co-culture, cells were placed on ice and stained for flow cytometric analysis. Cells were stained with viability dye (AF700, eBioscience), Fc-receptors were blocked, and FACS antibodies (CD4 (clone SK3=Leu3a, BV786, BD), CD8a (clone RPA-T8, PerCP-Cy5.5, BD), mTCRβ (clone H57-597, PE, BioLegend)) were used for extracellular staining. Cells were fixed as described before and intracellularly stained with TNFα (clone Mab11, BV711, BioLegend). Flow cytometric data was acquisitioned on a BD FACS Lyric device.

2.21 TCRβ deep sequencing

DNA from tissue, blood or FFPE tissue was isolated as described before. Libraries were prepared using the hsTCRB Kit V4b (Adaptive Biotechnologies) according to the manufacturer's protocol by the Immune Monitoring Unit (DKFZ Heidelberg, Germany) and sequenced on an Illumine MiSeq device. Sequencing was performed by the Genomics & Proteomics Core Facility (DKFZ Heidelberg, Germany).

Data was processed using the immunoSEQ platform from Adaptive Biotechnologies, and data was analyzed using the immunarch package (Nazarov V, Tsvetkov V, Fiadziushchanka S, Rumynskiy E, Popov A, Balashov I, Samokhina M (2023). *immunarch: Bioinformatics Analysis of T-Cell and B-Cell Immune Repertoires*. https://immunarch.com/, https://github.com/immunomind/immunarch) in RStudio.

2.22 IFNγ ELISpot

ELISpots were used to quantify the number of IFNγ secreting T cells. White-bottom ELISpot HTS plates (Millipore, MSIPS4W10) were coated with anti-IFNγ antibody by hydrophilizing the membrane with 30 µL of 35% EtOH for 1 min. The plate was immediately washed five times using 150 µL autoclaved distilled H_2O, respectively. A total of 100 µL human anti-human IFNγ antibody (clone 1-D1K, Mabtech, 3420-3-1000) at a concentration of 15 µg/mL in PBS was added per well and incubated overnight at 4°C. ELISpot plates were blocked with X-Vivo20 supplemented with 1% BSA after washing the plate five times with PBS using a Vaccu-Pette. After 1 h of blocking, the plate was washed once more using X-Vivo20. To prevent the plate from drying out, 20 µL of X-Vivo20 were added per well.

Peptides used for re-stimulation were diluted in X-Vivo20 and plated for restimulation at a concentration of 10 µg/mL (for MOG, IDH1-wildtype, IDH1R132H). PMA/ionomycin (4 ng/0.2 µg), staphylococcal enterotoxin B (SEB) (1 µg; Sigma, S4881-1MG-PW) or Cytomegalovirus (CMV) (0.05 µg; PepTivator CMV pp65, Miltenyi, 130-093-435) with adenovirus (AdV) (0.05 µg; PepTivator AdV5 Hexagon premium grade, Miltenyi, 130-093-496) were used as positive controls. Wells without peptide were used as negative controls to monitor background activation of T cells.

If PBMCs were used for ELISpot, cells were thawed as described before and rested overnight in X-Vivo20 using 50 mL Falcon Tubes with slightly twisted open lids. Post-ESPEC samples were harvested one day before ELISpot and rested overnight in X-Vivo20 supplemented with 2% AB serum but without cytokines. Cells were counted using trypan blue and $3*10^5$ PBMCs or $2.5*10^4$-$2.5*10^5$ ESPEC-derived cells were loaded per well in triplicates, or in duplicates if cell numbers were limited. After 40 hours, IFNγ-secreting cells were detected after repeated washing cycles using a Vaccu-Pette: first, the plate was washed five times with PBS, incubated for one minute with distilled H_2O to lyse remaining cells and to reduce assay background, then washed again five times with PBS before adding 100 µL of 1:1000 diluted filtrated (0.22 µm polyvinylidene fluoride (PVDF) membrane; Merck, SLGV0033RS) biotinylated anti-IFNγ biotin antibody (clone 7-B6-1, Mabtech, 3420-6-1000) per well. After 2 h of incubation at RT, plates were washed five times with PBS and 100 µL of 1:1000 diluted streptavidin-ALP (Mabtech, 3310-8-1000) were added per well. After 1.5 h of incubation at RT, plates were again washed five times with PBS. AP conjugate substrate solution (Bio-Rad, 1706432) was prepared according to the manufacturer's recommendations and filtrated using a 0.45 µm filter (mixed cellulose esters (MCE) membrane; Merck, SLHAR33SS). Substrate was removed as soon as spots became visible and after a maximum of 40 min, and plates were immediately washed five times using H_2O. After 3 min of incubation with H_2O, residual water was removed and the plate was dried while wrapped in tissue. IFNγ spot counts were quantified using an ImmunoSpot Analyzer (ImmunoSpot/CTL Europe).

If peptide-pulsed DCs and CD4+ or CD8+ T cell subsets were co-cultured in ELISpot, immature DCs were prepared and harvested as described before. A total of 15,000 DCs were plated per well of a coated and blocked ELISpot plate and pulsed with either MOG peptide (2 µg), IDH1-wt (2 µg), IDHR132H (2 µg), CEF pool (0.1 µg; jpt, PM-CEF-S-3) as a positive control for MHC I stimulation, or CEFX Ultra SubSet MHC II (PM-CEFX-3) (0.1 µg; jpt, PM-CEFT-S-3) as a positive control for MHC II-restricted antigen responses in 50 µL volume. PBMCs were thawed and rested in X-Vivo20 as described before. The next day, CD4+ and CD8+ cells were negatively enriched using magnetic bead-based kits (CD4+ enrichment: Miltenyi, 130-096-533; CD8+ enrichment: Miltenyi, 130-096-495) according to the manufacturers

protocol. Purity of CD4 positive and CD8 positive enriched populations was analyzed using flow cytometry (viability dye (AF700, eBioscience), CD3 (clone HIT3A, BV510, BD), CD4 (clone SK3=Leu3a, BV786, BD), CD8a (clone RPA-T8, PerCP-Cy5.5, BD)). 75,000 T cells were loaded per well. SEB (1 µg) was used as a positive control. Total culture volume in all wells was 200 µL. ELISpots were stopped after 40 h and analyzed as described before.

2.23 Mass spectrometry of peptide-pulsed B-LCLs

B-LCLs were expanded to have between 2.5-4*10^7 cells available per condition. Cells were pulsed with 20-mer IDH1R132H or 20-mer IDH1-wildtype peptides (p123-142, GWVKPIIIGHHAYGDQYRAT and GWVKPIIIGRHAYGDQYRAT) at a concentration of 10^{-5} M. After 22-24 h at 37°C, cells were incubated for 1 h in peptide-free media in a 37°C CO_2 incubator, washed twice with PBS, and a pellet was frozen at -80°C for later mass spectrometry analysis by Jonas Becker (DKFZ Heidelberg, Germany).

Immunoprecipitation of HLA class I:peptide complexes was performed as previously described (Chong et al. 2018). Lyophilized peptides were dissolved in 12 µl of 5% ACN in 0.1% TFA and spiked with 100 fmol Peptide Retention Time Calibration (PRTC) Mixture (Pierce) and transferred to QuanRecovery Vials with MaxPeak HPS (Waters). All samples were analyzed using an UltiMate 3000 RSLCnano system coupled to an Orbitrap Exploris 480 equipped with a FAIMS Pro Interface (Thermo Fisher Scientific). For chromatographic separation, peptides were first loaded onto a trapping cartridge (Acclaim PepMap 100 C18 µ-Precolumn, 5µm, 300 µm i.d. x 5 mm, 100 Å; Thermo Fisher Scientific) and then eluted and separated using a nanoEase M/Z Peptide BEH C18 130A 1.7µm, 75µm x 200mm (Waters). Total analysis time was 120 min and separation were performed using a flow rate of 0.3 µl/min with a gradient starting from 1% solvent B (100% ACN, 0.1% TFA) and 99% solvent A (0.1% FA in H2O) for 0.5 min. Concentration of solvent B was increased to 2.5% in 12.5 min, to 28.6% in 87 min and then to 38.7% in 1.4 min. Subsequently, concentration of solvent B was increased to 80% in 2.6 min and kept at 80% solvent B for 5 min for washing. Finally, the column was re-equilibrated at 1% solvent B for 11 min. The LC system was coupled on-line to the mass spectrometer using a Nanospray-Flex ion source (Thermo Fisher Scientific), a SimpleLink Uno liquid junction (FossilIonTech) and a CoAnn ESI Emitter (Fused Silica 20 µm ID, 365 µm OD with orifice ID 10 µm; CoAnn Technologies). The mass spectrometer was operated in positive mode and a spray voltage of 2500 V was applied for ionization with an ion transfer tube temperature of 300 °C. For ion mobility separation, the FAIMS module was operated with standard resolution and a total carrier gas flow of 4.6 l/min. Each sample was injected twice using either a compensation voltage of -50 V or -70 V for maximal orthogonality and thus increased immunopeptidome coverage. Full Scan MS spectra were acquired for a range of 300 – 1650 m/z with a resolution of 120.000 (RF Lens 50%, AGC Target 300%). MS/MS spectra were acquired in data-independent mode for a cycle time of 3s using 40 previously determined dynamic mass windows optimized for HLA class I peptides with an overlap of 0.5 m/z. HCD collision energy was set to 28% and MS/MS spectra were recorded with a resolution of 30000 (normalized AGC target 3000%).

MS raw data was analyzed using Spectronaut software (version 17; Biognosys (Bruderer et al. 2015)) and searched against the UniProtKB/Swiss-Prot database (retrieved: 21.10.2021, 20387 entries) supplemented with an entry for the IDH1 protein with R132H mutation. Search parameters were set to non-specific digestion and a peptide length of 7 -15 amino acids. Carbamidomethylation of cysteine and oxidation of methionine were included as fixed modifications. Results were reported with 1% FDR at the peptide level. Peptides identified by Spectronaut were further analyzed using NetMHCpan 4.1 binding predictions (Reynisson et al. 2020), Gibbs 2.0 clustering of peptide sequences (Andreatta, Alvarez, and Nielsen 2017), and retention time prediction by DeepLC (Bouwmeester et al. 2021). IDH1-

derived peptide sequences were manually validated using Skyline (version 22 (Pino et al. 2020)). Additionally, spectral libraries were in silico generated using PROSIT (Gessulat et al. 2019) and all possible binders (8 – 14mers) derived from the pulsed peptides were manually searched using Skyline.

2.24 Data visualization

Data was visualized using GraphPad Prism (GraphPad Software, San Diego, California USA, http://www.graphpad.com/), BioRender (http://www.BioRender.com/), or RStudio (RStudio Team, 2021. *RStudio: Integrated Development Environment for R*, Boston, MA. Available at: http://www.rstudio.com/.).

2.25 Materials

Table 1. Antibodies for flow cytometry.

Marker	Fluorophore	Clone	Company	Reference number
CD107a	APC-H7	H4A3	BD	561343
CD11b	BB515	ICRF44	BD	564517
CD235a	APC	HI264	BioLegend	349113
CD3	BV510	HIT3A	BD	564713
CD3	APC	HIT3A	BD	561804
CD31	APC	WM59	BioLegend	303115
CD34	PE	563	BD	550761
CD4	BV786	SK3=Leu3a	BD	563877
CD4	APC	SK3=Leu3a	BD	566915
CD45	APC-H7	2D1	BD	560178
CD45	FITC	2D1	BD	345808
CD69	APC	FN50	BD	555533
CD8a	PerCP-Cy5.5	RPA-T8	Invitrogen	45-0088-42
HLA-ABC	APC	W6/32	ThermoFisher	17-9983-42
HLA-DP	PE	B7/21	BD	566825
HLA-DQ	BV421	Tu169	BD	564808
HLA-DQ	FITC	Tu169	BD	555563
HLA-DR	PerCP-eF710	L243	ThermoFisher	46-9952-42
HLA-DR	BV711	L243	BioLegend	307644
HLA-DR	PE	L243	BioLegend	307606
mTCR-beta	PE	H57-597	BioLegend	109208
TNF-alpha	BV711	MAb11	BioLegend	502940

Table 2. Live/dead marker for flow cytometry. DCM= dead cell marker.

Marker	Fluorophore	Clone	Company	Reference number
DCM	AF700	n.a.	eBioscience	65-0866-14

Table 3. Antibodies for cell surface barcoding.

Antibody	Barcode sequence	Clone	Company	Reference number
TotalSeq-C0251	GTCAACTCTTTAGCG	LNH-94; 2M2	BioLegend	394661
TotalSeq-C0252	TGATGGCCTATTGGG	LNH-94; 2M2	BioLegend	394663
TotalSeq-C0253	TTCCGCCTCTCTTTG	LNH-94; 2M2	BioLegend	394665
CiteSeq - CD4	TGTTCCCGCTCAACT	RPA-T4	BioLegend	300567
CiteSeq - CD8	GCGCAACTTGATGAT	SK1	BioLegend	344753

Table 4. Primer sequences.

Primer name	Primer sequence
pSMARTer_EF1a_seqF_v2	TAAGTGCAGTAGTCGCCGTG
pSMARTer_apoB_seqR_v2	TGGTGTCTTCATGTGCCACA
MmTRAC_co mRNA rev	TCAGCTGGACCACAGTCTCAGG
T7 EF1a F	TAATACGACTCACTATAGGGACAGAACACAGGCCACCATG
Primer_F	TACAGAGTAATACGACTCACTATAGG
Primer_R	CTTGGGAGGTGTCTGGAAC

Table 5. Cell culture media.

Name	Ingredient	Supplier and ordering number
MeWo growth media	MEM 10% FBS 100 IU/mL Penicillin, 100 µg/mL Streptomycin	Life Technologies, 11095080 Merck, S0615-500ML Life Technologies, 15140122
BT21 and JURKAT growth media	RPMI1640 10% FBS 100 IU/mL Penicillin, 100 µg/mL Streptomycin	Sigma, R8758-500ML Merck, S0615-500ML Life Technologies, 15140122
TIL expansion media	X-Vivo15 2% HSA 2.5 µg/mL Fungizone 20 µg/mL Gentamicin 100 IU/mL Penicillin, 100 µg/mL Streptomycin	Lonza, BE02-060Q Behring, CH.-B.: P100245582 Gibco, 15290-018 Roth, 2475.1 Life Technologies, 15140122
REP media	X-Vivo15 2% Human AB serum 2.5 µg/mL Fungizone 20 µg/mL Gentamicin 100 IU/mL Penicillin, 100 µg/mL Streptomycin	Lonza, BE02-060Q Sigma Aldrich, H4522-100ML Gibco, 15290-018 Roth, 2475.1 Life Technologies, 15140122

Tumor growth media	DMEM/F12 (15 mM HEPES, L-Glutamin)	Thermo Fisher Scientific, 11554546
	100 IU/mL Penicillin, 100 µg/mL Streptomycin	Life Technologies, 15140122
	1x B-27 supplement	Thermo Fisher Scientific, 17404044
	20 ng/mL epidermal growth factor (EGF)	R&D Systems, 236-EG-200
	20 ng/mL fibroblast growth factor (FGF)	Thermo Fisher Scientific, PHG0021
B-LCLs growth media	RPMI 1640 Medium, GlutaMAX™ Supplement	Thermo Fisher Scientific, 61870044
	10% FBS	Merck, S0615-500ML
	100 IU/mL Penicillin, 100 µg/mL Streptomycin	Life Technologies, 15140122
	0.1 mg/mL Kanamycin Sulfate	Thermo Fisher Scientific, 15160047
	1 mM Sodium Pyruvate	Thermo Fisher Scientific, 11360039
	0.1 mg/mL MEM non-essential amino acid solution NEAA	Thermo Fisher Scientific, 11140035
	55 µM 2-Mercapthoethanol	Thermo Fisher Scientific, 21985023
B95-8 growth media	RPMI 1640 Medium, GlutaMAX™ Supplement	Thermo Fisher Scientific, 61870044
	10% FBS	Merck, S0615-500ML
	100 IU/mL Penicillin, 100 µg/mL Streptomycin	Life Technologies, 15140122

Table 6. List of peptides used for IDH1R132H screening. Aliquots were discarded after thawing them once. MOG=myelin oligodendrocyte glycoprotein. Note that peptides used for screening patients of the TCR-POC cohort are listed in the supplementary.

Peptide	**Sequence**
MOG (p35-55)	MEVGWYRSPFSRVVHLYRNGK
Flu (Influenza HA) (p306-318)	PKYVKQNTLKLAT
IDH1-wildtype (p123-142)	GWVKPIIIGRHAYGDQYRAT
IDH1R132H (p123-142)	GWVKPIIIGHHAYGDQYRAT
IDH1R132H (p126-134)	KPIIIGHHA

3. Results

3.1 Establishment of methods for TCR selection

TCR-engineered T cell therapy is a type of anti-tumor therapy, in which patient-autologous T cells are modified to express tumor-reactive T cell receptors of interest. TCRs selected for therapy have to be able to recognize tumor neoepitopes presented to the immune system via HLA alleles expressed on the patient's tumor cells. Identification of reactive TCRs is not only relevant for TCR-engineered T cell therapy, but also to gain a better understanding of treatment-induced anti-tumor T cell responses in patients by longitudinal and spatial tracking of reactive TCRs in peripheral blood and tissue, for example after application of anti-tumor vaccinations. To be able to screen for and characterize tumor-reactive patient-derived TCRs with a high success rate, it is crucial to define suitable methods for pre-selecting promising TCRs for cloning and testing. In this thesis, two TCR selection approaches were established, the first requiring information on the epitope-of-interest to be able to run peptide-based expansion cultures, and a second antigen-agnostic approach based on bioinformatic analysis of TIL (tumor infiltrating lymphocytes, in the following referring to T cells only) gene expression profiles (**Figure 3A**).

The first method uses epitope specific expansion cultures (ESPEC) with subsequent identification of TCRs (SUIT) to amplify T cell responses against the antigen-of-interest. This in vitro approach is based on culture of autologous cells with shared or private neoepitopes specific for individual patients and was developed to identify tumor-reactive TCRs from patient blood samples. In short, PBMCs are stimulated with the peptide-of-interest for 13 days and the expansion of antigen-reactive cells as compared to unstimulated cultures and baseline frequencies is assessed by TCR repertoire analysis (TCRβ bulk sequencing). TCRs of clones with strong expansion under mutated peptide as compared to the baseline PBMC sample and with low expansion in the no peptide control are selected for cloning and testing. Clones which strongly expand in the no peptide control are regarded as non-specific expanders, which are highly responsive to the cytokines added to the expansion culture. To obtain information on the correct alpha-beta chain pairing necessary for TCR cloning, single cell V(D)J sequencing is employed.

Where applicable, cultures with wild-type variants of the antigen-of-interest can be performed in parallel. As a quality control step, expansion of relevant T cell clones can be verified prior to sequencing by using functional assays to quantify cytokine-release after restimulation of expansion cultures with antigen-of-interest and controls. Such assays can be either ELISpot or intracellular cytokine staining with subsequent flow cytometry. Depending on the epitope, enrichment of CD4+ or CD8+ T cell subsets is performed prior to repertoire sequencing to gain deeper insights to the relevant TCR repertoire.

The assay was successfully applied in patients that received an anti-tumor peptide vaccination against shared neoepitopes (n=15 patients, n=7 representative datasets shown in this thesis) or private neoepitopes (n=2 patients) (see chapters 3.2 and 3.3), but also using PBMCs of one patient that did not receive any vaccination against private neoepitopes and thus likely had lower baseline frequencies of relevant clones (see chapter 3.3). Eleven post-ESPEC datasets of ten representative patients are described in this thesis, which were used as a basis to select and screen a total of 155 TCRs for reactivity with an overall success rate of 89% (range 57-100%) for clones selected on this basis. This protocol allowed for successful expansion of both CD4+ and CD8+ T cell responses. Moreover, TILs can be efficiently expanded with a slightly modified ESPEC protocol, using lower cell numbers and DCs as antigen presenting cells (not shown). In addition, expansion cultures utilizing peptide-pools instead of individual peptides expanded relevant clones reactive to individual peptides contained within the pools (see chapter 3.3).

In a second approach to identify tumor-reactive TCRs, gene signature characterizing reactive T cells in the TIL compartment can be used. As previously demonstrated by others for various tumor entities,

such as lung cancer, melanoma or gastrointestinal cancers, tumor-reactive T cells show differential gene expression patterns compared to non-reactive bystander cells (Caushi et al. 2021; Hanada et al. 2022; Oliveira et al. 2021; Veatch et al. 2022; Zheng et al. 2022; Lowery et al. 2022). Chin Leng Tan (DKFZ Heidelberg, Germany) is working on developing a gene signature for identification of reactive T cell clones in brain tumor samples using single cell sequencing datasets. I contributed to the project by processing brain tumor tissue samples, preparing single cell sequencing data and by testing TCRs for reactivity (see chapter 3.4). In this thesis, I will describe TCR reactivity data for patient BT21, for which I processed a brain tumor melanoma metastasis tissue sample and successfully validated reactivity of 46 TCRs in an in vitro co-culture assay using an autologous tumor cell line.

3.2 Methods for TCR testing

To assess TCR reactivity, two co-culture assays were developed, one using expanded PBMCs and the second assay using a JURKAT-reporter cell line as effector cells (see Materials and Methods, chapter 2.19 and 2.20). Reactivity of expanded PBMCs was assessed by quantifying CD107a and TNFα by flow cytometry. Expression of both markers correlated well when testing TCRs derived from either CD4+ or CD8+ clones, irrespective of the PBMC donor (**Figure 3C**). Furthermore, a low background signal in TNFα and CD107a in the unstimulated condition allowed for detection of slight changes of signal in the stimulated culture-of-interest and therefore identification of TCRs with lower degree of reactivity (**Figure 3D**). Gating on mTCRβ+ cells further enhanced sensitivity for TCRs with low cell surface expression levels and moreover served as normalization to allow for comparison of cytokine secretion between TCRs with either low or high mTCRβ expression.

Two JURKAT-reporter cell lines, JURKAT-TPR-CD8ab and JURKAT-NF-κB eGFP, were obtained from the laboratory of Peter Steinberger and characterized with the aim to select a sensitive screening tool for medium throughout in vitro co-culture assays for testing the reactivity of candidate TCRs (Jutz et al. 2017; Jutz et al. 2016). Both lines are engineered to express fluorescent proteins after TCR activation, which can be either quantified via flow cytometry or plate-based fluorescence detection, the latter increasing TCR screening throughput and reducing costs compared to FACS-based readouts (**Figure 3B**). Both JURKAT lines showed low CD4 co-receptor expression compared to PBMCs, with 44% positive cells for the NF-κB eGFP cell line and 6% positive cells among TPR-CD8ab cells. CD8 expression was either absent (NF-κB eGFP) or present on only 4% of cells (TPR-CD8ab), even though the latter cell line was transduced to overexpress CD8 (**Figure 3E**). Moreover, JURKAT-NF-κB eGFP suffers from high basal background fluorophore expression despite absence of CD69 upregulation (19% GFP positive cells, **Figure 3F**), and JURKAT-TPR-CD8ab from low fluorescence brightness after stimulation and therefore lower sensitivity (**Figure 3G**). As the overall sensitivity and CD4 expression levels of the NF-κB eGFP cell line was higher, this line was selected for co-culture assays of CD4 derived TCRs using with peptide-pulsed DCs or B-LCLs as antigen presenters.

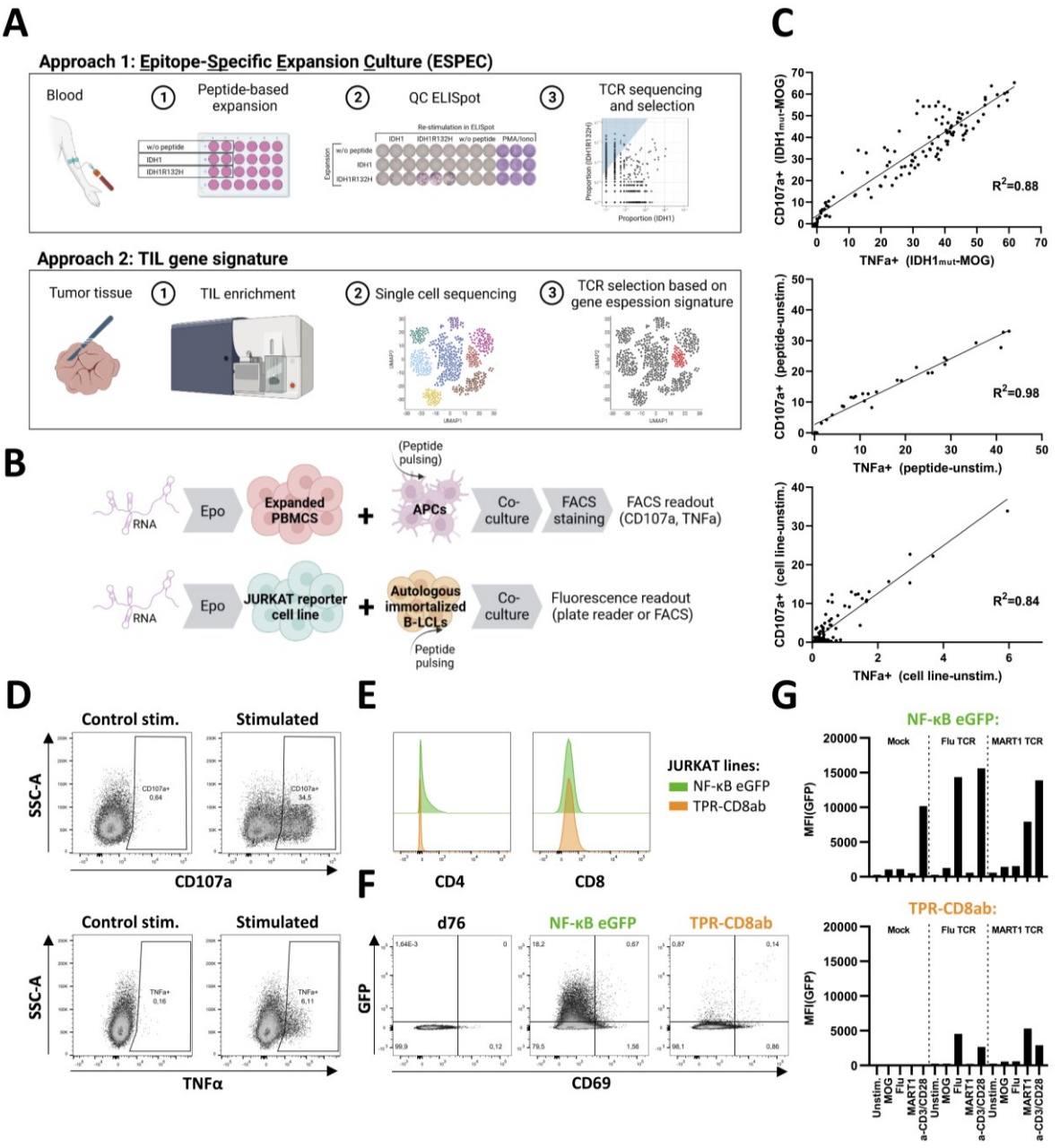

Figure 3. Methodology used to screen for reactive TCRs. A) Schematic overview of two approaches used for pre-selecting TCRs for cloning and testing in the scope of this thesis: ESPEC-SUIT or TIL gene expression signatures. **B)** To validate selected TCRs, TCR-encoding RNA was electroporated into expanded PBMCs or into JURKAT-reporter cell lines. TCR reactivity in expanded PBMCs was assessed by quantifying CD107a and TNFα secretion using flow cytometry. JURKAT reporter cell lines express fluorescent proteins upon TCR stimulation and activation of response elements. Fluorescence can be either quantified by flow cytometry or using a plate reader. **C)** CD107a and TNFα levels after co-culture of individual TCRs with APCs, gating on viable mTCRβ+ cells. From top to bottom: IDH1R132H CD4-derived TCRs (see chapter 3.2), TCR-POC-001 CD4-derived TCRs (see chapter 3.3), BT21 CD8-derived TCRs (only one CD4-derived TCR) (see chapter 3.4). In each plot, a different PBMC donor was used for co-culture. Signals per TCR are normalized by subtracting the respective background signal after co-culture with DCs pulsed with MOG peptide (top), B-LCLs without peptide (middle), or T cells that were used in a co-culture assay without APCs (bottom). **D)** Flow cytometric data of CD107a and TNFα expression in expanded PBMCs after electroporation with an IDH1R132H-reactive TCR and co-cultivation with (I) MOG peptide-pulsed DCs ("control stim.") or (II) IDH1R132H-pulsed DCs ("stimulated"). **E)** Quantification of CD4 and CD8 co-receptor expression of JURKAT reporter cell lines. Neither cell line was positive for CD8 (only 4% CD8+ cells for TPR-CD8ab), but both expressed CD4 to a varying degree (44% NF-κB eGFP, 6% TPR-CD8ab). **F)** Background fluorophore expression of JURKAT reporter cell lines without stimulation in co-culture but two days after mock electroporation. Quantification of CD69 as activation marker and of GFP expression using flow cytometry. **G)** Analysis of the MFI of GFP amongst viable cells of the NF-κB eGFP and TPR-CD8ab JURKAT reporter cell lines after 18 h of co-culture with peptide-pulsed DCs (1:10 ratio). JURKAT cell lines were electroporated as (I) mock control, with (II) Flu TCR (41%/64% mTCRβ+) and with (III) MART1 TCR (44%/45% mTCRβ+) SMAR DNA two days before co-culture (% for NF-κB eGFP / TPR-CD8ab, respectively, measured on day of co-culture).

For co-culture assays with tumor cells, expanded PBMC were used as effector cells instead, in an effort to compensate for lower antigen levels presented on these non-professional APCs. Tumor cells express lower amounts of MHC I and II molecules on their surface as compared to professional APCs (Wickstrom et al. 2019), frequently exhibit loss of MHC I and/or lack of MHC II expression (Axelrod et al. 2019; Shklovskaya and Rizos 2021), and likely present less amounts of individual antigens as compared to APCs pulsed with supraphysiological amounts of peptide, a result of the large number of possible antigens being processed and presented per cell.

3.3 IDH1 TCR discovery

Around three quarter of all WHO grade II/III diffuse glioma cases carry the IDH1R132H mutation (Platten et al. 2021). TCR-engineered T cell therapy is an attractive therapeutic option for these patients due to homogenous expression of the mutation within tumor tissue (Schumacher, Bunse, Wick, et al. 2014), but its applicability is currently limited by the fact that screening for reactive TCRs and subsequent production of virus or plasmids for T cell engineering is a time-consuming task. To be able to rapidly offer patients with IDH1R132H-mutant gliomas off-the-shelf transgenic T cell therapies, a TCR warehouse of well characterized IDH1R132H-reactive TCRs was established. As it was previously shown that IDH1R132H induces CD4+ T_H1 T cell mediated immunity, it was decided to focus on the CD4 T cell subset when screening for reactive TCRs (Schumacher, Bunse, Pusch, et al. 2014; Bunse et al. 2018). TCRs were selected using ESPEC-SUIT from PBMCs of patients that received a long IDH1R132H peptide vaccine with or without PD-L1 inhibitor avelumab (**Table 7**).

Table 7. List of patients included into the TCR screening campaign for CD4-derived IDH1R132H-reactive TCRs. In total, 123 TCRs were selected for testing. n.a.=not applicable, patients received the treatment on a compassionate use basis. VAC= peptide vaccination with IDH1R132H (p123-142); AVE = avelumab treatment; EOT= end of treatment.

Patient ID	Trial	Treatment	Visit used for ESPEC	Number of vaccinations before ESPEC	Number of TCRs selected by FEST	Number of TCRs selected for testing
ID1	NOA21	VAC + AVE	V7/EOT	3	120	25
ID2	NOA21	VAC	V6	2	115	28
ID3	NOA21	VAC + AVE	EOT	2	41	15
ID4	n.a.	VAC + AVE	V9	5	19	15
ID5	n.a.	VAC + AVE	V7	3	51	17
ID6	NOA16	VAC	V10	7	21	16
ID7	NOA16	VAC	V10	7	8	7

As PBMCs from several timepoints after vaccination were available per patient, samples for ESPEC-SUIT were selected based on ELISpot results showing high IDH1R132H response with low background signal for the IDH1-wildtype or MOG condition. Mean spot counts of PBMCS from visits selected for ESPEC were 103/100,000 (range 27-261 per 100,000 PBMCs) in ELISpot after IDH1R132H re-stimulation, whereas spot-counts after IDH1-wildtype re-stimulation were consistently lower (mean 51/100,000 PBMCs, range 9-129 per 100,000 PBMCs) (representative ELISpot data in Figure 4**A**). Post-ESPEC QC ELISpots revealed a strong enrichment of IDH1R132H specific T cell responses in all 12 assays upon IDH1R132H restimulation, with no spots observed in the unstimulated control cultures due to absence of IDH1R132H reactivity (n=12 assays, 25,000 cells/well). Reactivity to mutant IDH1 was frequently observed in both IDH1R132H and IDH1-wildtype stimulated cultures, but with the IDHR132H response in all cases strongly exceeding the IDH1-wildtype response (**Figure 4B**). Flow

cytometric analysis of post-ESPEC populations of patient ID2 showed that CD3+ T cells expanded and made up 55-92% of the expansion cultures, in which the overall fraction of CD4+ clones increased from 13% in the no peptide control to 53% after ESPEC with IDH1R132H-peptide. CD4+ T cells were further enriched by FACS sorting or by magnetic bead-based enrichment prior to TCRβ deep sequencing (**Figure 4C**). The FEST algorithm (Danilova et al. 2018) was used to select candidate TCRs for TCR cloning and testing (**Figure 4D**). After sorting the FEST output by frequency after expansion under IDH1R132H, the top TCRβ chains were selected for cloning. If clones showed a stronger expansion under IDH1-wildtype peptide as compared to IDH1R132H peptide, they were omitted from testing, as they were initially suspected to be non-specific expanders. A total of 123 representative TCRs were selected for testing (**Table 7**).

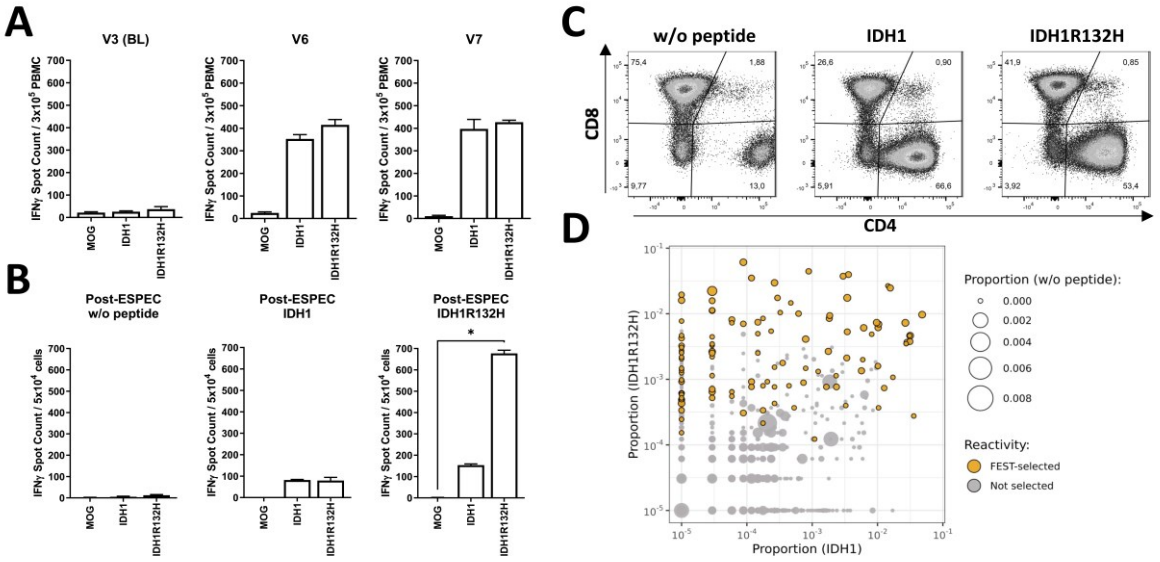

Figure 4. ESPEC workflow for pre-selection of putative IDH1R132H-reactive TCRs. A) Exemplary longitudinal ELISpot data of PBMCs isolated from patient ID2 at BL (V3), V6 and V7, after receiving three doses of IDH1R132H vaccination. 300,000 PBMCs/well. BL=baseline, V=visit. **B)** Post-ESPEC QC IFNγ ELISpot of patient ID2. PBMCs from V6 were selected for ESPEC and expanded against (I) no peptide, (II) the long IDH1 peptide, and (III) the long IDH1R132H peptide before restimulation. 25,000 cells/well. **C)** Determination of the fraction of CD4+ and CD8+ T cell subsets post-ESPEC. Gating on viable CD3+ cells. The overall fraction of CD3+ cells was 55/83/92% after expansion without (w/o) peptide, IDH1 or IDH1R132H, respectively. **D)** Bubble plot of TCRβ deep sequencing data depicting the frequency of individual TCRβ chains in post-ESPEC cultures for patient ID2 after CD4+ enrichment. Clones interesting for cloning based on output of the FEST-algorithm (Danilova et al. 2018) are highlighted in orange (n=115).

3.3.1 TCR warehouse of CD4-derived IDH1R132H reactive TCRs

In total, 123 TCRs from seven patients were selected for testing based on post-ESPEC TCRβ deep sequencing data. As alternative alpha-beta pairings were found in single cell sequencing data of either TIL or post-ESPEC cultures for a total of 23 selected TCRβ chains, two constructs with alternative alpha chains were cloned for each of these, making a total of 146 constructs available for testing. TCR-encoding RNA was electroporated into expanded PBMCs and used in co-culture assays with peptide-pulsed autologous DCs, or in the case of patient ID6 and ID7 with limited PBMC availability, against peptide-pulsed autologous expanded PBMCs as APCs. Each TCR was tested against APCs pulsed overnight with (I) MOG peptide as a negative control, (II) IDH1 20-mer wildtype peptide, (III) IDH1R132H 20-mer peptide, and (IV) anti-CD3/CD28 beads as positive control. Only TCRs with more than 2% mTCRβ expression were included in further analysis (n=143).

To classify TCRs as reactive or non-reactive, expression of CD107a and TNFα in mTCRβ+ cells was normalized by subtracting the signal measured after co-culture with MOG-pulsed DCs from the signal measured after co-culture with IDH1R132H peptide. The standard deviation (SD) of TNFα and CD107a positive cells after co-culture with MOG peptide (negative control) was determined for all TCRs of a given patient (SD range in individual patients: 0.07-2.98% (TNFα), 0.1-2.06% (CD107a)) and TCRs were classified as reactive, if the normalized percentage of both TNFα and CD107a positive cells was larger than two times the SD of the background of the respective marker for a given patient. If the threshold was not passed for either TNFα or CD107a, or neither of both markers, the TCR was classified as non-reactive. Reactive TCRs had a mean level of 27.8% TNFα (range 0.51-68.3%) and 30.7% CD107a (range 1.62-72%) after co-culture with IDH1R132H-pulsed DCs.

For n=23 TCRs, for which TCR-pairs with alternative alpha-beta pairings were ordered, either the non-reactive alternative alpha-beta pair or the alternative alpha-beta pair with lower read-counts in the single-cell sequencing data were excluded from further analysis. In total, 120 TCRs were available for final analysis, of which 106 TCRs (88%) showed reactivity against IDH1R132H.

Interestingly, 49 of the IDH1R132H-reactive TCRs also showed reactivity against the IDH1-wildtype peptide (**Figure 5, A and B**). Cross-reactivity of IDH1R132H reactive TCRs to IDH1 wildtype peptide was not expected, as no toxicities potentially associated with cross-reactivity were observed in patients. No strong differences in the number of IDH1-wildtype reactive TCRs amongst all reactive TCRs were observed depending on the treatments received by individual patients, with 35/68 (51%) TCRs for patients treated with the peptide vaccination and avelumab, or 22/38 (58%) TCRs for patients treated with only the long peptide vaccination) (**Figure 5C**). Also, no statistically significant differences in mTCRβ expression or expansion in ESPEC were observed between reactive and cross-reactive TCRs. Note that also no differences in mTCRβ expression can be observed in non-reactive TCRs (**Figure 5D**). As only 1/16 (6%) IDH1-wildtype reactive TCR was observed in reactive TCRs tested against expanded PBMCs (ID6 and ID7), but 48/90 (53%) in TCRs tested against DCs (ID1-ID5), it was suspected that supraphysiological levels of antigen presentation might be the cause for this observation (**Figure 5E**). DCs as professional antigen presenting cells likely carry higher amounts of MHC molecules on their surface as compared to expanded T cells, and exogenous loading with high amounts of peptide is expected to results in very high antigen density. A selection of cross-reactive TCRs was therefore tested in co-culture assays against DCs pulsed with decreasing amounts of IDH1-wildtype and IDH1R132H peptide. For non-cross-reactive TCRs, reactivity to the wildtype peptide cannot be observed at any of the indicated concentrations. While reactivity against IDH1R132H was observed at all concentrations for cross-reactive TCRs, reactivity against IDH1-wildtype peptide showed a dose-dependent decrease and was absent when dendritic cells were pulsed with 10^{-8} M peptide, supporting the hypothesis that observation of “cross-reactivity” is a result of high peptide concentrations in our in vitro assay system, with wildtype-reactive cells having an overall higher affinity (**Figure 5F**). TCRs for which reactivity against wildtype and mutant IDH1 peptide was observed are in the following referred to as high-affinity TCRs.

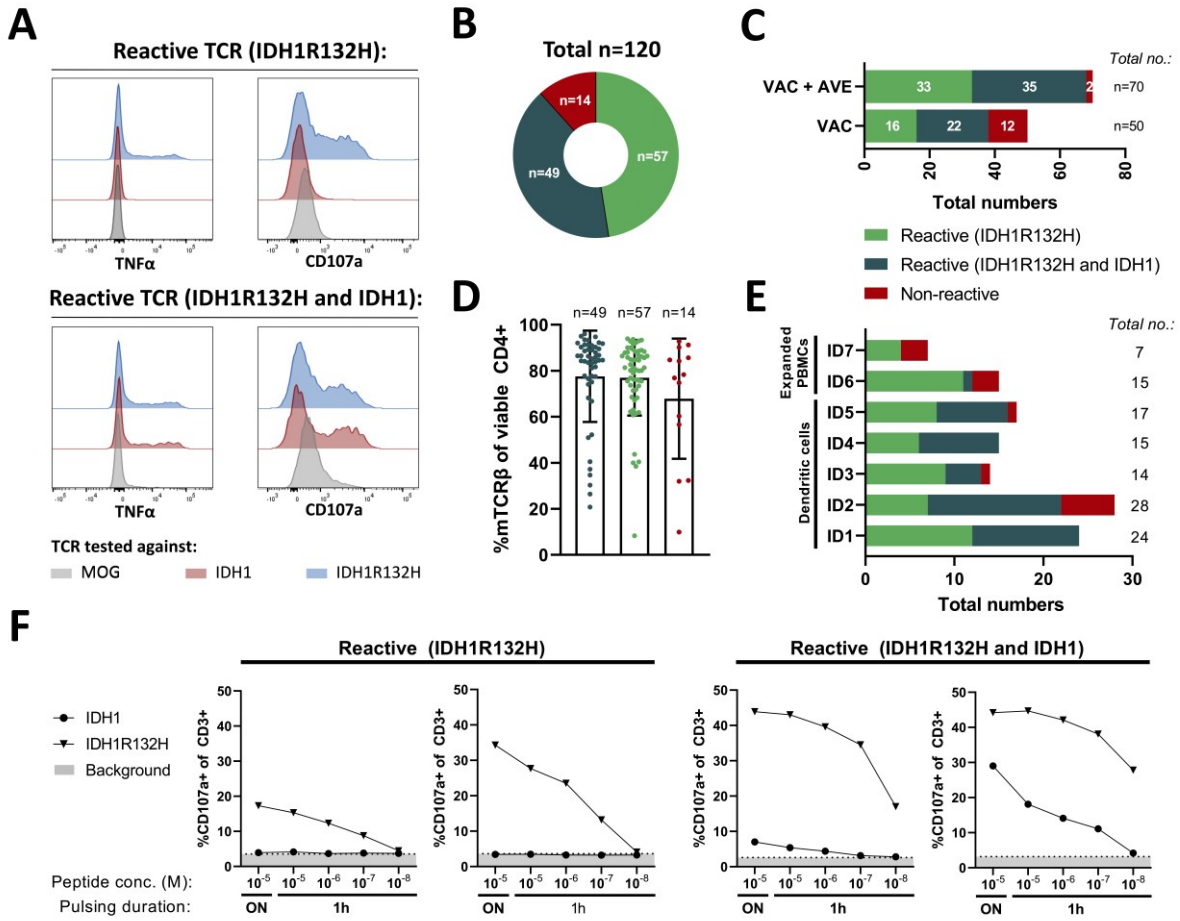

Figure 5. Warehouse of TCRs reactive against IDH1R132H and analysis of IDH1-wildtype reactivity. A) Flow cytometric data of TNFα and CD107a amongst mTCRβ+ cells for two exemplary IDH1R132H-reactive TCRs of patient ID1. TCR-encoding RNA was electroporated into expanded PBMCs, which were then co-cultured with peptide-pulsed DCs (MOG peptide, the 20-mer IDH1-wildtype peptide, or the 20-mer IDH1R132H peptide). **B)** Overall number of TCRs reactive to only IDH1R132H (47.5%), reactive to both mutant and wildtype IDH1 (40.8%), and non-reactive TCRs (11.7%). **C)** Number and reactivity of tested TCRs depending on the treatment received by individual patients. Patients were either treated with the long IDH1R132H peptide vaccine alone (VAC), or with a combination of the peptide vaccine and avelumab (VAC + AVE). **D)** Quantification of mTCRβ expression of TCRs reactive to both wildtype and mutant TCRs, TCRs reactive to only IDH1R132H, or TCRs classified as non-reactive. Three TCRs with mTCRβ expression levels below 2% were excluded from analysis and are not shown. **E)** Number and reactivity of tested TCRs per patient. The type of APC used for co-culture is annotated. **F)** Co-culture of TCRs from patient ID2 (TCR IDs from left to right: 96, 70, 68, 69) against DCs pulsed with decreasing concentrations of IDH1R132H or IDH1 peptide (10^{-5}-10^{-8} M) for one hour (h), or with 10^{-5} M of peptide overnight (ON). The latter peptide-pulsing condition was used to assess TCR reactivity in TCR testing co-culture assays when screening for reactive TCRs. Left: two TCRs with only reactivity to IDH1R132H. Right: two TCRs with reactivity to the mutated and wildtype IDH1 peptide. Background (grey): %CD107a+ cells after co-culture with MOG peptide at indicated concentrations.

3.3.2 Tracking of IDH1R132H reactive CD4-derived TCRs in blood and tissue

The availability of blood from different timepoints after vaccination allows for longitudinal tracking of the frequency of identified reactive TCR clones using TCRβ deep sequencing. For patients ID1-5, 78/90 (87%) of the identified reactive TCRs were absent in blood before they received their first dose of vaccination. Of the reactive TCRs found to be present at baseline, 11 had a low basal frequency of $2.9*10^{-4}$ - $3.9*10^{-3}$ % amongst all T cells in the periphery and only one was present at a relatively higher frequency of $4*10^{-2}$ % at baseline (ID1). This is also reflected in ELISpot data, in which IDH1R132H-responses cannot be detected in blood before onset of vaccination in patients of the NOA16 and NOA21 trial cohorts (data not shown; 300,000 PBMCs loaded per well; ELISpots were performed by

the Immune Monitoring Unit of the DKFZ). TCR frequencies increased strongly after the first vaccination doses and reached mean frequencies of $7.4*10^{-2}$ %, with maximum frequencies of up to 2.12% of the total peripheral T cell repertoire for a single TCR (ID5, Visit 7 (V7)) (**Figure 6A**). Cumulatively, identified reactive TCRs reached frequencies as high as 3.17% of the entire TCR repertoire per patient. However, note that the true cumulative frequency of IDH1R132H reactive TCRs per patient should be even higher as not all TCRs that could have been selected for testing based on the ESPEC output were cloned and tested.

The cumulative frequency of all tested reactive TCRs changed over time and did not follow a specific pattern between patients. For example, for patient ID4, cumulative frequencies of reactive TCRs first increased strongly and then decreased after V6, with the dynamics also being reflected in ELISpot data (**Figure 6**B and C, ELISpot data provided by the Immune Monitoring Unit of the DKFZ). Overall spot counts in ELISpot follow more or less the same dynamics as the cumulative frequency of TCRs tested to be reactive, indicating that TCRs included in the screening campaign are a good representation of the overall repertoire of IDH1R132H-reactive clones for these patients. The cumulative frequency of reactive TCRs in blood was not always highest at the timepoint selected for ESPEC, but was sometimes higher at other timepoints. This indicates that the assay does not only select for clones that are expanded at the timepoint selected for ESPEC, but that it also selects for clones expand at earlier or later timepoints. No statistically significant differences in fold-expansion between TCRs reactive to both mutated and wildtype or reactive to only IDH1R132H peptide in consecutive visits were observed (not shown).

The availability of single cell sequencing data of the TIL compartment for patients ID1-ID3 allowed quantification of the frequency of TCRs within on-trial tumor tissue after three doses of vaccination. The cumulative frequency of all identified reactive TCRs per patient from the same visit (V7) was consistently higher in tissue as compared to blood (**Figure 6D**). For two patients (ID6 and ID7), TCRβ deep sequencing datasets of tissue after pseudoprogression (PsPD) and after recurrence (rec.) were available, respectively. While none of the reactive TCRs were found within the recurrent tissue (34 weeks after first vaccination, no longer received vaccination when tumor was obtained), the pseudoprogressive tissue was infiltrated with IDH1R132H reactive TCRs (12 weeks after first vaccination, received IDH1R132H-vaccination at timepoint of surgery) (**Figure 6B**, bottom panel). The overall T cell infiltration was lower within the rec. tissue as compared to the one after PsPD, as observed for other patients (Ma et al. 2019). There is a strong overlap between clones expanded after ESPEC with the IDH1R132H peptide and clones found within PsPD tissue for patient ID6 (**Figure 6E**). Patient ID6 is still alive and has stable disease more than 80 months after diagnosis, whereas patient ID7 passed away 148 weeks after diagnosis (Platten et al. 2021).

For ID3, pre-vaccination FFPE tissue was available and used for TCRβ deep sequencing. One TCR that was later found to be IDH1R132H-reactive was observed at a frequency of 2.3% within this tissue sample 776 days before inclusion into the NOA21 trial and receiving a first vaccination dose with IDH1R132H peptide. The same TCR was absent in blood at baseline, where no ELISpot response against mutant IDH1 was detected. The clone expanded after onset of vaccination to a frequency of 0.034% in blood at visit 7 and further expanded strongly ex vivo in ESPEC to a frequency of 1.56% (**Figure 6F**). Interestingly, the clone was found at a lower frequency of 0.13% in TCRβ deep sequencing data of on-trial tumor tissue, showing that the intratumoral T cell repertoire is consistently subject to dynamic changes in TCR composition.

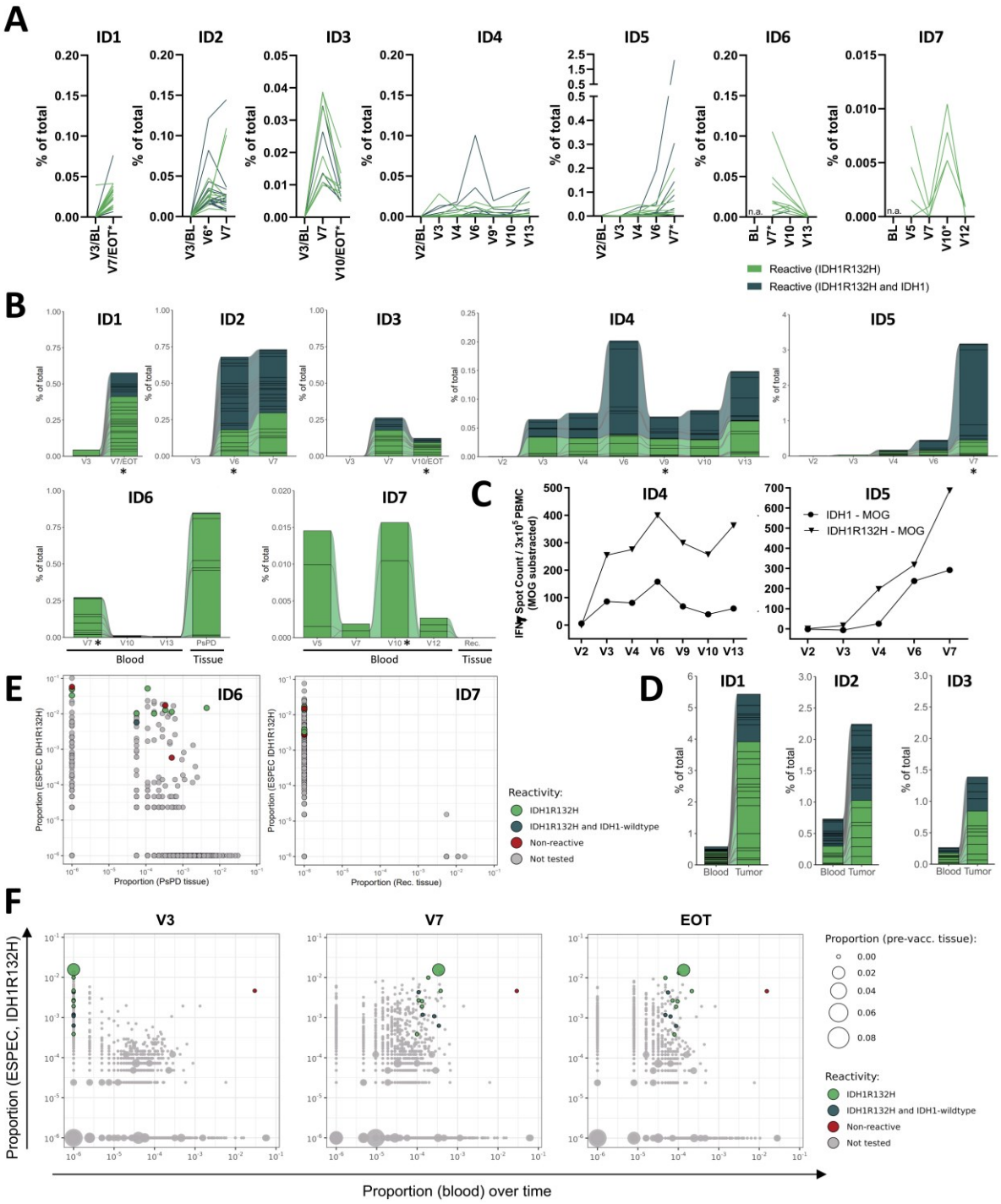

Figure 6. Tracking of IDH1R132H-reactive T cells in peripheral blood and tissue. A) Tracking of individual IDH1R132H-reactive TCRs in blood over time based on TCRβ deep sequencing data. Asterisks indicate which timepoint was used to set up ESPEC cultures for pre-selection of TCRs for cloning. (V=visit) **B)** Cumulative frequencies of TCRs tested to be reactive over time. Asterisks indicate the timepoint used to set up ESPEC cultures. **C)** IFNγ ELISpot data of PBMCS from different visits of patient ID4 and ID5. Spot counts after stimulation with MOG peptide were subtracted from spot counts after IDH1R132H and IDH1 stimulation. 300,000 PBMCs/well. **D)** Quantification of frequencies of reactive TCRs in blood (based on TCRβ deep sequencing data) and in tissue (TCRβ deep sequencing data for ID1 and ID3, and based on single cell V(D)J sequencing data for ID2). Blood and tissue were obtained at visit 7 after three doses of vaccination. **E)** Bubble plots of TCRβ deep sequencing data of patients ID6 and ID7 comparing frequencies after ESPEC with IDH1R132H peptide (ID6: V7, ID7: V10) and frequencies in tissue after PsPD (12 weeks after the first vaccination) or after recurrence (rec.) (34 weeks after the first vaccination). **F)** Bubble plots depicting the proportion of individual TCRβ chains of patient ID3 in post-ESPEC cultures with long IDH1R132H peptide after enrichment of CD4+ clones (y-axis), and blood at visit 3, 7 and 10 (end of treatment (EOT)) (from left to right, x-axis). The size of individual bubbles indicates the frequency of a respective clone in pre-vaccination FFPE tissue, which was obtained 776 days before onset of vaccination.

3.3.3 IDH1R132H reactive TCRs are not restricted to only one MHC II allele per patient

B-LCLs were used to analyze the HLA-restriction of IDH1R132H-reactive TCRs. HLA alleles transcribed from HLA-DR, -DP and -DQ alleles were targeted by CRISPR-Cas using gRNAs previously validated by others (Lee et al. 2020). Knockout efficiencies were confirmed by flow cytometry and B-LCLs were used in co-culture assays without any further enrichment, as CRISPR efficiencies were sufficiently high and similar to efficiencies reported by Lee et al. (~80%/~80%/~90%, here 79%/86%/98% for DRA/DPA/DQA) (**Figure 7A**). B-LCLs without knockout, or with individual knockouts, were pulsed with IDH1R132H-peptide and co-cultured with JURKAT NF-κB eGFP reporter cells expressing TCRs that were previously validated to be IDH1R132H-reactive using autolgous DCs. A decrease in the percentage of GFP and in the MFI of CD69 after 18h of co-culture indicates that a TCR is restricted to a given HLA-allele (red squares). Out of 14 TCRs of patient ID2, 13 were restricted to a HLA-DR allele and only one (TCR ID76) was restricted to HLA-DQ (**Figure 7B**). All TCRs were previously shown to be reactive against both wildtype and mutant IDH1 peptide. Seven additional TCRs included in the screening failed to recognize IDH1R132H pulsed on B-LCLs despite expression of sufficient amounts of mTCRβ (23.8-70.9%), of which six were previously reactive to IDH1R132H but not IDH1-wildtype pulsed on DCs (not shown).

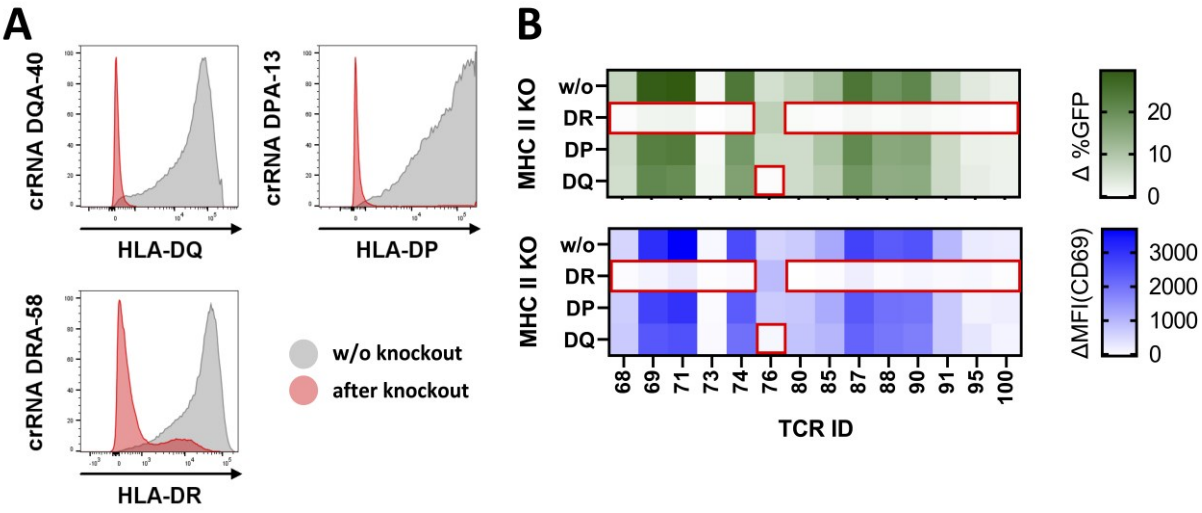

Figure 7. HLA-restrictions of IDH1R132H-reactive TCRs. A) Flow cytometry data of autologous B-LCLs of patient ID2 quantifying HLA-DQ, -DR and -DP expression seven days after CRISPR-based knockout of the respective alleles (red). The same B-LCL line without CRISPR-Cas knockout was used as a positive control (grey). Knockout efficiencies were 98% for HLA-DQ, 79% for HLA-DR, and 86% for HLA-DP. **B)** Co-culture of JURKAT NF-κB eGFP reporter cells electroporated with a selection of reactive TCRs derived from patient ID2 (RNA-based electroporation) and autologous B-LCLs after CRISPR-Cas knockout of HLA-DQ, -DR and -DP alleles. B-LCLs without (w/o) CRISPR-Cas knockout were used as a positive control, and B-LCLs of each of the four conditions were either pulsed with IDH1R132H peptide or without peptide as negative control. The differential percentage of GFP positive cells and the differential MFI of CD69 between conditions with IDH1R132H peptide or without were quantified after 18h of co-culture using flow cytometry. All depicted TCRs were reactive to both mutant and wildtype IDH1.

The presented data indicates that IDH1R132H long peptides can be presented by different MHC II alleles. The number of MHC II alleles able to present IDH1R132H peptide should be even larger, indicated by the overall high fraction of patients developing T cell responses against the IDH1-peptide-vaccine in the NOA16 trial cohort (26/32), where patients were recruited irrespective of their HLA allelotype (Platten et al. 2021). Moreover, patients included in this thesis for which CD4 T cell-mediated

IDH1R132H-responses were detected express a multitude of different MHC II alleles (**Supplementary table 1**).

As a total of 13 TCRs that were restricted to HLA-DR alleles were identified, I aimed at identifying common motifs in the CDR3 amino acid sequences, which was not possible as larger numbers of CDR3 sequences would be required to provide statistically significant analysis. No intuitive motifs were discovered looking at the CDR3 sequences of TCR beta chains (

Table 8). However, some TRBV and TRBJ genes were observed several times within the group of TCRs classified as reactive and DR-restricted, such as TRBV27 (n=3/13) or TRBJ1-5 (n=4/13), which are both shared by TCR IDs 73 and 74, indicating that a higher number of reactive TCRs with known HLA restriction might allow to decipher a CDR3 motif for IDH1R132H-reactive TCRs.

Table 8. List of CDR3 amino acid sequences, V- and J-genes of beta chains of IDH1R132H-reactive TCRs with tested HLA-restriction. Diversity sequences in between V- and J-genes are highlighted.

TCR ID	Restriction	CDR3	V gene	J gene
68	DR	CASSL**DWGA**YEQYF	TRBV5-1	TRBJ2-7
69	DR	CASS**LTGA**GANVLTF	TRBV11-2	TRBJ2-6
71	DR	CASS**QNPGG**NQPQHF	TRBV9	TRBJ1-5
73	DR	CASS**SKGFL**QPQHF	TRBV27	TRBJ1-5
74	DR	CASS**WN**SNQPQHF	TRBV27	TRBJ1-5
76	DQ	CSA**TRDGSL**YNEQFF	TRBV20-1	TRBJ2-1
80	DR	CASS**ASPGQA**QFF	TRBV9	TRBJ2-1
85	DR	CASS**LRGGAW**YNSPLHF	TRBV27	TRBJ1-6
87	DR	CASS**PRAGV**ATNEKLFF	TRBV2	TRBJ1-4
88	DR	CASSL**TP**SNQPQHF	TRBV7-8	TRBJ1-5
90	DR	CASS**QGGV**TEAFF	TRBV10-1	TRBJ1-1
91	DR	CASS**QKGQG**HGYTF	TRBV6-5	TRBJ1-2
95	DR	CASS**FKG**NSPLHF	TRBV12-4	TRBJ1-6
100	DR	CASSL**GSGGLS**EQYF	TRBV7-9	TRBJ2-7

3.3.4 IDH1R132H reactive TCRs show a distinct gene expression profile

CD3+ CD45+ T cells from on-trial tumor tissue from patient ID1, ID2 and ID3 was used for FACS-based enrichment and single cell sequencing. Gene expression as well as V(D)J data were used for differential gene expression analysis of (I) CD4+ clonotypes with confirmed reactivity and (II) all other CD4+ clonotypes that were not tested. The latter could potentially include reactive clones. Top up- and downregulated genes were depicted as a heatmap (**Figure 8A**, analysis performed by Chin Leng Tan (DKFZ Heidelberg, Germany). Reactive clones express higher levels of CD40 ligand (CD40LG), long intergenic non-protein coding RNA 892 (LINC00892) with slight upregulation of Granzyme K (GZMK), whereas expression of IL-7 receptor (IL7R) and genes associated with cytotoxicity such as granzyme B (GZMB) was decreased (**Figure 8B**). IDH1R132H reactive clonotypes were classified as T helper cells.

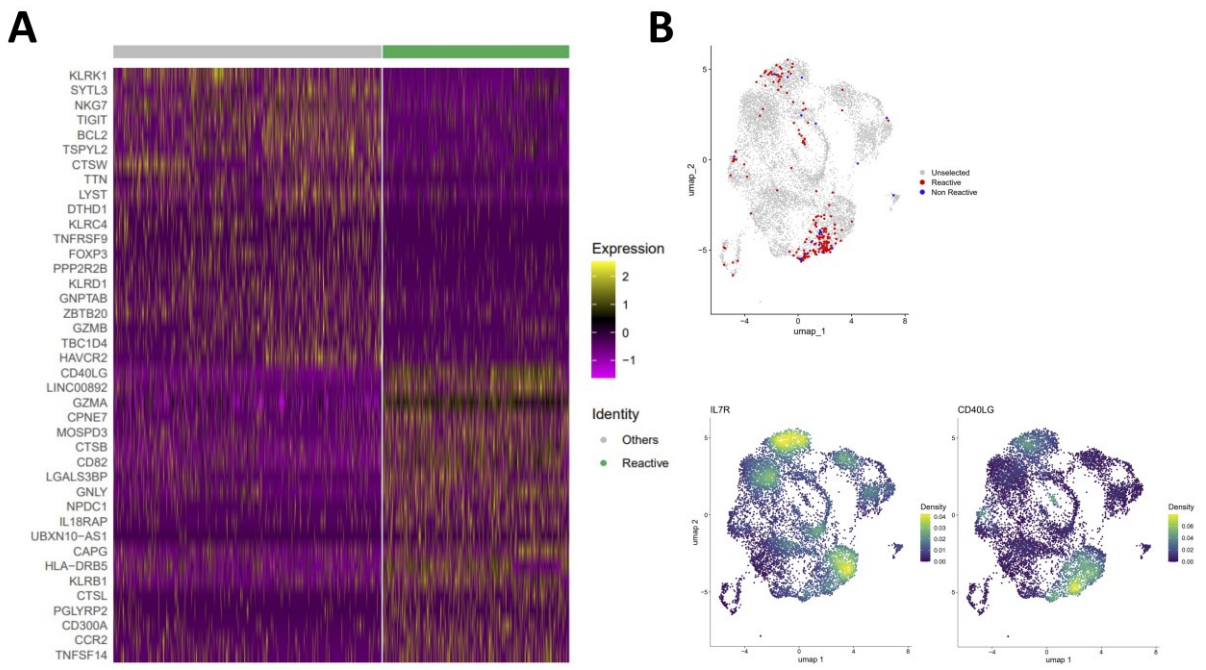

Figure 8. Single cell gene expression analysis of IDH1R132H-reactive TILs. CD3+ CD45+ CD11b- TILs were FACS sorted from on-trial tumor tissue for NOA21 patients ID1, ID2 and ID3 after they received two to three doses of vaccination ± avelumab. **A)** Differential gene expression analysis of reactive CD4+ T cell clones (green) and CD4+ clones that were not tested for reactivity (gray, downsampled for visualization). Mitochondrial and V(D)J genes were removed from analysis. **B)** UMAP projection of gene expression profiles of patients ID1-ID3, with clones that were tested to be reactive highlighted in red, and clones with high IL7R and CD40LG expression highlighted below. (Single cell sequencing analysis was performed by Chin Leng Tan.)

3.3.5 IDH1R132H can be presented on MHC I and elicits a CD8 T cell response

The current literature mainly focuses on CD4+ IDH1R132H reactive T cells due to previous observations that reported the absence of a CD8 response in IDH1R132H (p123-142) vaccinated A2.DR1 mice, which were engineered to express humanized MHC alleles (HLA-A*02:01, DRB1*01:01, DRA1*01:01). It was also shown that a depletion of CD4+ T cells abrogated the anti-tumor response in these mice (Schumacher, Bunse, Pusch, et al. 2014). In addition, a reduced CD8 T cell proliferation was observed in IDH1R132H+ glioma tissue, while CD4 proliferation was unaffected, further strengthening the impression that CD8+ T cells do not play a major role in IDH1-mutant gliomas (Bunse et al. 2018).

To test whether CD8+ T cell responses can be found in patients of the NOA21 trial, which carry a diverse set of MHC I alleles, ELISpot assays of CD4+ and CD8+ enriched T cells against peptide-pulsed DCs were performed in an autologous setting. DCs are able to process and cross-present exogenously loaded long peptides as short peptides on MHC I (Joffre et al. 2012). CD4+ and CD8+ enriched cells were analyzed by flow cytometry to show the purity of CD4+ and CD8+ populations after magnetic column-based enrichment (**Figure 9A**, left). Interestingly, CD8+ T cell responses were observed in two out of three tested patients in ELISpot. The overall number of reactive CD8+ T cells was lower than the overall number of reactive CD4+ T cells, as reflected by spot counts in ELISpot (mean spot counts for IDH1R132H, CD4/CD8: ID2 (365/213), ID14 (220/39)) (**Figure 9A**, right). For both CD4+ and CD8+ cells, reactivity to the IDH1-wildtype peptide was observed.

To be able to identify the short IDH1R132H peptides and the associated MHC I alleles recognized by CD8 T cell clones for both patients, mass spectrometric analysis of B-LCLs pulsed with the long 20-mer IDH1-wildtype and -R132H peptides was performed. For patients ID2 and ID14, one and three short

peptides presented on HLA-B*07:05 and HLA-B*35:01 were identified, respectively. For patient ID2, no wildtype counterpart to the identified mutated peptide was detected, whereas for patient ID14, two short mutated peptides along with the wildtype version of one of the peptides were detected (**Table 9**). HLA-B*07:05 and HLA-B*35:01 cover 12.3% of the German population taking HLA supertype families into account (data from IEDB population coverage tool (Bui et al. 2006)).

Table 9. Short IDH1 peptides and associated MHC I alleles discovered in patients ID2 and ID14. Both were identified using mass spectrometric analysis of autologous B-LCLs pulsed with 20-mer IDH1-wildtype and IDH1R132H peptides (p123-142) after MHC I pulldown for patients ID2 and ID14. Data acquisition and analysis was performed with two independent replicates by Jonas Becker (DKFZ Heidelberg, Germany).

Patient ID	HLA allele	Peptide sequence	Peptide length	Position
ID2	HLA-B*07:05	KPIIIG**H**HA	9	p126-134
ID14	HLA-B*35:01	KPIIIG**H**HAY	10	p126-135
ID14	HLA-B*35:01	KPIIIG**R**HAY	10	p126-135
ID14	HLA-B*35:01	IG**H**HAYGDQY	10	p130-139

To test reactivity against the identified 9-mer peptide for patient ID2, the 20-mer IDH1-wildtype and -R132H peptides, as well as the identified 9-mer peptide were added to PBMCs of visit 7 and TNFα/CD107a were quantified after five hours of co-culture. Quantification of TNFα indicates that the short peptide is recognized by a population of CD8+ cells (0.05% increase over background in CD8+ cell population), also visible as a clear TNFα/CD107a double positive population in FACS (**Figure 9B**). Long IDH1R132H peptide also elicited a small response with 0.07% increase of TNFα+ cells over background, most likely reflecting the response against cross-presented peptide. To be able to select TCRs for cloning and to test their reactivity, ESPEC-SUIT was performed using PBMCs of patient ID2 and the IDH1R132H 9-mer peptide. The post-ESPEC quality control ELISpot was indicative for a strong expansion of reactive clones. A total of 6.7% of cells were CD8+ TNFα+ in a subsequent TNFα secretion assay. The double positive population was enriched by FACS-sorting and used for single cell V(D)J sequencing. The single cell sequencing dataset was dominated by a single large clone (89.4% of the entire repertoire), which was moreover also found in the single cell sequencing dataset of TILs isolated from on trial tissue of this patient (0.24% of the repertoire, 20th largest clone) (**Figure 9C**). A total of seven TCRs that were found in both the post-ESPEC and TIL V(D)J single cell sequencing datasets were selected for cloning and testing, covering 93.9% of the post-ESPEC repertoire. TCR testing revealed reactivity of the first largest post-ESPEC clones against both the short 9-mer and long 20-mer IDH1R132H peptide as quantified using CD107a and TNFα. The second largest post-ESPEC clone only showed reactivity against the long IDH1R132H peptide, but not the short 9-mer used for expansion. This indicates that this TCR is indeed reactive against the short peptide, which needs to be confirmed in a second experiment (**Figure 9D**). Autologous DCs were used as APCs, which most likely processed the long version of the peptide and presented the appropriate 9-mer peptide in co-culture.

The cumulative frequency of both reactive clones together was 0.74% within the entire TIL repertoire isolated from on trial tissue at V7, and made up 0.54% of the entire repertoire in blood isolated at the same timepoint. Frequencies observed in TCRβ deep sequencing datasets from blood are higher than the aforementioned frequencies observed after peptide-pulsing PBMCs with short peptide and quantification of TNFα+ cell populations (**Figure 9, E and B**). The cumulative frequency of both CD8+ clones in blood at V7 is comparable to the cumulative frequency of CD4+ IDH1R132H-reactive clones at the same timepoint identified through ESPEC (**Figure 6B**, 0.73%). Clones were absent before onset of vaccination, indicating that they were induced through vaccination with the IDH1R132H long peptide vaccine.

A 3D model of the pMHC::TCR interaction of top TCR 1 revealed that the histidine amino acid of at position 132 of IDH1R132H interacts with a serine at position 96 of the TCR-beta chain, which is the 6th amino acid of the CDR3 sequence within the D region. Gene expression analysis of TILs revealed that both clone top 1 as well as top 2 are part of a granulysin (GNLY) positive cluster.

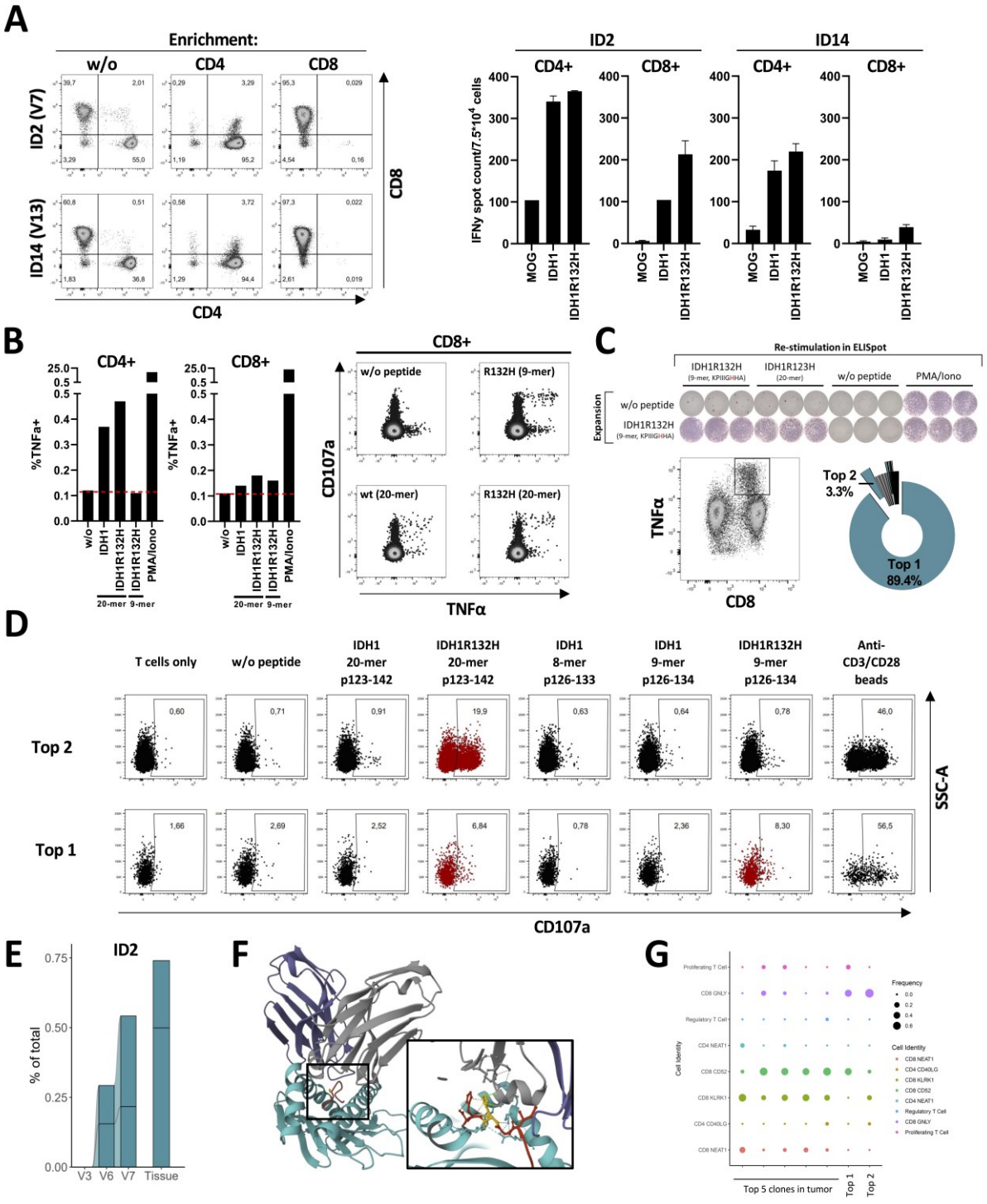

Figure 9. Discovery of CD8+ IDH1R132H-reactive TCRs. A) ELISpot of CD4+ and CD8+ T cells against peptide pulsed DCs of patients ID2 (V7) and ID14 (V13). DCs were pulsed overnight with (I) MOG peptide, (II) 20-mer IDH1-wildtype peptide and (III) 20-mer IDH1R132H peptides to allow for cross-presentation of short peptide fragments on MHC I. CD4+ and CD8+ T cells were separately negatively enriched using magnetic columns. Their purity was confirmed using FACS (left panel, T cells before enrichment were gated on viable CD3+ singlets and used as a control). 75,000 cells/well (duplicates were used if number of cells was limited). Number of spots counted for CD8+ cells after IDH1R132H stimulation of ID14 is significantly higher as

compared to the number of spots counted after MOG stimulation (p=0.014, Kruskal-Wallis test). **B)** FACS-based quantification of TNFα-secretion after pulsing PBMCs of patient ID2 (V7) with either the 20-mer IDH1-wildtype and IDH1R132H peptides (p123-142), or with the 9-mer IDH1R132H peptide (p126-134), which was identified using MS analysis. Co-culture was performed as described for TCR testing assays (Methods chapter 2.20, without TCR electroporation). Gating on viable CD3+ singlets, and either CD4+ or CD8+ populations. FACS raw data (right panel) depicting the same dataset as in the bar plot, quantifying CD107a and TNFα in CD8+ cells. 63,000 cells depicted per plot. **C)** Top: Post-ESPEC quality control ELISpot of PBMCs of patient ID2 (V7) after expansion with the 9-mer IDH1R132H peptide KPIIIGHHA (p126-134) and re-stimulation with IDH1R132H 20-mer and 9-mer peptide (25,000 cells/well). Bottom left: TNFα secretion assay after restimulation with the 9-mer IDH1R132H peptide and FACS-based enrichment of the CD8+ TNFα+ cell population. Bottom right: Proportion of TCRs within the single cell sequencing dataset generated from cells sorted after TNFα secretion assay. **D)** TCR testing results for the top two clones identified in C. TCR encoding RNA was electroporated into expanded PBMCs and co-cultured against peptide pulsed DCs. TNFα and CD107a were quantified using flow cytometry. One day after electroporation, TCR 2 was expressed at 70.8%, whereas TCR 1 was only expressed at 4.7% based on mTCRβ data. After gating on mTCRβ+ cells, the percentage of CD107a and TNFα positive cells was quantified. **E)** Tracking of reactive TCRs in blood and tissue of patient ID2, using TCRβ deep sequencing data from blood and single cell sequencing data from FACS sorted TILs. **F)** Model of the interaction of the KPIIIGHHA peptide (red) with HLA-B*07:05 (light blue) and the top 1 TCR (alpha chain in dark blue, beta chain in grey). The R132H mutation is highlighted in yellow. Interactions with Ser96 of the CDR3-beta chain are highlighted in green. The 3D model was generated using ImmuneScape (Li et al. 2019). **G)** Gene expression analysis of both reactive clones within the TIL compartment as compared to the top 5 CD8+ clones found within the tumor.

3.4 TCR discovery in non-brain tumor patients

Besides screening for TCRs reactive against shared neoepitopes such as IDH1R132H, ESPEC-SUIT was used to screen for reactivity against private neoepitopes of individual patients. Private neoepitopes are defined after analysis of the tumor mutanome based on whole exome sequencing (WES) and for patients described in the following covers single nucleotide variants (SNVs) as well as antigens resulting from gene-fusion events. Optimally candidate antigen expression is verified using transcriptome sequencing (RNAseq). Binding predictions can reduce the number of possible targets in high-mutational load tumors and, if available, immunopeptidomics data derived from MS analysis of tumor tissue can confirm MHC presentation of candidate antigens. WES, RNAseq, sequencing data analysis, immunopeptidomics and selection of candidate neoepitopes of patients POC-001, POC-004 and POC-005 described in the following were performed by partners at DKFZ within the scope of the TCR-POC consortium which aims to establish an optimized workflow for TCR-transgenic therapies.

Beyond tissue analysis for antigen selection, a leukapheresis is collected to allow comparison of diverse TCR pre-selection assays in terms of efficiency for selecting reactive TCRs. For some patients, repeated blood sampling allowed tracking of selected TCRs over time. TCR POC follows an all-comers approach, including patients suffering from various tumor entities as long as requirements for sample availability are met. Tumor entities covered herein were: colorectal cancer (primary tumor and liver metastasis, POC-001), liposarcoma (POC-004), and metastatic melanoma (POC-005). Patients POC-001 and POC-004 received repeated doses of vaccinations with long peptides covering their respective tumor mutanome to elicit an anti-tumor response, whereas POC-005 only received vaccinations covering shared epitopes, but not the tumor mutanome.

Patient POC-001 received six doses of vaccination containing a total of 18 long peptides per dose (HD-Pep-1773 to HD-Pep-1790) on days 0, 33, 55, 89, 179, and 630. These peptides cover SNVs as well as gene-fusions (**Table 10**). Tumor tissue was obtained at day -211 (colon cancer) and day -99 (liver metastasis) before start of vaccination. A leukapheresis withdrawn on day 405 was used to set up ESPEC against all 18 vaccine peptides. The post-ESPEC QC ELISpot showed successful expansion of reactive clones against 17/18 peptides (**Figure 10A**). A representative set of 28 TCRs with highest degree of expansion (0.7-10.1%) in post-ESPEC cultures were selected for cloning and testing based on TCRβ deep sequencing and single cell V(D)J sequencing data of the cultures. Only 3/28 selected TCRs were found in the MOG negative control expansion culture with a low proportion of $8.3*10^{-5}$ – $1.5*10^{-3}$. One day after RNA-based electroporation into expanded PBMCs, all constructs passed the

threshold of 2% mTCRβ expression and were used for co-culture assays (**Figure 10B**). In total, 25/28 (89%) tested TCRs showed reactivity based on TNFα and CD107a expression, and were further analyzed. Quantification of the fraction of CD4+ and CD8+ cells amongst mTCRβ+ TNFα+ expanded PBMCs after co-culture revealed that clones with higher TNFα secretion contained a higher fraction of CD8+ cells (31.7% for TCR 48) as compared to clones with lower amounts of TNFα secretion (4.2% for TCR 65). Given the fact that all TCRs were derived from CD4+ clones, this indicates that some clones are less dependent on the CD4 co-receptor for stabilization of the pMHC::peptide – TCR axis, possibly due to higher TCR affinities to the target epitope, and thus achieve higher TNFα secretion by broadening the responder population to CD4- T cells. (**Figure 10C**). Analysis of the frequency of reactive clones in pre- and post-expansion cultures showed that reactive clones had baseline frequencies of 0-0.06% in blood, with a 118-9847 fold expansion of clones that were present at baseline (n=18) in ESPEC (**Figure 10D**). Reactive clones were tracked over time in blood, showing that all of them were absent at day 0 and induced through vaccination. Two clones were found in pre-vaccination tissue on basis of TCRβ deep sequencing data, with frequencies of $1.3*10^{-4}$ % and $4.2*10^{-5}$ % (**Figure 10E**). Both clones were found to be reactive against HD-Pep-1773 and -1774, respectively.

Table 10. Peptides used for vaccination and for ESPEC cultures of patient POC-001. Peptides were selected based on the mutanome after analysis of WES and RNAseq data. The peptide amino acid sequences are listed with the mutated amino acid highlighted in red. In case of fusion peptides, red amino acids indicate those parts of the sequence belonging to the second gene. Patient-derived xenografts (PDXs) of the colon tumor and liver metastasis were generated in mice, and analyzed using WES and RNAseq. Presence of the indicated mutation or fusion event in liver metastatic tissue and both xenografts is annotated.

HD-Pep ID	Peptide sequence	Length	Gene	Mutation expressed in liver metastasis and both PDX models?	Number of tested / reactive TCRs
1773	GDAEAVKGIGSSKVLKSGPQDHV	23	LGMN	Yes	2 / 1
1774	SEIEARIAATTANGQPRRRSIQD	23	MAP3K7-A	Yes	1 / 1
1775	NILDVPEIVISANGQPRRRSIQD	23	MAP3K7-B	Yes	1 / 1
1776	ESLMHYQPFSFSKNASVPTITAK	23	MEP1A	Yes	2 / 2
1777	NPCAEGWMDWAVSKISGWTQALP	23	NDRG1	No	2 / 2
1778	ESDLDKVFHLPITTFIGGQESAL	23	OGDH	Yes	2 / 2
1779	FPLSSPFRQVVQPRVEGKPVNPP	23	TRAPPC9	Yes	2 / 1
1780	WDSETGENDSFTGKGHTNQVSRM	23	WDR1	Yes	-
1781	HQVTLLDFGASREFTDHYIEVVKA AAD	27	ADCK4	Yes	3 / 3
1782	RVQVLPDAVLYYILPRKVLQMDFL VHPA	28	APC	Yes	4 / 4
1783	PAYLNSLNNFLLRLTCQNTMLPDM ASSCIAILIQECKTKNKPQSAV	46	ABCA12	Yes	2 / 2
1784	GNPRDLRVSDPMTSTMKLSWSGA	23	COL12A1	No	1 / 1
1785	EQRFTCYMEHSRNHGTHPVPSGK	23	MICB	No	2 / 2
1786	EVDTLSTLSLSNAQHWTQAKEKG	23	SETBP1	Yes	-
1787	KCLEENNGVDKHVTRFVLPVGAT	23	SLC1A3	No	-
1788	AIFAPNPSLMLCLDVQSEKSEGN	23	WDR44	Yes	-
1789	WSPSAARLVSSHSGWFPRIPQAQ	23	NRP2	No	2 / 1
1790	PGPRDAQAHPGHPRAVPTQCDVP	23	GAA	No	2 / 2

ESPEC-SUIT was also performed for patient POC-005, where a total of 44 long peptides and 145 short peptides representative for the tumor mutanome (melanoma metastasis growing in the lymph node) were used for testing. Viral peptides (n=8 short peptides, n=6 long peptides) were included as positive controls. To decrease the number of ESPEC cultures (and thus cells) needed, short peptides were tested in 50 peptide pools with up to 14 single peptides per pool, with each pool containing the mutations identified in one gene. Short peptides had a length of 8-12 amino acids, with the respective mutation located at a different position within the individual peptides. MHC I binding predictions with algorithms such as NetMHCpan-4.1 were performed to narrow down the number of short peptides to be tested per gene as much as possible.

Post-ESPEC, cultures were re-stimulated with the individual peptides contained in the pool, allowing analysis of individual peptide-specific responses. Different from POC-001, patient POC-005 did not receive any anti-tumor vaccinations prior to ESPEC, therefore any observed response in the QC ELISpot is indicative for a pre-existing anti-tumor immune response. Only 3/145 (2%) short peptides caused a peptide-specific expansion covering SNVs in FKBP Prolyl Isomerase 8 (FKBP8), WD Repeat Domain 12 (WDR12) and Synapse Defective Rho GTPase Homolog 1 (SYDE1), of which reactivity to WDR12 and SYDE1 was confirmed in two independent assays (**Figure 10G** and **Table 11**). Post-ESPEC QC ELISpots did not reveal any reactivity against wildtype versions of the short peptides which elicited a positive response (not shown). ESPEC with long peptides was performed in two independent replicates, with 15/44 (34%) long peptides causing an increase in spot counts in post-ESPEC QC ELISpots for both assays, and 17/44 (39%) long peptides causing an increase in spot counts in only one of both assays (**Figure 10H**, showing only data of one assay, and **Table 11**). 12/44 (27%) long peptides did not cause a peptide-specific expansion in either of both assays. Long peptides covering mutations that previously caused a positive expansion after ESPEC with short peptides only elicited responses for FKBP8 (n=1 assay) and SYDE1 (n=2 assays), whereas no response to the long peptide of WDR12 was detected.

Based on the FEST-algorithm, a total of 48 TCRs will be cloned and tested for the three short peptide hits (WDR12: 16, FKBP18: 18, SYDE1: 14). However, only 34 (WDR12: 14, FKBP18: 13, SYDE1: 7) of them were present in tumor TCRβ deep sequencing data (proportions in tumor compartment between $8.26*10^{-6}$ - $4.96*10^{-4}$) representing the most promising anti-tumor TCR candidates. As a large number of possible responses were detected in the ESPEC assays using long peptides, a representative number of 18 post-ESPEC cultures were used for TCRβ deep sequencing and to select TCRs. A total number of 666 TCRs could be cloned and tested based on output of the FEST algorithm, though functional validation will be focused either on top expanded clonotypes or on selected antigens.

Patient POC-004 (liposarcoma) received two individual peptide vaccine cocktails: two vaccinations with HD-Pep-2592 – 2596 (n=5 long peptides, representative for SNVs in HIVEP2, MEGF8, PIGO, PRMT5 and TCF3, administered on days 0 and 232), and one vaccination with HD-Pep-2977 – 2983 (n=7 long peptides, representative for fusion peptides 12, 13, 24, 26/28, 36 and 8, administered on day 232). Tumor tissue for antigen selection was obtained on day -274. A leukapheresis of day 330 was available for ESPEC, in which 20 peptide pools (encompassing the vaccine peptides plus additional candidate antigens) containing a total of 97 short peptides were used for expansion, while individual single peptides contained in the pool were used for restimulation in post-ESPEC QC ELISpots. Heavy labelled peptides that were utilized for immunopeptidomics analysis were tested in 22 additional separate short peptide pools, but caused a high background in post-ESPEC QC ELISpots, and were therefore omitted from analysis. Therefore, it was not possible to cover the entire mutanome and all vaccination peptides with peptide pools no. 4-23, and two peptides that were identified after immunopeptidomics analysis of the tumor tissue could not yet be included into further analysis.

Despite these limitations, 16/97 (16%) short peptides from the tumor mutanome caused a positive response in post-ESPEC QC ELISpots (**Figure 10I**, highlighted in red), of which 13/16 were included in

the administered vaccine. Positive responses were also detected for 2/4 viral control peptides. Expansion of PBMCs using short EBV peptides (pool 2, five peptides) caused a high background in ELISpot. Cells that were plated without any restimulation in ELISpot secreted high amounts of IFNγ and were therefore excluded from analysis. No responses against peptides that were not included in the vaccination scheme were detected.

Table 11. Overview of peptides and genes tested and reactive in ESPEC assays for patient POC-005. ESPEC assays using short and long peptides were performed with PBMCs and in two independent replicates, each. Short peptides were tested in peptide pools, with individual peptides contained in the pool and used for restimulation in QC ELISpots being visualized as squares in the table. HD-Pep IDs refer to peptide IDs of long peptides. Colors indicate the number of assays in which a peptide caused an increase in IFNγ spot count in post-ESPEC QC ELISpots. Viral control peptides are labelled in blue. Green: detected in n=2 assays; Yellow: detected in n=1 assay; Grey: detected in none of both assays.

Running number	HD-Pep ID (long peptides)	Gene	Short peptide (pools)	Long peptides
1	3053	NRAS		
2	3054	CCT3		
3	3055	WWC3		
4	3056	SNRPA		
5	3057	EIF4EBP2		
6	3058	SELENBP1		
7	3059	NRD1		
8	3060	TRIM51		
9	3061	NGDN		
10	3062	OSGEP		
11	3063	DOPEY2		
12	3064	SUPT6H		
13	3065	SMU1		
14	3066	TSPAN17		
15	3067	INO80		
16	3068	GMPS		
17	3069	WDR12		
18	3070	RPL27		
19	3071	MAGEC1		
20	3072	CD320		
21	3073	FKBP8		
22	3074	RCC2		
23	3075	KIAA0368		
24	3076	MGAT1		
25	3077	RBM8A		
26	3078	COASY		
27	3079	TOMM40L		
28	3080	NDUFA4		
29	3081	NOSIP		
30	3082	UBR4		
31	3083	SLC38A10		
32	3084	CKAP2L		
33	3085	SRCAP		
34	3086	MEF2D		
35	3087	MTOR		
36	3088	SYDE1		
37	3089	PPRC1		
38	3090	SLC22A15		
39	3091	FRMD8		
40	3092	ACAD10		
41	3093	TBC1D22B		
42	3094	fusion1		
43	3095	fusion7		
44	n.a.	FLNA		n.a.
45		JKAMP		
46		TRIM27		
47		GCH1		
48		HDAC6		
49		ADAMTSL4		
50		MET		
51	3101	fusion 1		
Viral control peptides	n.a.	CMV		
	3096	CMV (pp65)		
	3097	Influenza (PB1)		
	3098	EBV (BZLF-1)		
	3099	EBV (EBNA3A)		
	3100	CMV (IE1)		

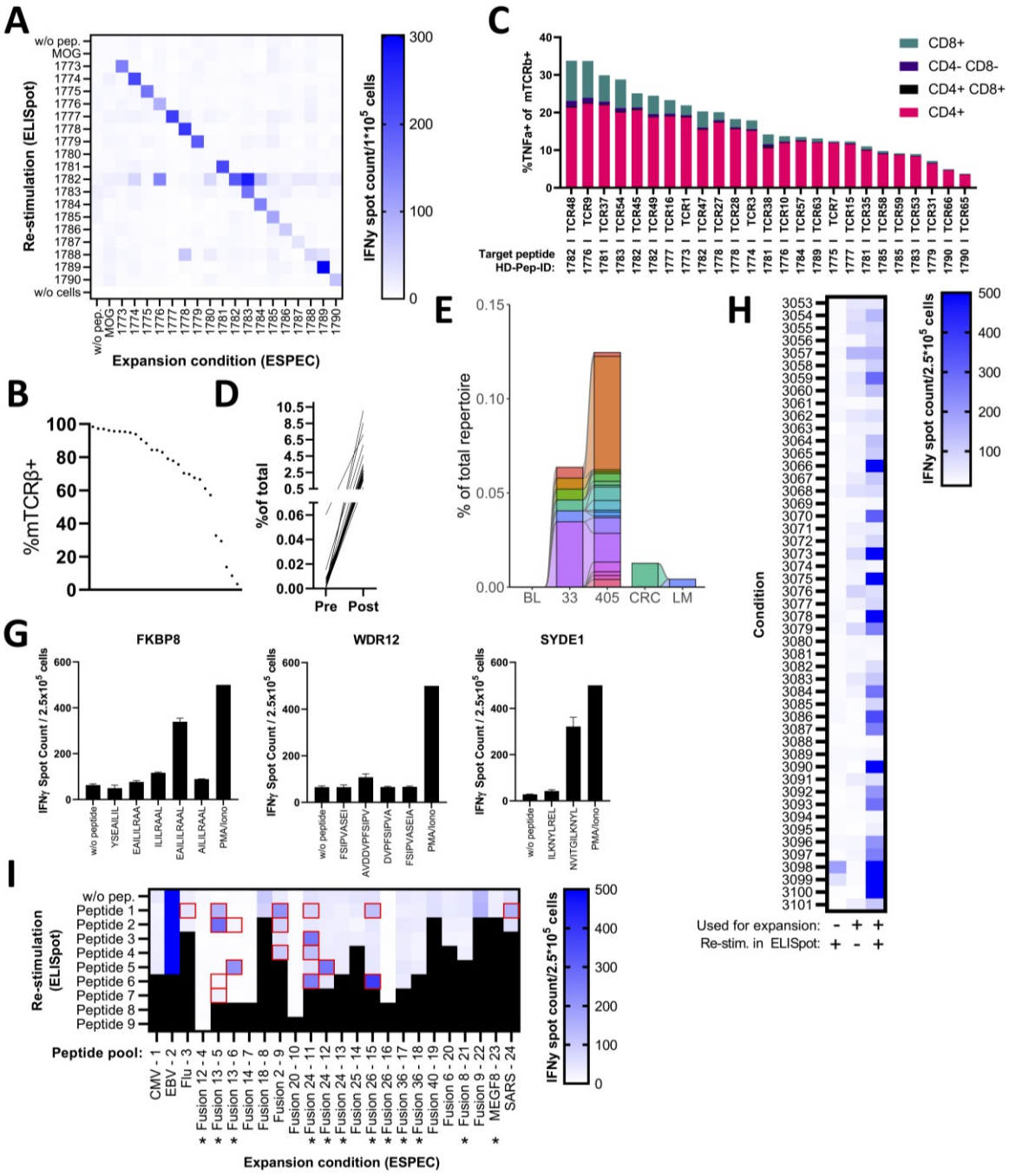

Figure 10. ESPEC-SUIT with patients of the TCR-POC cohort. A) Heatmap of all post-ESPEC QC ELISpots for patient POC-001. Numbers plotted on the x- and y-axis refer to HD-Pep IDs used for expansion in ESPEC or restimulation, respectively, as listed in **Table 10**. 100,000 cells/well in duplicates. **B)** Flow cytometric quantification of mTCRβ for POC-001 ESPEC-selected TCRs after electroporation of TCR-encoding RNA into expanded PBMCs. Expression levels are sorted by decreasing frequency. **C)** Quantification of TNFα in mTCRβ+ cells of reactive TCRs in expanded PBMCs after co-culture with peptide-pulsed B-LCLs. For patient POC-001, 25 of 28 tested TCRs were classified as reactive. The percentage of CD4+, CD8+, CD4+ CD8+ and CD4- CD8- cell populations amongst TNFα+ cells is annotated. **D)** Frequency of reactive TCRs of patient POC-001 before ESPEC in blood and in post-ESPEC cultures as quantified by TCRβ deep sequencing. **E)** Tracking of TCRs tested to be reactive of patient POC-001 in blood over time. BL = baseline sample before onset of vaccination with peptides listed in **Table 10**. X-axis = days since first vaccination. PBMCs of the leukapheresis from day 405 were used for ESPEC. CRC=colorectal cancer, LM=liver metastasis. **F)** Quantification of the overall frequency of TCRs tested to be reactive of patient POC-001 in tissue based on TCRβ deep sequencing data. **G)** Post-ESPEC QC ELISpots after expansion of POC-005 PBMCs with short peptide pools, and re-stimulation with individual short peptides contained in the pool. Only pools with positive responses in ELISpot are shown. 250,000 cells/well. **H)** Heatmap of post-ESPEC quality control ELISpots for patient POC-005. Numbers plotted on the x- and y-axis refer to HD-Pep IDs, as listed in **Table 11**. 250,000 cells/well in duplicates. **I)** Summary of post-ESPEC QC ELISpots for patient POC-004. PBMCs were expanded in peptide pools (Pool 1 – Pool 24) and re-stimulated with individual peptides contained in the

pool in ELISpot. Conditions for which a positive expansion was detected were highlighted in red, as some of them are of low magnitude. Asterisks indicate peptide-pools which contained short peptides expressing SNVs or fusions that were also covered by the long peptides used for vaccination. 250,000 cells/well.

3.5 Gene signature-based TCR discovery in brain tumor patients

To be able to analyze gene expression patterns of T cells in the brain tumor environment, brain tumor tissues of 20 patients were processed (11/20 processed by myself and 9 by other colleagues from the CCU) with the aim of generating tumor cell lines and single cell V(D)J and transcriptome sequencing datasets of T cells. In total, six patient-derived brain tumor cell lines were generated and 146 T cell receptors were selected using an in silico approach and tested for in vitro reactivity against autologous targets.

An initial batch of 63 TCRs were selected for testing by Chin Leng Tan based on a classifier that was defined based on available literature. TCRs introduced into expanded PBMCs by RNA-based electroporation were co-cultured with patient-derived brain tumor cell lines that were stimulated with IFNγ to increase MHC I and II expression. MHC I/II expression was verified by flow cytometry (data not shown). Despite mTCRβ expression levels >2% of 59/63 tested TCRs, no reactive TCRs were identified, while the positive control, Mart-1 specific DMF5 TCR co-cultured with the Mart1+ MeWo cell line performed well in all assays.

As an alternative approach, the top 83 clonotypes within the TIL repertoire of a melanoma brain tumor metastasis of patient BT21 were cloned and tested for reactivity against the corresponding tumor cell line. Cloning and TCR testing was performed in cooperation with Edward Green, Chin Leng Tan and Gordon Haltenhof, who developed a new method for high-throughput cloning of TCR constructs together with Tamara Boschert (all DKFZ Heidelberg, Germany). As alternative alpha chains were available for 12 TCRs, they were also included in testing (total n=95 TCRs), but were later excluded from analysis if the corresponding alternative alpha-beta pairing was tested to be reactive. From 83 TCRs included in testing, one had to be excluded from analysis due to low viability of the expanded PBMCs after electroporation, and eight did not pass the threshold for >2% mTCRβ expression (**Figure 11A**). Therefore, a total of 74 TCRs were used for a co-culture assay with the BT21 tumor cell line, which expressed high levels of MHC I (96.2% positive cells) but low levels of MHC II (2.1% positive cells) after stimulation with IFNγ (**Figure 11B**). After co-culture, n=46 TCRs were classified as reactive based on CD107a expression, including 45 CD8-derived and only one CD4-derived TCR (**Figure 11C**). TNFα expression was not used to classify TCRs as reactive or non-reactive as expression levels showed fluctuations in TCRs with lower reactivity, therefore repetitions of this assay are planned to confirm reactivity of TCRs with low CD107a expression. The overall mTCRβ expression between reactive and non-reactive TCRs did not differ significantly, indicating that a lack of reactivity is not due to low expression levels of the tested TCR (**Figure 11D**). In total, the reactivity of 36.5% of the tumor TIL repertoire were characterized, with 27.7% of this TIL subset being reactive and 8.8% being non-reactive (**Figure 11E**). Individual reactive clones had a higher mean proportion within the tumor as compared to non-reactive clones, whereas the opposite was true within blood (**Figure 11F**). Moreover, reactive clones showed a clear enrichment within the tumor, with CD107a expression after co-culture not correlating with the size of a TCR clone within the tissue (**Figure 11G**). However, TCRs with a higher degree of reactivity contained higher fractions of CD4+ expanded PBMCs within CD107a+ cells. As all but one TCR are derived from CD8+ T cells, this again indicates that cells less dependent on the CD4 or CD8 co-receptor due to higher affinities of the pMHC complex to the respective TCR achieve a higher degree of cytokine secretion (**Figure 11H**). Based on the single cell gene expression data of reactive clones for patient BT21, a classifier characterizing reactive T cell clones will be defined by Chin Leng Tan.

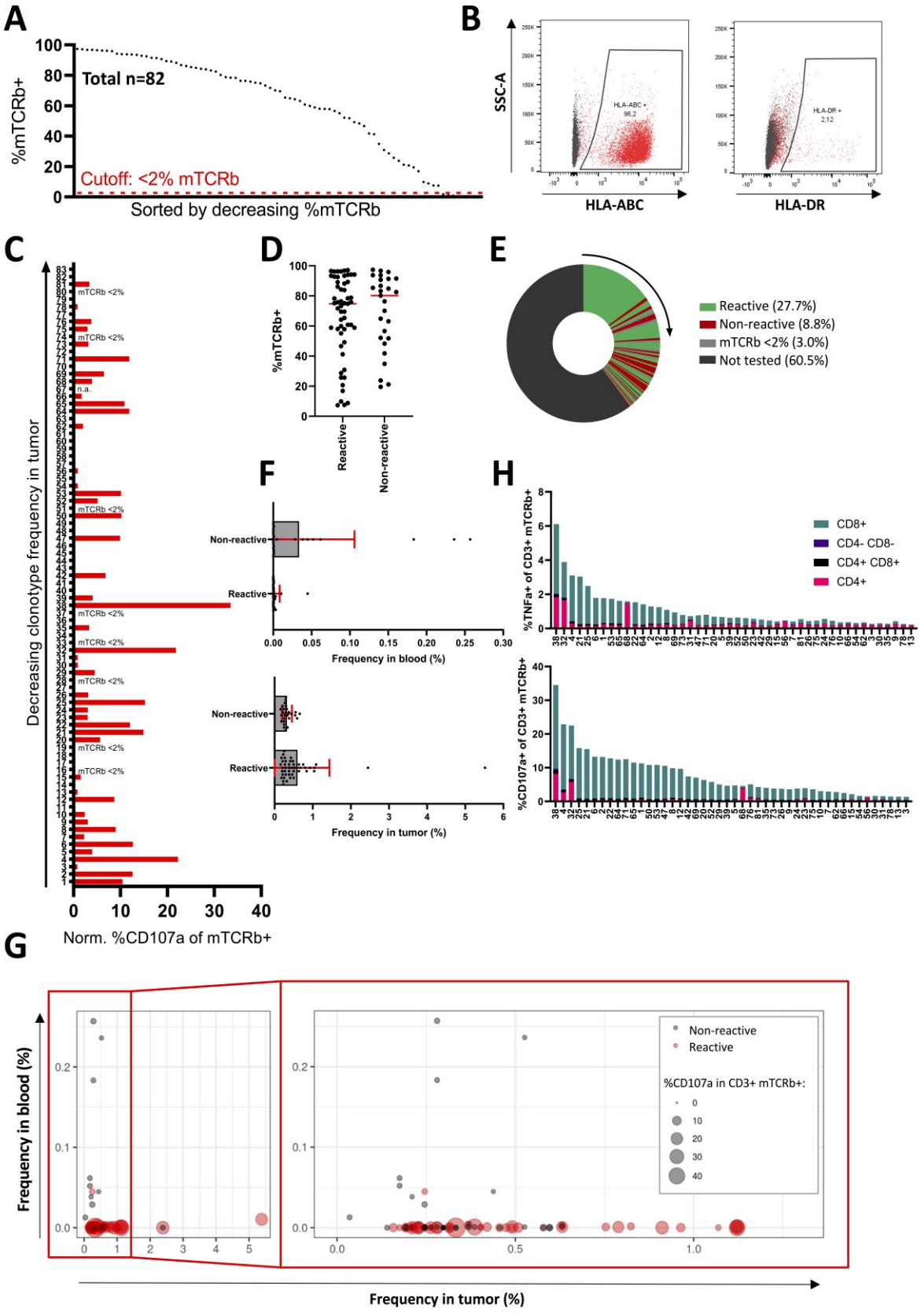

Figure 11. Testing TCRs from the TIL compartment of the melanoma brain metastasis BT21 for reactivity. A) mTCRβ expression of the top 82 TCRs of the TIL compartment of patient BT21. Quantification of mTCRβ of one TCR (ID67) was not performed due to low cell viability. Eight TCRs were excluded from analysis due to mTCRβ expression below 2%. **B)** Flow cytometric quantification of MHC I and II expression of the BT21 tumor cell line after two days of stimulation with 300 IU/mL IFNγ. **C)** Flow cytometric quantification of CD107a expression within CD3+ mTCRβ+ cells after electroporation of TCR-encoding RNA into expanded PBMCs and co-culture with the BT21 tumor cell line after IFNγ stimulation. TCR clonotypes were ordered

by decreasing clonotype frequency within the TIL compartment. CD107a expression was normalized per TCR by subtracting the percentage of CD107a+ cells measured after co-culture with the tumor cell line minus the unstimulated condition, and by also subtracting the normalized signal measured for mock transfected T cells. TCRs were regarded as reactive and labelled in red if the resulting CD107a signal is at least >2x the SD measured for all unstimulated conditions. Reasons for excluding TCRs from analysis are annotated. **D)** Comparison of mTCRβ expression levels between reactive and non-reactive TCRs after omitting TCRs with mTCRβ expression levels below 2% and TCR ID67 due to low cell viability after TCR transfection from analysis. **E)** Fraction of reactive (n=46) and non-reactive (n=28) TCRs within the TIL repertoire. TCRs that were excluded from analysis (n=9) or that were not included for testing are labelled in grey. TCRs are sorted by decreasing frequency as indicated by the arrow. **F)** Comparison of the frequency of reactive and non-reactive T cell clones in tumor and blood as quantified with single cell V(D)J sequencing data and TCRβ deep sequencing data, respectively. **G)** As in F, but with annotation of the percentage of CD107a release within the co-culture assay. **H)** Quantification of CD107a and TNFα in mTCRβ+ cells of reactive TCRs in expanded PBMCs after co-culture with the BT21 cell line. The fraction of CD4+, CD8+, CD4+ CD8+ and CD4- CD8- cell populations amongst TNFα+ or CD107a+ cells is annotated.

4. Discussion

4.1 Discussion of TCR screening approaches

This thesis aimed at identifying and validating neoepitope-specific T cell receptors. Thus, pre-selection of TCRs for testing and cloning as well as establishing assays for validation of reactivity are fundamental. Two types of assays were used to validate reactivity of TCRs against either peptide-pulsed APCs, such as DCs or B-LCLs, or against tumor cell lines.

Expanded PBMCs were electroporated with TCR-encoding RNA and reactivity was assessed upon flow cytometric quantification of CD107a and TNFα after co-culture. Both markers were shown to correlate well (**Figure 3C**) and to have little amounts of background expression (**Figure 3D**), thereby allowing to screen TCRs with a high degree of sensitivity, making these effector cells ideal for testing TCRs against tumor cell lines with little antigen expression. Correlation of both markers makes sense, as CD107a is a degranulation marker (Betts and Koup 2004). As shown in **Figure 3C** (bottom), overall lower levels of CD107a and TNFα can be expected upon co-culture with tumor cell lines, even after IFNγ treatment to increase MHC I/II expression on target cells (Seliger, Ruiz-Cabello, and Garrido 2008), as compared to co-cultures with peptide-pulsed APCs (top and middle). Sensitivity of co-culture assays can be further increased by expanding only CD4+ or only CD8+ T cells prior to co-culture, if TCRs from only CD4+ or CD8+ clones are to be tested, respectively, as higher cell numbers of relevant populations can be analyzed in flow cytometry.

Downsides of the PBMC-based co-culture assay are high costs for FACS antibodies, and a laborious and time-consuming assay setup, as PBMCs have to be expanded over a time course of two weeks and since co-cultures assays without flow cytometric measurements can easily take 12 hours, if a decent number of TCRs are screened per assay. Also, using different PBMC donors for expansion can cause variability between assays. Such variability can be prevented by expanding a larger batch of PBMCs, cryopreserving them and thawing them as needed, as done when testing IDH1R132H TCRs derived from CD4+ clones.

On the other hand, the JURKAT-NF-κB eGFP and JURKAT-TPR-CD8ab reporter cell lines can be used to assess TCR reactivity. They can be electroporated with either DNA or RNA, making the overall assay setup more flexible as compared to expanded PBMCs (**Figure 3A**). Moreover, fluorescence can be quantified using a plate reader, which is faster and cheaper as compared to flow cytometric analysis, and in contrast to using expanded PBMCs, co-cultures can be run overnight, thereby resulting in more convenient timings of readout. In contrast to flow cytometric analysis, gating on mTCRβ positive cells is not possible, which might decrease the sensitivity when analyzing reactivity of TCRs with lower expression levels.

Both reporter cell lines that were used to establish JURKAT-based assays, especially JURKAT-NF-κB eGFP, expressed fluorescent markers in culture conditions that should not lead to activation (**Figure 3F**). This background signal might be an issue when screening TCRs with lower degree of reactivity or when assessing TCR reactivity in co-culture with tumor cell lines, as the background signal impairs sensitivity of the assay. Tumor-derived cell lines express lower amounts of MHC I molecules due to loss or downregulation to escape anti-tumor immunity, often lack MHC II expression, and should present less antigenic peptide as compared to APCs that were pulsed with supraphysiological amounts of peptide (Shklovskaya and Rizos 2021; Axelrod et al. 2019). It is therefore important to always quantify MHC I and II expression on tumor cell lines when using them for co-culture assays.

On top of that, MFI of GFP of activated TPR-CD8ab cells was low in co-culture assays, which might further decrease sensitivity in future plate reader-based assays (**Figure 3G**). CD4 and CD8 co-receptor expression were low or even absent in both lines, further decreasing sensitivity of JURKAT lines, as especially the CD8 co-receptor is important to stabilize interaction of a TCR and pMHC class I (**Figure**

3E) (Morch et al. 2020). It was surprising to see little to no expression of CD8 in TPR-CD8ab cells, as this cell line was engineered to overexpress CD8, and overexpression of CD8 was shown in the original publication (Rosskopf et al. 2018). JURKAT-TPR-CD8ab available in the laboratory had low proliferative capacities and were difficult to electroporate with TCR constructs, as this usually resulted in low cell viability and lower mTCRβ expression levels, despite culturing the cells according to the recommendations. Seeing that the JURKAT-NF-κB eGFP cell line had superior proliferative capacities, viability and mTCRβ expression levels after electroporation lead to the decision to use this cell line for future co-culture assays despite higher background expression of GFP. Co-electroporation of TCR constructs and a CD8ab-expressing construct might allow to also screen TCRs derived from CD8+ clones with higher sensitivity, as previously reported by others (Muller et al. 2020).

In summary, JURKAT reporter cell lines are well suited for screening TCRs against peptide-pulsed APCs, but should not be used to screen TCRs against tumor cell lines. They are a promising tool that might allow to scale up the TCR screening efforts while keeping material costs low and at the same time saving time as compared to using expanded primary cells as effectors. The possibility of using JURKAT reporter cell lines for high-throughput screenings for reactive TCRs was shown by the laboratories of Dirk Busch and Peter Steinberger (Muller et al. 2020). They used the TPR-CD8ab cell line discussed herein and showed functionality by screening TCRs against cytomegalovirus (CMV) peptides, but mostly focused on multimer staining of TCR-transduced cells and on comparison of the CD8+ transduced and CD8 negative TPR cell line, but did not discuss possible problems with background fluorophore expression. It would have been interesting to see if this pipeline could also be used to screen TCRs with lower affinity or target antigen expression as compared to CMV-reactive TCRs against peptide-pulsed PBMCs, as background activation could pose a problem for such TCRs. Low background of the TPR-CD8ab cell line was shown in a previous publication, but TCRs in this publication were expressed after retroviral transduction (Rosskopf et al. 2018). Possibly higher background reporter gene expression levels have to be expected upon electroporation of TCR-encoding DNA, as for example NF-κB is known to be an effector of the cGAS-STING pathway, which is activated in presence of cytosolic DNA (Liao, Du, and Wang 2020). Inhibition of this pathway could decrease background GFP expression of the JURKAT-NF-κB eGFP cell line, but would at the same time most likely affect TCR signaling. It would be interesting to run a side-by-side comparison of electroporated TCR-encoding DNA or RNA and to compare background activation, as single stranded RNA should not trigger this pathway.

Multiple laboratories in house and external collaboration partners are currently working on establishing new JURKAT reporter cell lines to screen TCRs in high throughput format with high sensitivity (Schmid et al. 2023). It is planned to use such cell lines for comparison with the JURKAT-NF-κB eGFP cell line, thereby also testing different reporter genes. A variety of add-ons are described in the literature to further increase the throughput for TCR testing. For example, T cell hybridoma lines were generated to express a NFAT reporter gene which induces expression of a fluorescent protein upon activation. Each line was engineered to additionally constitutively express a different fluorescent protein. After electroporation of each line with a single TCR construct and pooling of all cell lines together for co-culture as a multiplex, acquisition on a flow cytometer and gating on the fluorescent marker characteristic for each individual cell line allows for analysis of reactivity of individual TCR contained within the multiplex (Mann et al. 2020). Others use promising microfluidic approaches to co-culture TCR-transduced JURKAT cells and APCs in individual droplets and subsequently use FACS to sort out only those reaction compartments which express fluorescent proteins after reporter activation for sequencing (Kula et al. 2019; Li et al. 2023).

4.2 Performance and advantages of using ESPEC-SUIT for TCR discovery

ESPEC-SUIT was established to expand patient-derived PBMCs with reactivity against a peptide-of-interest, thereby allowing to pre-select TCRs for cloning and testing. After expansion, target populations of interest, such as CD4+ cells, CD8+ cells or TNFα secreting cells, can be further enriched prior to TCRβ deep sequencing to gain deeper insights into the relevant TCR repertoire.

Overall this assay allowed to screen for TCRs derived from either CD4+ or CD8+ clones in both vaccinated and non-vaccinated patients. For vaccinated patients, IDH1R132H-reactive TCRs from both CD4+ and CD8+ clones were identified, with an overall success rate of 88% for those derived from CD4+ clones. For both the NOA21 trial as well as the recently started INTERCEPT trial (ClinicalTrials.gov identifier NCT04808245), ESPEC will be used as a routine procedure for immune monitoring to be able to track relevant clones over time in blood. For example, ESPEC cultures were successfully used to identify TCRs derived from CD4+ clones reactive against the H3K27M epitope, highlighting the relevance of the H3K27M vaccine for a long-term survivor of midline glioma (pre-print available on bioRxiv, (Boschert et al. 2023)).

ESPEC cultures were also used to identify reactive TCRs against more diverse target epitopes in the scope of the TCR-POC consortium encompassing various tumor entities, using peptides for expansion that were selected based on analysis of the tumor mutanome. Two of three patients received anti-tumor vaccinations representative of their tumor mutanome prior to ESPEC, whereas one patient was not vaccinated with such a set of peptides. It was possible to expand relevant clones for all three patients, and so far, 25 reactive TCRs for patient POC-001 were identified. TCRs with higher levels of CD107a and TNFα after co-culture as quantified by flow cytometry seemed to be less dependent on the co-receptor, as cells positive for these markers contained a higher fraction of CD8+ T cells as compared to cells with lower levels of CD107a and TNFα expression. This indicates that both low and high affinity TCRs can be identified through ESPEC.

It is planned to screen a higher number of TCRs for patients POC-004 and POC-005, where ESPEC cultures were performed using peptide pools containing 97 and 203 individual peptides, respectively. Peptide pools reduce the number of PBMCs required for expansion and further strongly decrease the workload when running larger ESPEC cultures. Re-stimulation with individual peptides contained within the respective pools in QC ELISpot cultures allowed to immediately decode which individual peptide caused expansion of putative reactive clones. Moreover, this data helps to decide which post-ESPEC cultures should undergo TCRβ deep sequencing and which cultures can be excluded from sequencing, thereby saving costs. One possible downside of using peptide pools for expansion could be that single peptides might cause a strong expansion of individual clones, which could hinder clones with lower degree of reactivity or with reactivity against other epitopes contained in the pool from proliferation. A similar situation was observed when CMV peptide was included in a peptide-pool containing five individual peptides for ESPEC-based expansion of PBMCs from healthy donors. One clone took over 55% of the entire post-ESPEC repertoire, even suppressing post-ESPEC ELISpot responses against Flu peptide that was contained within the same pool, which elicited a strong response in QC ELISpots if used alone for expansion (not shown).

Other reasons for this observation could be that single peptides with high affinity could compete with lower affinity peptides for MHC binding, which could further inhibit expansion of individual clones. Moreover, some clones have low precursor frequencies in blood, making it harder for them to expand in ESPEC cultures with only $1*10^6$ PBMCs available per well at baseline. Even if multiple wells with the same condition are plated for expansion (which was the case for POC-004 and POC-005), such clones could easily suffer from proliferative restrictions if other clones with higher baseline frequencies take over the culture. All these reasons could potentially explain why replicates of ESPEC cultures for patient POC-005 did not always result in responses against the same peptides contained within the peptide

pools despite using the same culture conditions and using cryopreserved PBMCs from the same timepoints for expansion.

Also, if multiple peptides from the same pool elicit a signal in the QC ELISpot, TCRs expanding in this culture have to be tested against multiple peptides to identify the true target. As an alternative, a second ESPEC with only one peptide per condition can be performed after a first initial screening assay in which peptide pools are used.

ESPEC assays performed with heavy labelled peptides from MS analysis for POC-004 showed that these peptides caused high background upon re-stimulation in ELISpot as compared to in-house synthesized peptides. This underlines the importance of using peptides of high quality to prevent non-specific expansion. A second lesson learned from ESPEC cultures of patient POC-004 is that background in post-ESPEC QC ELISpots can depend on the degree of reactivity against a specific target epitope, which can cause strong T cell activation. Using EBV peptide for expansion caused such strong T cell activation, that in the post-ESPEC QC ELISpot quantification of spot counts, even in wells containing cells without re-stimulation was, impossible.

Interestingly, patient POC-005 did not receive any of the peptides used for screening as vaccination prior to ESPEC, but it was possible to expand clones reactive against 15 of 189 tested peptides in at least one assay, highlighting the relevance of ESPEC cultures to identify putatively tumor-reactive TCRs and putative immunogenic antigens in tumor patients. None of these peptides were predicted to be presented based on MS data, which is in accordance to observations by others, who found incomplete overlap of the set of neoepitopes that were detected by reactive T cells and the set of neoepitopes identified using immunopeptidomics (Wickstrom et al. 2019). Overall this indicates that MS analysis does not necessarily reflect the true tumor immunopeptidome due to limitations in assay sensitivity, or, as suggested by Wickstrom et al. (2019), instability of pMHC class I complexed and lower sensitivity of MS in regards to detection of hydrophobic peptides or peptides containing cysteine residues. Patient POC-005 was suffering from a melanoma metastasis contained within the lymph node. Melanomas are known for their overall high mutational load, which can increase the possibility of identifying reactive TCRs (Chalmers et al. 2017; Jardim et al. 2021). Tumor reactive CD8+ TCR clones were also identified in lung cancer patients using the MANAFEST assay, a peptide-based expansion assay described in detail below (Caushi et al. 2021). It would be interesting to test ESPEC-SUIT for tumor samples with lower mutational load, such as primary brain tumor samples, for which it was not possible to identify reactive TCRs when using preliminary gene signatures (see chapter 3.5) (Chalmers et al. 2017). The Rosenberg laboratory successfully identified a tumor-reactive TCR from blood of one of five tested glioblastoma patient using peptide- and TMG-based expansion assays, indicating that such an approach could be successful (Leko et al. 2021).

For patient POC-005, it is planned to screen a maximum of 666 TCRs derived from post-ESPEC cultures for reactivity, depending on how many of them can be found in single cell sequencing datasets. Validation of a larger number of TCRs will be possible soon, as high-throughput assays for cloning of TCR-encoding RNA were established and since high-throughput JURKAT-based assays for screening of TCRs are becoming available (see chapter 4.1). Screening a higher number of TCRs per ESPEC run will further allow to re-define the procedure used for selection of TCRs based on TCRβ deep sequencing data. At the moment TCRs are selected using the FEST algorithm from Danilova et al. (2018), but T cells with high expansion in ESPEC were frequently observed to be excluded from analysis by this algorithm as their frequency at baseline before ESPEC was low. Most clones that strongly expanded in ESPEC against IDH1R132H but with proportions between 10^{-5} -10^{-4} at baseline were not suggested for further analysis by FEST. Seeing that clones with such low frequencies were able to expand dramatically in ESPEC underlines the sensitivity of ESPEC and points out the need to re-think how TCRs are selected using on post-ESPEC TCRβ deep sequencing data.

The FEST algorithm was designed to analyze data from MANAFEST (Mutation-Associated Neoantigen Functional Expansion of Specific T cells), a peptide-based expansion assay that is similar to ESPEC, but differs in the culture conditions used for expansion and was designed for expansion of CD8+ T cells. In MANAFEST, T cells are isolated from PBMCs using column-based magnetic enrichment, with the T cell-negative fraction being irradiated and co-cultures being set up with an equal number of non-irradiated T cells and irradiated cells, which are both stimulated with the peptide-of-interest. After three days, cytokines are added to boost proliferation.

In contrast to MANAFEST, ESPEC cultures use rested PBMCs without prior irradiation or T cell enrichment: 50% of cells are pulsed with peptide for four hours before pooling non-pulsed and pulsed PBMCs together. This prevents intra-culture fratricide of peptide-loaded T cells and simplifies the protocol considerably. MANAFEST was designed to monitor expansion of CD8+ clones only, whereas both CD4+ and CD8+ responses can be detected using ESPEC, again underlining that ESPEC cultures are useful for analyzing the overall T cell responses against epitopes of interest in patients using blood instead of only the CD8+ T cell responses. As discussed later in chapter 4.3.5, both CD4 as well as CD8 T cell responses are important to mount an anti-tumor immune response.

Over the last few years, a variety of creative assays for pre-selection of TCRs for cloning and testing were published, which I shortly want to touch on and compare with ESPEC. For example, T cells from PBMC were expanded against patient-derived organoids (Dijkstra et al. 2018). At first sight this seems to be a promising alternative to ESPEC cultures, as tumor-derived organoids should only express the target epitopes of interest and are not biased by bioinformatic analysis of the tumor mutanome. T cells from PBMCs used for expansion should not target autologous tissue, and it is not required to synthesize peptide for expansion assays, thereby saving both costs as well as time. Downsides of this assay are that it is might not always be possible to obtain sufficient amounts of tissue for such analysis. The authors claim that biopsies are sufficient to run the assay, but only used tumors with high mutational load and high tumor cell densities for their expansion cultures. Furthermore, organoids could potentially change their mutational landscape while being cultivated ex vivo, with some mutations being lost and others potentially being expressed but presented at a lower level as compared to in vivo, which could prevent expansion of relevant clones in culture.

In another approach, TILs were co-cultured with DCs that expressed neoantigens encoded by tandem minigenes (TMGs), which were designed and cloned based on analysis of the tumor mutanome. After co-culture, T cells were then used for single cell sequencing to obtain information on gene expression profiles as well as V(D)J sequences associated with each clone. T cells that upregulated IFNγ as well as IL-2 upon co-culture were selected for cloning and testing (Lu et al. 2021). One major advantage of this assay is that it can performed with small numbers of TILs, thereby abolishing the need for pre-expansion of TILs using standard expansion protocols without peptide stimulation, as such cultures were reported to cause loss of tumor-reactive clones over time (Poschke et al. 2020). Besides that, TILs should contain higher numbers of tumor-reactive clones as compared to PBMCs as they are actively recruited to the tumor, increasing the probability of identifying reactive clones (Melero et al. 2014). However, costs for single cell sequencing are high and clones with low precursor frequencies could potentially be missed in single cell analysis, or clones with background activation could misleadingly be regarded as reactive. On top of that, tumor-reactive clones that underwent exhaustion within the TME might be less responsive to stimulation in co-culture. ESPEC assays are more robust and less sensitive to such small variations as T cells are expanded over a period of two weeks, allowing for proliferation of clones with small precursor frequencies and exclusion of irrelevant clones by parallel expansion of cells without peptide. Tumor-reactive clones are more likely to have smaller frequencies in blood as compared to tissue, but can be expanded from blood from low precursor frequencies as observed for reactive TCRs identified from TCR-POC patients (**Figure 10D**).

Another useful tool to pre-enrich putatively reactive TCRs against an epitope of interest can be multimers. Multimers are engineered MHC molecules loaded with a peptide-of-interest, which bind to TCRs reactive against this particular pMHC complex. If coupled to a fluorophore, FACS allows for enrichment for subsequent sequencing of putatively reactive clones; If coupled to a DNA-barcode, relevant clones can be identified in single cell sequencing data. Downsides of this type of assay are high costs associated with production of the multimers and that the HLA-allele presenting a peptide-of-interest has to be known a priori, making this approach less flexible as compared to ESPEC cultures. Moreover, not all MHC I alleles and most MHC II alleles were not yet successfully used for production of multimers, further limiting the number of epitopes that could be in principle used for screening analysis. In addition, such screening approaches are extremely slow in case new multimers have to be designed and cloned for individual patients, and T cell clones with low precursor frequencies are difficult to enrich (Chang 2021).

Thus, ESPEC is a promising approach for pre-selection of interesting TCRs for cloning and testing, which can compete with other wetlab-based approaches that are currently available in the field. The assays can be run using either peripheral blood or TILs. Peptide pools instead of single individual peptides can be used for expansion with some limitations, thereby decreasing the need for a large number of PBMCs as starting material and reducing the burden of having to withdraw high amounts of blood from patients. It was shown that clones with low precursor frequencies in blood can be expanded and tracked over time in blood and tissue. ESPEC does help to identify reactive TCRs against a pre-defined antigens-of-interest, but in contrast to multimer analysis, it does not rely on pre-definition of a specific HLA-allele of interest. ESPEC assays are easy to perform and can be implemented as a standard method for immune monitoring.

4.3 Screening for IDH1R132H-reactive TCRs

4.3.1 Affinity of IDH1R132H-reactive TCRs

Vaccinations with long IDH1R132H peptide were highly successful in pre-clinical studies with mice as well as in the NOA16 phase I clinical trial where safety as well as immunogenicity were shown in patients with newly diagnosed WHO grade III and IV IDH1-mutant astrocytomas (Schumacher, Bunse, Pusch, et al. 2014; Platten et al. 2021).

To gain a deeper understanding of the T cell response induced in patients that received the long IDH1R132H peptide vaccine, a total of 123 TCRs derived from CD4+ T cells were selected through ESPEC assays and screened for reactivity, of which 106 were tested to be reactive in co-culture assays with peptide-pulsed DCs. Surprisingly, 49 of 106 TCRs were also reactive against IDH1-wildtype peptide in in vitro assays (**Figure 5B**), which is in contrast to previous literature where no cross-reactivity to IDH1-wildtype (p123-142) was described in ELISpot assays using splenocytes of vaccinated A2.DR1 mice (Schumacher, Bunse, Pusch, et al. 2014). However, reactivity to IDH1-wildtype peptide was observed in IFNγ ELISpot assays upon restimulation of PBMCs of patients included in the NOA16 and NOA21 trial using IDH1-wildtype peptide (p123-142), with consistently less wildtype reactive cells as compared to cells reactive against mutant IDH1 being detected (unpublished data and **Figure 4A**). Despite these findings, no adverse effects, such as auto-immunity, related to potential cross-reactivity were observed in patients that received the peptide vaccine (Platten et al. 2021).

Using peptide-titration assays in TCR co-culture assays revealed that reactivity of seemingly cross-reactive TCRs to the wildtype and mutant peptide decreased in a dose-dependent manner if decreasing peptide concentrations were used for peptide-pulsing of DCs. While reactivity to the IDH1-wildtype peptide was absent using peptide-pulsing concentrations of 10^{-8} M peptide, reactivity against IDH1R132H was still well detectable. Reactivity to mutated IDH1 peptide as quantified with %CD107a+

cells after co-culture decreased by 50% if concentrations between 10^{-7}-10^{-8} M peptide were used for peptide-pulsing of DCs (1 h incubation) (**Figure 5F**). Matching these observations, a 50% inhibition of TCR::peptide-MHC II interactions were reported for concentrations between 10^{-4}-10^{-7} M as measured using soluble pMHC or soluble TCRs for a small set of TCRs in other early studies (Eisen, Sykulev, and Tsomides 1996). Later publications mention that TCRs with an affinity higher than 10^{-7} M might not lead to any functional advantages, as prolonged TCR-pMHC interactions could potentially lead to exhaustion (Slifka and Whitton 2001).

Overall, this data could indicate that TCRs with a positive signal upon co-culture against high amounts of IDH1-wildtype peptide could have an overall higher affinity to IDH1R132H peptide, which might cause the TCRs to also weakly bind to APCs presenting IDH1-wildtype peptide. Upon supraphysiological presentation of IDH1-wildtype peptide, TCRs might have repeated short and weak encounters with pMHC complexes presenting IDH1-wildtype peptide, with the sum of all interactions potentially causing a positive T cell response. The amount of peptide presented on DCs in in vitro assays is likely higher as compared to the amount of antigen presented in vivo due to (I) lower amounts of MHC II molecules presented on the surface of tumor cells or associated APCs in the tumor microenvironment (TME) as compared to professional APCs such as DCs (Axelrod et al. 2019), and (II) high peptide-pulsing concentrations used in vitro. If this is true and if the amount of IDH1-wildtype peptide presented is sufficiently low, an in vivo autoimmune response of wildtype-reactive TCRs is unlikely.

It is planned to run further titration assays for additional seemingly cross-reactive TCRs to validate previous observations on a larger set of TCRs, covering those with low, medium and high reactivity as quantified by the percentage of CD107a+ or TNFα+ cells after co-culture with mutated peptide. The peptide-titration curves of the two seemingly cross-reactive TCRs presented in **Figure 5** showed a relatively high reactivity to IDH1R132H in co-culture assays as compared to other TCRs from the same patient (range %TNFα+ cells upon co-culture with 10^{-5} M IDH1R132H peptide for patient ID2: 5.4-55.7%, both TCRs expressed 55.7% or 36.9% TNFα, respectively). It will be interesting to see whether TCRs with lower degree of cytokine secretion behave similar to the previously discussed TCRs. Moreover, it could be interesting to also determine the IC50 values by titrating soluble peptide-MHC II tetramers on T cells transduced with TCRs of interest and to be able to compare this data to previous publications. IC50 values cannot be precisely determined using peptide-pulsed DCs, as the amount of peptide that is presented depends on the duration of peptide pulsing and the capability of DCs to take up antigen, which might vary between donors.

Quantification of the amount of IDH1-wildtype or -R132H peptide presented in tumor samples would be interesting to translate our findings on TCR reactivity under varying peptide concentrations to the in vivo situation. Unfortunately, it is difficult to determine the absolute amount of pMHC complexes per cell. Using MS approaches for quantification, bias could be easily be introduced during sample preparation due to loss of peptide during cleanup steps (Hassan et al. 2014). A second problem is that absolute quantifications of pMHC molecules per cell is not possible since the number of (tumor) cells per tissue sample cannot be determined (Stopfer et al. 2021). As an alternative approach to quantify pMHC complexes per cell, antibodies against pMHC complexes of interest could be generated using a laborious method that is based on an antibody phage display library (Cohen et al. 2003). These antibodies could then be used to stain tumor single cell suspensions of patients that carry the HLA allele of interest. The relative amount of pMHC presented on the cell surface could be quantified using fluorophore-coupled antibodies and flow cytometry. However, no public data on antibodies generated against peptide-MHC II complexes were found in the literature, it seems only antibodies against peptide-MHC I complexes were produced so far (Vest Hansen et al. 2001; Cohen et al. 2003). Recombinant expression of MHC II molecules before presentation to the phage-display library is likely

more difficult compared to recombinant expression of MHC I molecules, as reported for pMHC class II tetramers (Lantz and Teyton 2022).

Another option to analyze presentation of pMHC II on tumor cells is based on the use of a proximity ligation assay (PLA). Our laboratory previously showed co-localization of IDH1R132H peptide and HLA-DR in human paraffin-embedded tissue by using antibodies able to bind to both epitopes (Bunse et al. 2015). Binding of the antibody to IDH1R132H peptide in complex with HLA-DR was shown using an immune-competitive ELISA. Proximity between the anti-IDH1R132H and anti-HLA-DR antibodies was demonstrated using secondary antibodies that carry short DNA sequences. A rolling circle PCR allows for amplification of DNA only if both antibodies bind in close proximity to another, thereby allowing DNA to hybridize into a circular structure, which can then be amplified using fluorescently-labeled complementary oligonucleotide probes and detected by fluorescence microscopy (Alam 2018). If both antibodies do not bind in close proximity to another, no DNA can be amplified and no fluorescent signal is measured. For IDH1R132H and HLA-DR, a positive signal at both the extracellular membrane as well as within intracellular vesicles was detected in a glioma cell line, indicating co-localization (Bunse et al. 2015). When analyzing tissue samples of patients with IDH1R132H-mutant gliomas, 7/46 samples were non-evaluable due to high background, and assay background was also partially observed in cell lines used for evaluation of co-localization. Due to these drawbacks, it could be difficult to effectively quantify the number of peptide-MHC II molecules presented on the cell surface using PLA assays.

4.3.2 Reactivity against processed IDH1R132H peptide and discussion of wildtype reactivity

Another open question to be answered is whether IDH1R132H-reactive TCRs identified in the scope of this thesis are only reactive against APCs that were exogenously loaded with peptide, or whether they can also recognize intracellularly processed peptide. Interesting studies from Unanue and colleagues 27 years ago showed that vaccination of mice against the hen egg lysozyme (HEL) antigen with subsequent generation of T hybridoma lines results in two different types of T cell hybridomas. While “type A” hybridomas show similar response curves to naturally intracellularly processed peptides and exogenously loaded synthetic peptide, “type B” hybridomas are either unresponsive to intracellularly processed HEL peptide or require several magnitude higher concentrations to elicit IL-2 secretion. The peptide sequences presented on murine MHC II haplotype I-A^k after intracellular processing and exogenous loading of peptide were the same (Viner et al. 1996).

The Unanue laboratory showed that one and the same immunogenic peptide sequence can be presented in two different 3D conformations within a given MHC II molecule, depending on the mode of loading (Viner et al. 1996). The presence of two different 3D conformations was also shown for other antigenic peptides on murine MHC II, such as one derived from pigeon cytochrome *c* (PCC; p89-104) (Schmitt et al. 1999), myelin basic protein 2K 4A (MBP to which 2K 4A mutations were introduced to increase binding affinities to MHC II) found in a stable long-lived and less stable short-lived conformation (Rabinowitz et al. 1997), or sperm whale myoglobin (p110-121) peptide with low affinity to murine MHC II I-E^d (Beeson and McConnell 1994).

A later publication revealed that while exogenously loaded peptide binds to MHC II in early endocytic compartments (or in a peptide-exchange reaction directly to MHC II molecules on the cell surface (Beeson and McConnell 1994)), naturally processed peptide interacts with MHC II molecules in late endosomal/lysosomal vesicles under the presence of HLA-DM, which only allows formation of the most stable peptide-MHC II interactions (Pu et al. 2004). As a result, two types of T cell responses against two antigenically diverse targets can potentially be generated. Immunizations with exogenously loaded peptide (e.g. by vaccination) elicits T cell responses that are reactive against (I) the stable conformation found after intracellular natural processing (observed 70% of T cell clones after

immunization of mice with HEL antigen) and (II) the less stable peptide-MHC II conformation observed after exogenous loading of peptide but not after intracellular processing (30% of T cell clones after immunization with HEL antigen) (Pu et al. 2004). T hybridomas that are reactive against the less stable conformation resulting from exogenous peptide loading require an at least 100-fold greater concentration of intact HEL protein as compared to peptide for half-maximal stimulation, whereas T hybridomas induced from naturally processed antigen and therefore reactive against the stable conformation have similar responses to peptide or intact HEL protein (Viner et al. 1996).

What are the implications of these findings for the IDH1R132H-reactive TCRs described in this thesis? First, it has to be considered that some of the TCRs that were found to be reactive might solely recognize exogenously loaded peptide, but not naturally processed IDH1R132H peptide. It is therefore important to test reactivity of all tested TCRs against IDH1R132H-mutant tumor cell lines. As it was not possible to generate such cell lines from any of the analyzed tumor samples so far, tissue-derived organoids are currently investigated as an alternative approach for T cell co-culture assays in an autologous setting. Moreover, it is planned to use CRISPR-Cas to introduce the R132H point mutation into autologous B-LCLs to have unlimited numbers of APCs with naturally processed peptide available for co-culture assays, or to use a U87 glioma cell line with heterozygous expression of R132H after CRISPR-engineering.

Second, it might be interesting to analyze whether TCRs with IDH1-wildtype reactivity might have been induced by exogenous peptide loading. Reactivity to wildtype peptide was not expected when screening TCRs, as immune responses with potential autoreactivity should be eliminated during thymic selection. As also shown in another publication by the Unanue laboratory, T cells reactive only to exogenously loaded peptide are unaffected by thymic selection, as only naturally processed peptide is presented by APCs within the thymus (Peterson et al. 1999). This could indeed apply to TCRs that might solely be reactive against exogenously loaded peptide, as suspected for IDH1R132H TCRs that are reactive to both wildtype and mutant IDH1 if supraphysiological peptide concentrations are used.

Further evidence for this hypothesis comes from a publication by Rabinowitz et al. (1997). They found that the MBP 2K 4A peptide can be presented as two structurally different isomers on the murine MHC II haplotype I-A^k, either as a short-lived intermediate or in a long-lived conformation. Both isoforms were specifically recognized by two different T cell clones which differed in their TRBV gene usage (Rabinowitz et al. 1997). Interestingly the T cell clone recognizing the short-lived intermediate pMHC structure also showed reactivity against MBP-wildtype peptide, which was hypothesized to be due to structural similarities of the short-lived pMHC MBP 2K 4A complex and the wildtype peptide (Rabinowitz et al. 1997). This would match observations for IDH1R132H-reactive TCRs which are reactive against IDH1-wildtype peptide, which I hypothesize to bind to and be similar in structure to a short-lived conformation of IDH1R132H on MHC II.

To challenge this hypothesis, one could co-culture potentially cross-reactive TCRs with APCs or tumor cells that naturally processed the IDH1R132H antigen. Based on aforementioned findings, it would be expected that TCRs with wildtype and mutant reactivity respond little or not at all to endogenously processed IDH1R132H.

Another hypothesis for IDH1-wildtype reactivity could be that the wildtype epitope is not or only weakly presented by MHC II, which could also allow for thymic escape of wildtype-reactive clones and would not result in auto-immunity. As no adverse effects of IDH1-wildtype reactive TCRs are observed in patients, little or no presentation of the IDH1-wildtype epitope is very likely (unpublished data). To fully exclude the potential of generating immunogenic cross-reactive TCRs by vaccination, one could consider using mRNA-based vaccines instead of peptide-based vaccines, which generate pMHC complexes that have to undergo intracellular natural peptide loading. It would be interesting to test

whether vaccinations of mice with mRNA-encoded IDH1R132H does indeed not induce any cross-reactive clones, or if mRNA or full protein pulsed on APCs fails to stimulate IDH1-wildtype reactive clones in vitro. This could have implications for future vaccination studies, as the risk of accidentally generating a truly autoreactive cross-reactive TCR could be reduced using mRNA vaccines.

Importantly, as (I) a R132H but non-wildtype-reactive TCR was found within the pre-vaccination FFPE tissue of patient ID3 which later expanded in blood upon vaccination, and since (II) a R132H- TCR but non-wildtype reactive was found expanded at baseline of patient ID1 (as based on TCRβ deep sequencing data, $4*10^{-2}$ % of the peripheral repertoire), it can be presumed that natural processing of IDH1R132H and induction of an immune response is possible in vivo. Vaccination with the p123-142 peptide can boost this immune response, as both of these TCRs expanded after vaccination (**Figure 6, B and F**). The presence of pre-induced immune response in few non-vaccinated IDH1-mutant glioma patients further supports this hypothesis (Schumacher, Bunse, Pusch, et al. 2014). No IDH1-wildtype reactivity was observed in ELISpot for one patient for which IFNγ ELISpot analysis at baseline before onset of vaccination is available, but wildtype reactivity was induced upon vaccination (unpublished, data by Theresa Bunse (DKFZ Heidelberg, Germany), data not shown). However, it has to be noted that a total of 12/90 TCRs identified in this thesis using ESPEC were found at very low frequencies within TCRβ deep sequencing data of blood ($2.9*10^{-4}$ - $3.9*10^{-3}$ % of the entire repertoire), of which four were later tested to be cross reactive (frequencies of $2.9*10^{-4}$ – $5.7*10^{-4}$ %). A pre-existing immune response against wildtype and mutant IDH1R132H peptide could indicate that either the discussed hypothesis of pMHC isomers induced by exogenous loading of peptide is wrong, or that exogenous peptide loading can occur in vivo, for example upon cell death and release of peptide, which needs to be further analyzed.

In contrast to that, further overall support for the above-mentioned hypothesis that vaccination with IDH1R132H might generate two antigenically diverse targets can be drawn from co-culture experiments with peptide-pulsed B-LCLs when screening for HLA restrictions (**Figure 7**). A total of 21 reactive TCRs were included in the screening (6 with only R132H-reactivity, 15 with reactivity to both wildtype and R132H peptide, as tested before using peptide-pulsed DCs), of which seven did not elicit a positive response after co-culture with peptide-pulsed non-modified B-LCLs despite sufficiently high mTCRβ expression. None of the TCRs with only R132H-reactivity showed reactivity upon co-culture with peptide-pulsed B-LCLs.

The initial screening to classify TCRs as reactive or “cross-reactive” was performed using DCs, which take up IDH1R132H peptide by micropinocytosis or phagocytosis (Liu and Roche 2015), thereby naturally processing the peptide and putatively generating a stable pMHC class II isoform. B cells present antigen after B cell receptor (BCR)-mediated endocytosis and then naturally process and present peptide on MHC molecules, also putatively generating the stable isoform (Adler et al. 2017). In general, peptide can be loaded on MHC molecules that are already present on the cell surface by a simple exchange reaction between the presented peptide and a suitable second peptide found in solution (Schmitt et al. 1999). As immortalized autologous B-LCLs, which were expanded from a small number of B cell clones, were used for CRISPR-based co-culture screens of HLA restrictions, it is likely that most of the IDH1R132H peptide was being introduced to MHCII by exogenous loading, independently of a BCR. This could generate a short-lived pMHC class II isomer that is only detected by TCRs with wildtype and R132H reactivity. In contrast to that, DCs most likely are able to present a mixture of both isomer forms, as the stable conformation can be generated after peptide uptake and intracellular processing, while the less-stable conformation originates from a parallel reaction through peptide exchange on pMHC class II molecules presented on the cell surface. Further assays testing the reactivity of IDH1 TCRs with wildtype reactivity against peptide-pulsed B-LCLs are required to confirm these results.

In the study by Rabinowitz et al. (1997), the fraction of long-lived pMHC molecules increased with longer peptide pulsing times for MBP 2K 4A. One could expect that longer peptide-pulsing durations with IDH1R132H would therefore favor presentation of the long-lived stable pMHC isoform. This could be reflected in the decrease in %CD107a+ cells of R132H-reactive TCRs when pulsing 10^{-5} M peptide on DCs for one hour instead of overnight using the same concentration of peptide (**Figure 5F**, left side). A decrease in %CD107a+ cells cannot be observed for wildtype and R132H-reactive cells under the same conditions, which could be explained by the fact that these TCRs bind to short-lived less stable pMHC isoforms, which are more rapidly formed as compared to intracellularly processed peptide (**Figure 5F**, right side). Peptide titration assays of a higher number of TCRs are required to confirm these results.

Overall, the presence of two isoforms of pMHC complexes for IDH1R132H could also be the reason why previous peptide affinity screening assays resulted in data that was difficult to interpret (data not shown; NeoScreen assay by Immunitrack, Copenhagen, Denmark). The assay was performed as described before and stability of the peptide-MHC class II complex was measured after heating the complex at 60°C for 30 min, 1 h, 2 h and 4 h (Justesen et al. 2009). Notably peptide-MHC complexes were generated by re-folding MHC II molecules in presence of peptide. Suboptimal affinities of the peptide to DRB1*01 were detected, with wildtype IDH1 peptide seemingly having higher affinity as compared to mutant peptide. DRB1*01:01 is expressed by A2.DR1 mice along with DRA*01:01 in preclinical vaccination studies in which a vaccine-induced anti-IDH1R132H T cell response was observed, so binding of the long IDH1R132H peptide vaccine to this allele is expected (Schumacher, Bunse, Pusch, et al. 2014). Difficulties in interpretation of peptide affinity screening data could be in part due to exogenous loading of the peptide for these assays instead of using pMHC class II complexes that were naturally loaded through intracellular processing under guidance of HLA-DM.

It would be interesting to analyze the 3D structure of IDH1R132H and IDH1-wildtype peptide within the associated relevant MHC II binding pocket to understand the mode of interaction between a reactive TCR and the IDH1R132H peptide bound to MHC II. This might allow us to understand why IDH1-wildtype peptide can elicit a T cell response in about half of the TCRs presented in this thesis if used at supraphysiological concentrations in in vitro co-culture assays. Off note, no IDH1R132H-reactivity was generated in mice that were vaccinated with the IDH1-wildtype peptide and no growth suppression of their IDH1R132H-expressing sarcomas was observed (Schumacher, Bunse, Pusch, et al. 2014).

Accurate bioinformatic predictions of peptide-MHC II interactions are currently still problematic. With limited understanding on how interactions between peptide and MHC II molecules are mediated, pipelines to model 3D structures of pMHC class II complexes are difficult to implement, as they require structural templates, which are not always available (Cheng et al. 2021). Moreover, they require information on anchor residues for peptide binding, which are partially conserved for MHC I and II, but for which also non-canonical peptide anchor positions were reported (Marzella et al. 2022). New pipelines to understand the 3D structure of long peptides presented on MHC II are currently being established in multiple laboratories which could potentially be used to model 3D structures of IDH1R132H in MHC II alleles or at least pave the way for improved structural modelling of peptide-MHC II complexes (Marzella et al. 2022; Li et al. 2019; Mikhaylov and Levine 2023).

Most publication on the existence of two pMHC isoforms are more than two decades old and such analyzes are not mentioned in publications nowadays, especially not in those trying to model the structure of pMHC II complexes. If the isomer hypothesis turns out to be true for IDH1R132H-reactive TCRs, it would be interesting to collaborate with laboratories working on structural modelling of peptide MHC II complexes to understand how a single peptide sequence can possibly elicit two different types of T cell responses. It would also be interesting to analyze if these findings can be

applied to analyze if other peptide vaccines are also at risk to be presented as two antigenically diverse isomers with different immunogenicity, which could potentially limit their efficiency. Furthermore, such analysis could potentially help to understand autoimmune diseases, which emerge if T cell responses are not removed by thymic selection (also called central tolerance) or peripheral tolerance (Khan and Ghazanfar 2018). Autoimmunity is frequently found to be associated with specific MHC alleles (Khan and Ghazanfar 2018). Potentially they could be caused by specific peptide sequences which are presented in two different 3D conformations, with one of them being similar to an autogenic antigen.

4.3.3 HLA restrictions of IDH1R132H reactive TCRs

Modelling the 3D structure of peptide-MHC II interactions and use of TCRs for TCR-transgenic therapy requires information on which HLA allele presents the IDH1R132H peptide to a given reactive TCR. Restrictions to HLA-DR, -DP and -DQ isotypes were tested by CRISPR-based targeting of individual isotypes in B-LCLs and using the resulting cell lines as APCs for co-culture assays (**Figure 7**). A total of 13/14 TCRs were restricted to HLA-DR, with only one TCR being restricted to HLA-DQ. While this dataset is currently limited in size as TCRs of only one patient were tested, the predominant restriction to HLA-DR is in accordance with pre-clinical studies in A2.DR1 mice (expressing human HLA-DRA*01:01 and HLA-DRB1*01:01), in which a DR-restricted anti-IDH1R132H immune response was generated after vaccination with the 20-mer peptide p123-142 (Schumacher, Bunse, Pusch, et al. 2014). Moreover, HLA-DR blocking was shown to hinder T cell response in vaccinated mice and moreover the IFNγ PBMC ELISpot response in at least one patient with pre-existing IDH1R132H reactive T cells (Schumacher, Bunse, Pusch, et al. 2014). Taken together, this data suggests that the long IDH1R132H peptide binds promiscuously to a variety of HLA-DR alleles. It is planned to confirm these results by analyzing the HLA-restriction of further TCRs that were found to be reactive from patients ID1 and ID3-ID7. Moreover, it is planned to determine which precise HLA alleles are able to present the long IDH1R132H peptide using either knockout experiments in autologous B-LCLs, or by overexpressing specific HLA alleles in non-autologous B-LCL lines, which do no elicit a positive TCR signal if used as APCs in co-culture in their unmodified state.

Interestingly, vaccination with IDH1R132H peptide resulted in a positive T cell response in most patients participating in both the NOA16 trial (26/32 patients, (Platten et al. 2021)) and the NOA21 trial (ongoing, unpublished data) as quantified by IFNγ ELISpot analysis, despite patients not being pre-selected based on their HLA allelotype. This indicates that a large number of MHC II alleles is able to bind and present the long peptide vaccine, which could be, as discussed previously, based on promiscuous binding of IDH1R132H peptide to diverse alleles of the HLA-DR isotype. Promiscuous binding of peptides to different HLA-DR alleles has been described for a variety of target epitopes, for example for tetanus toxin (Panina-Bordignon et al. 1989) or a vaccine containing six melanoma-related peptides (Hu et al. 2014; Consogno et al. 2003).

DR molecules might be particularly susceptible for promiscuous binding of peptides as they are made up of a monomorphic alpha chain (HLA-DRA1 gene) and a polymorphic beta chain (HLA-DRB1, -DRB3, -DRB4 and -DRB5 genes), with more than 700 possible beta chains but only five possible alpha variants being available for combination (Panina-Bordignon et al. 1989; van Lith, McEwen-Smith, and Benham 2010; Suzuki et al. 2021). In contrast to that, HLA-DP (encoded by HLA-DPA1 and -DPB1 genes) and HLA-DQ (encoded by HLA-DQA1 and -DQB1) are made up of two polymorphic chains, thereby vastly increasing the number of possible alpha-beta chain combinations as compared to HLA-DR (van Lith, McEwen-Smith, and Benham 2010; Racle et al. 2023; Heijmans, de Groot, and Bontrop 2020). Polymorphic residues of alpha and beta chains define which peptides are able to bind to a given MHC II allele. They are positioned at the peptide-binding site with positions P1, P4, P6/7 and 9 being

common anchor positions for peptides, defining the amino acids that are pointing towards the peptide-binding groove, while remaining residues are open for interaction with a TCR (Racle et al. 2023; Unanue, Turk, and Neefjes 2016). With the alpha chain being invariant, chances are higher that HLA-DR molecules that differ in their beta chain can bind to the same peptide. Promiscuous binding of the IDH1R132H peptide to various HLA-DR alleles could be the reason why the vaccine can generate a positive T cell response in large proportions of the population carrying variable HLA alleles.

At the moment it is not yet possible to define a CDR3 motif based on the number of TCRs for which HLA restrictions were determined (**Table 8**). It is planned to establish a larger dataset of putatively reactive TCRs by co-culturing post-ESPEC cultures with IDH1R123H-expressing cells that underwent HLA-DR, -DP, and -DQ knockout, respectively. FACS will be used to enrich for TNFα secreting cells which will then undergo TCRβ deep sequencing, thereby allowing to distinguish between clones with specific HLA restrictions and possibly allowing for motif analysis.

4.3.4 Tracking IDH1R132H-reactive T cell clones over time and in space

As discussed, two types of IDH1R132H-reactive TCRs were identified, either reactive against only mutant (n=57), or reactive against both mutant and wildtype IDH1 peptide (n=49). Comparing the proliferative capacity of both types of clones did not reveal preferential expansion of one or the other group of TCRs when tracking TCRs identified to be reactive over time in peripheral blood (**Figure 6, A and B**). The overall kinetics of the cumulative frequency of clones tested to be reactive per timepoint as based on TCRβ deep sequencing data of PBMCs appears similar to the kinetics observed in IFNγ ELISpot analysis of PBMCs (**Figure 6, B and C**). In addition to that, the kinetics of the cumulative frequency of TCRs reactive against only IDH1R132H matches the kinetics observed in IFNγ spot counts upon stimulation with IDH1R132H minus IDH1-wildtype peptide (**Figure 6, B and C**). This confirms that indeed a representative set of relevant TCRs were selected for cloning and testing based on post-ESPEC data, despite not cloning all TCRs suggested by the FEST algorithm (15/19 (ID4) or 17/51 (ID5), **Table 7**).

Most clones were induced through vaccination and were absent in blood at baseline, whereas those present at baseline (12/90, only taking patients with baseline TCRβ deep sequencing data into account) had low basal frequencies of $2.9*10^{-4}$ - $3.9*10^{-3}$ % as compared to maximum frequencies of up to $6.6*10^{-3}$ - $1*10^{-1}$ % of the same TCRs after receiving the IDH1R132H vaccine. Potentially more TCR clones were present at baseline which could be detected if the sequencing depth and input material would be even further increased. Only one clone with a relatively higher frequency of $4.0*10^{-2}$ % was found within the peripheral repertoire of patient ID1, which did not expand strongly after the patient received two doses of vaccination ($4.1*10^{-2}$ % at V7/EOT). Eight of these pre-existing clones were later shown to be reactive against only IDH1-mutant, including the aforementioned pre-expanded clone of patient ID1 (frequencies at baseline $3.5*10^{-4}$ – $3.9*10^{-3}$ %, excluding the expanded clone). Four clones were reactive against both wildtype and mutant IDH1, which had a slightly lower baseline frequency of $2.9*10^{-4}$ – $5.7*10^{-4}$ %.

No positive responses against IDH1R132H were observed at baseline before onset of vaccination for any of these patients in IFNγ ELISpot, for which 300,000 PBMCs were analyzed per well. Considering that the fraction of CD3+ T cells amongst PBMCs is usually around 70-85% in healthy donors (Kleiveland 2015), this would result in a positive spot count of less than one to 10 spots per ELISpot well for 11 of these TCRs, which could be easily considered as background in this assay. As mentioned before, one clone was present at a slightly higher baseline frequency of $4*10^{-2}$ %, which would result in 84-102 spots per well in ELISpot, which were however not observed (mean spot counts per well of patient ID1 at baseline: 15 for IDH1R132H, 14 for MOG; data not shown).

ELISpot is a functional readout quantifying the ability of T cells to respond to antigen stimulation. One could conclude that this particular clone was exhausted and therefore lacked capacity to express IFNγ, which would be in accordance with a previous publication describing reduced IFNγ expression of exhausted CD4+ T cells in patients with chronic HBV infection (Dong et al. 2019). Exhaustion of CD4+ clones was previously described in the literature to not only be associated with negative effects in regards to cytokine secretion, but also decreased proliferation, decreased antibody production in B cells and lower effector functions of CD8+ T cells, with immune-regulatory proteins being upregulated on exhausted cells as compared to non-exhausted cells (Miggelbrink et al. 2021). Exhaustion could be the reason why pre-existing anti-IDH1R132H immune responses (Schumacher, Bunse, Wick, et al. 2014) frequently fail in controlling tumor growth. It could be interesting to investigate whether the secretion of cytokines beyond IFNγ could be used to monitor IDH1R132H T cell responses, as for example T_H2, T_H17 or T regulatory cell (T_{reg}) cells do not secrete IFNγ (Miggelbrink et al. 2021). T_H17 cells were observed in blood of vaccinated patients of the NOA16 trial (Platten et al. 2021), but it is not yet clear to what extend they are found in non-vaccinated patients. It would be interesting to characterize the CD4 T cell subset of the clone found to be expanded at baseline using flow cytometry after determining its HLA restriction to be able to design tetramers for staining. This could shed light on the immune response in IDH1-mutant patients before onset of vaccination, which could either indicate a pre-existing anti-tumor response which is boosted upon vaccination, or - in case T_{reg} are present - suppress anti-tumor immunity.

Observing that pre-existing immune responses might not always be reflected in positive ELISpot counts could indicate that such T cell responses were missed by IFNγ ELISpot analysis of other patients and that a higher fraction of patients than what is expected might have IDH1R132H-reactive TCRs before vaccination. Baseline immune response were found in 4/25 patients in pre-clinical studies based on IFNγ ELISpot data (Schumacher, Bunse, Pusch, et al. 2014), but were not observed in patients of the NOA16 trial (n=32) (Platten et al. 2021) or in any of the patients that were recruited to the NOA21 trial so far (unpublished data).

More evidence for pre-existing immune responses in non-vaccinated patients can be concluded from the fact that an IDH1R132H-reactive clone was observed within tissue obtained before onset of vaccination in patient ID3. The TCR had an overall high frequency of 2.3% in tissue 776 days before vaccination, but was absent in blood at baseline as based on TCRβ deep sequencing data and lack of reactivity in ELISpot. The same clone was not found in the single cell sequencing dataset of the tumor biopsy of the same patient but at a low frequency within TCRβ deep sequencing data of the same tissue (0.13%) after receiving three doses of vaccination. It expanded in the periphery upon onset of vaccination and moreover expanded strongly in ESPEC cultures (**Figure 6F**). These findings emphasize that T cell clones undergo a constant dynamic expansion and contraction. Sequencing of additional FFPE tissues of patients before vaccination will allow us to analyze whether a pre-existing IDH1R132H response can be detected in further patients and to track these clones over time and both in tissue and blood. It will be interesting to determine the CD4 T cell subset of this clone using flow cytometry and IDH1R132H tetramers.

Analyzing the peripheral immune repertoire also revealed that individual reactive T cell clones temporarily expanded strongly between two visits, but often later decreased in frequency (**Figure 6, A and B**). Dynamic enrichment and contraction of clones is commonly observed after vaccinations, for example in a study in which patients were vaccinated against yellow fever (YF) and in which individual clones were tracked over time using TCRβ deep sequencing data (Minervina et al. 2020). Many of the observations from this study match to what was observed when vaccinating patients against IDH1R132H. For example, it was shown that most clones reactive against the target epitope expand after the first vaccination, with a smaller number of new additional clones being induced by a second

dose of vaccination 18 months later (Minervina et al. 2020). Similar observations can be reported for IDH1R132H-vaccinated patients, in which the time interval between vaccinations is shorter, but where most clones were induced after the first vaccination (V3/BL, V4, V6: bi-weekly vaccinations, followed by 5 times at monthly intervals and a last vaccination approximately 4 months after the last dose). Similar observations where moreover made when vaccinating patients with midline glioma using a long H3K27M peptide vaccine (Boschert et al. 2023). The overall fraction of YF-responding clones within the periphery was between 10^{-2} – 10^{-1}, similar to what was observed for the cumulative frequency of IDH1R132H-reactive clones for five of seven patients that were analyzed in this thesis (**Figure 6D**). Patient ID5 had a higher cumulative response highly dominated by one clone, whereas patient ID7 had an overall lower cumulative response.

The number of TCRs available for testing of patient ID7 based on ESPEC was rather low (7 of 8 clones suggested by FEST were tested, **Table 7**) and potentially further clones could have been selected manually for testing based on their strong expansion (**Figure 6E**, right side, y-axis). Patient ID7 passed away 148 weeks after diagnosis with none of the clones that were tested to be IDH1R132H-reactive or clones expanded in ESPEC found in TCRβ deep sequencing data of tissue obtained 68 weeks after diagnosis and after vaccination (**Figure 6E**, right side) (Platten et al. 2021). In contrast to that, for patient ID6 a remarkably high cumulative frequency of IDH1R132H-reactive TCRs can be observed in PsPD tissue obtained 24 weeks after diagnosis while the patient still received the long peptide vaccine (**Figure 6E**, left side) (Platten et al. 2021). PsPD is characterized by contrast enhancement on MRI due to strong infiltration with immune cells, which are difficult to differentiate from true tumor progressions (Ma et al. 2019). The patient is currently still alive more than 80 months after diagnosis, underlining the potentially positive effect of a vaccination-induced anti-IDH1R132H immune response on survival.

For patients included in the NOA21 trial, enrichment of IDH1R132H-reactive clones could be observed comparing the cumulative frequency of TCRs tested to be reactive in blood and tissue from the same timepoint (V7) after the patients received two doses of vaccination, which confirms immunogenicity of the IDH1R132H-targeting peptide vaccine and can be taken as a positive signal with respect to trial outcome (**Figure 6D**).

4.3.5 Role of CD8+ IDH1R132H-reactive TCRs

I showed that CD4+ T cells with reactivity against IDH1R132H can be found in vaccinated patients, which is in accordance with the literature (Platten et al. 2021; Schumacher, Bunse, Pusch, et al. 2014). In contrast to what was reported so far in human patients, I also found CD8 T cell responses against IDH1R132H in 2/3 tested patients in ELISpot, and could so far identify at least one IDH1R132H reactive CD8-derived TCR (**Figure 9**). In ELISpot, 0.49% (0.29%) of CD4+ T cells and 0.28% (0.05%) of CD8+ T cells were reactive against the long IDH1R132H peptide for patient ID2 (numbers in brackets correspond to patient ID14).

MS-based analysis of MHC I molecules after pulldown from peptide-pulsed B-LCLs was used to identify short IDH1R132H peptides presented on MHC class I molecules as well as the corresponding relevant MHC I allele. Analysis of TCR reactivity against the 9-mer peptide identified for patient ID2 (**Table 8**) is at an advanced stage. Reactivity of CD8+ cells from peripheral blood against the short peptide as well as the long peptide was observed using flow cytometric analysis of peptide-pulsed PBMCs, with the long peptide likely being processed and presented on MHC I (**Figure 9B**). Upon gating on the CD8+ cell population, a total of 0.05-0.07% TNFα+ cells were observed in FACS upon pulsing with short or long IDH1R132H peptide, which is lower than the previously observed frequency of 0.28% CD8+ cells positive in IFNγ ELISpot analysis using blood of the same visit. This could likely be due to the fact that

T cells were co-cultured against DCs in ELISpot, whereas only 0.5-2% of PBMCs are DCs, suggesting that less short IDH1R132H peptide was presented on MHC I in flow cytometric analysis (Wojciechowska-Durczynska et al. 2021).

As expected, CD4+ T cells did not secrete TNFα upon co-culture with short peptide, but reactivity against the long wildtype (0.25%) and mutated long peptide (0.35%) were observed in flow cytometric data (blood from V7, %TNFα+ of CD4+ cells over background). Similar to observations in CD8+ populations, this number is lower as compared to the frequency of IFNγ+ spots in ELISpot if only CD4+ cells from the same visit were loaded (wildtype peptide: 0.45%, mutant peptide: 0.49%). Both the frequencies determined in ELISpot and by flow cytometric analysis are lower than the reported cumulative frequency of 0.73% CD4+ T cell clones with proven reactivity against IDH1R132H at V7 taking all CD3+ cells into account (0.43% reactive against wildtype and mutated peptide, 0.30% reactive against only mutated peptide as based on TCRβ deep sequencing data). At V7, 55% of CD3+ PBMCs were classified as CD4+ (**Figure 9A**), meaning that at least 1.33% of all CD4+ cells were indeed reactive against the long peptide. While it is difficult to make quantitative comparisons between assays and while it is likely that not all cells are equally functional, this could indicate that the in vivo frequency of IDH1R132H-reactive CD8+ clones could as well be higher as compared to the frequency of positive events observed in ELISpot or in flow cytometric analysis.

ESPEC cultures with subsequent FACS-based enrichment of TNFα secreting cells upon restimulation and VDJ single cell sequencing were successfully used to enrich for CD8+ clones expanded against the IDH1R132H short peptide. Two clones with strong expansion, called top 1 and top 2, made up 89.4% and 3.3% of the enriched post-ESPEC repertoire and were selected for cloning and testing (**Figure 9C**). The top 1 clone was tested to be reactive against the identified short peptide as well as the long IDH1R132H peptide pulsed on and cross-presented by DCs, but not against short or long IDH1-wildtype peptides. The top 2 clone interestingly only showed strong reactivity against the long IDH1R132H peptide, but not against the short IDH1R132H peptide which was used for ESPEC (**Figure 9D**). It is planned to repeat this co-culture assay to assess whether these results can be replicated or if reactivity against the 9-mer IDH1R132H peptide can be observed.

Tracking the top1 and top2 TCRs in blood reveals that both were induced by vaccination with the long IDH1R132H peptide as they are absent at baseline (**Figure 9E**). Both TCRs have a cumulative frequency of 0.54% in peripheral blood at V7 (0.33% for top 1 clone, based on TCRβ deep sequencing) and 0.74% at the same timepoint in tissue (0.24% for top 1 clone, quantification based on single cell sequencing data). As CD3+ PBMCs of patient ID2 consist of 39.7% CD8+ cells at V7, this means a total of 1.36% of CD8+ cells express top 1 and top 2 TCRs in vivo (0.83% for top 1 clone). In contrast to that, only 0.05-0.07% increase in TNFα+ cells over background was detected upon co-culture of PBMCs from V7 with the short IDH1R132H peptide, and 0.28% positive CD8+ cells were observed in ELISpot (**Figure 9, A and B**). As described before for confirmed CD4+ TCRs, the proportion of reactive clones as based on TCRβ deep sequencing data is most likely higher than the proportion of reactive clones observed in ELISpot or by flow cytometric analysis.

This could be in accordance to observations of a lack of IFNγ ELISpot responses at baseline while some TCRs later tested to be reactive were actually present at baseline as based on TCRβ deep sequencing data. Possibly only a fraction of T cells is responsive to re-stimulation in ELISpot or when using flow cytometric analysis, which could be due to exhaustion.

Analysis of the gene expression pattern of the top 1 and 2 clone in TILs isolated from on-trial tumor tissue showed that both are enriched in the cluster of GNLY positive CD8+ clones (**Figure 9G**). GNLY is a marker of cytotoxic T cells and mediates tumor cell death (Krensky and Clayberger 2009). In case these CD8+ T cells are indeed cytotoxic, this could cause dying tumor cells to release antigens which

are then processed by surrounding T_H1-activated APCs, which allows to prime an anti-tumor immune response against additional tumor antigens. This process, called epitope spreading, can contribute to a sustained anti-tumor response (Brossart 2020). Analysis of CD8+ IDH1R132H-reactive T cell responses in a broader patient population could help to understand whether these responses are determinant for a positive clinical outcome in glioma patients and how frequently they can be observed. The NOA16 patient cohort would be well suited for this type of analysis, as long-term survival data as well as cryopreserved blood samples of patients that were recruited between May 2015 to November 2018 are available (Platten et al. 2021).

Preliminary analysis of the 3D conformation of the top 1 TCR and pMHC class I revealed that histidine at position 132 of the IDH1R132H short peptide might interact with a serine at position 96 of the TCRβ chain (**Figure 9F**). More detailed structural analysis is required to confirm this interaction. It remains to be shown that IDH1R132H-reactive TCRs derived from CD8+ cells show reactivity against IDH1R132H-mutant tumor cell lines and that these T cells are indeed cytotoxic. Besides deeper analysis of confirmed TCRs, it is planned to screen further patients in the context of CD8+ IDH1R132H immune responses to establish a larger dataset on (I) MHC I alleles that are able to present the peptide and (II) to also identify additional reactive TCRs derived from CD8+ T cell clones. The overall aim is to identify short peptides on a larger number of MHC I alleles that cover a higher fraction of HLA alleles of the general population to be able to either offer a short peptide vaccine, or a TCR transgenic therapy to patients. At the moment, only 12.3% of the German population are covered by HLA-B*07:05 and HLA-B*35:01 taking HLA supertype families into account, but it is possible to cover 99% of the world population including 15 additional B-LCL lines available from IDH1R132H-vaccinated patients for screening (data from IEDB population coverage tool (Bui et al. 2006)).

CD8+ T cell responses against IDH1R132H were not observed in human patients so far, and cytotoxic CD8+ T cells are usually not found in healthy brain parenchyma, which is considered a mechanism to prevent neuroinflammation (Wischnewski et al. 2023). Evidence for a CD8+ mediated anti-tumor immune responses come from studies by Pellegatta et al. (2015) with mice, where IDH1R132H-expressing murine GL261 tumor cells were intracranially injected. Using short peptide vaccines (two 9-mers (p126-134 and p128-136) and two 10-mers (p131-140 and p123-132)) to target IDH1R132H in mice was reported to induce a specific cytotoxic CD8+ T cell response as well as an antibody response, causing superior survival as compared to vaccinations with a long 16-mer (p126-141) peptide (Pellegatta et al. 2015). Vaccinations with long peptide in these studies also induced CD8+ responses but failed at inducing antibody responses, and lower survival of mice after vaccination with long peptide was attributed to the lack of antibody response (Pellegatta et al. 2015). The lack of antibody response after vaccination is in contrast to previous findings from the NOA16 trial, in which a 20-mer (p123-146) vaccine was used and in which antibody responses in vaccinated patients were detected, but seemingly no CD8+ T cell responses (Platten et al. 2021).

While these discrepancies could be attributed to differences between the human and murine immune system, it seems that CD8+ responses in pre-clinical studies as well as in the NOA16 trial might have been overlooked. In pre-clinical studies with A2.DR1 mice, a strong focus was put on the HLA-A*02:01 allele, where vaccination with IDH1R132H long peptide did not induce CD8+ T cell responses (Schumacher, Bunse, Pusch, et al. 2014). This is in accordance to MS-based analysis in this thesis, for which a peptide-pulsed B-LCL line of the HLA-A*02:01 positive patient ID14 was used, but where no short peptides binding to this allele were identified. Moreover, CD8+ T cell responses can be easily overlooked in FACS-based assays, where CD4+ responses are a lot more prominent (**Figure 9B**). ESPEC assays, which allow expansion of relevant T cell responses before cloning and testing, were not yet available when analysis of immune responses of the NOA16 trial were performed.

In contrast to the publication by Pellegatta et al., which would suggest superior outcome upon vaccination of a short IDH1R132H peptide, a multitude of studies showed that a more sustained immune response and favorable outcome is expected if both CD4 and CD8 T cells are simultaneously activated by using long peptide vaccines (Kissick et al. 2014; Krug et al. 2010; Alspach et al. 2019). As shown for example in a vaccination trial targeting p53, higher numbers of CD4+ reactive T cells increased tumor infiltration with reactive CD8+ T cells (Speetjens et al. 2009). Seeing that both CD4+ and CD8+ T cells with anti-IDH1R132H reactivity were found in at least one patient (ID2) of the NOA21 trial suggests that patients included in the trial could benefit from a combined CD4+ and CD8+ T cell response. It is plausible that co-vaccination with the long (p123-142) peptide vaccine in combination with a short peptide vaccine that is selected based on a patients' HLA-allelotype, or using adjuvants that increase cross-presentation, could yield a synergistic effect with even higher frequencies of reactive CD8+ T cells (Ho et al. 2018).

The role of CD4+ T cells in anti-tumor immunotherapy has been investigated extensively in the last years, and it is commonly accepted that CD4+ T cells help CD8+ T cells to become cytotoxic effector cells. Basic work on this relationship was already performed more than 25 years ago, when it was found that activated CD4+ T helper cells express CD40LG, which binds to CD40 expressed on DCs or other APCs such as B cells or macrophages, thereby stimulating them to enhance antigen presentation as well as co-stimulation, so-called licensing. These APCs can then activate a cytotoxic CD8+ T cell response (Schoenberger et al. 1998). Strong CD40L expression was observed in CD4+ IDH1R132H-reactive TILs, suggesting that they might indeed play a role in activation of APCs and priming a cytotoxic CD8+ response (**Figure 8, A and B**).

Our laboratory just recently reported another mechanism highlighting the importance of CD4+ T cell responses for anti-tumor immunity in brain tumors. It was found that loss of MHC II can drive CD8+ T cells into exhaustion due to a lack of activated CD4+ T cells. Activated CD4+ T cells were found to inhibit osteopontin expression by blood-borne myeloid cells. Thus, a lack of MHC II leads to higher levels of osteopontin, which chronically activates NFAT2 in reactive CD8+ T cells, thereby triggering TOX-mediated exhaustion (Kilian et al. 2023). Co-presentation of epitopes targeted by CD4+ and CD8+ T cells on the same tumor cells was highly favorable for T cell mediated tumor rejection (Alspach et al. 2019).

Besides the aforementioned roles in anti-tumor immunity mediated through enhanced maturation and activation of APCs, CD4+ T_H1 cells are also known to secrete IFNγ, which can either directly kill tumor cells by inducing apoptosis (Zhou et al. 2008) or cause upregulation of MHC I and II molecules, thereby increasing visibility of tumor cells to the immune system (Gocher, Workman, and Vignali 2022). Secretion of cytokines by CD4+ T cells furthermore causes an inflammatory TME, allowing for activation of a large number of immune cells (Speiser et al. 2023). For example, CD4+ cells are known to mediate B cell activation through the CD40-CD40L axis, antibody class switching, B cell maturation and affinity maturation (Speiser et al. 2023), or interaction of CD4+ T cells with NK cells were reported to activate and support NK cell functions (Ni et al. 2016; Horowitz et al. 2010). Interestingly, some CD4+ T cells were also reported to be cytotoxic, as shown after an adoptive T cell transfer of CD4+ T cells in melanoma, which will be further discussed in chapter 4.3.6 (Quezada et al. 2010). Finally, CD4+ T cells were also reported to inhibit angiogenesis in tumors (Speiser et al. 2023)

To further analyze the relevance and function of CD4+ and CD8+ IDH1R132H-reactive T cells for glioma anti-tumor immunity and their role within the TME, it would be interesting to vaccinate mice that express human MHC I and II alleles that are confirmed to play a role in IDH1R132H immunity with the long IDH1R132H peptide vaccine.

4.3.6 Intratumoral gene expression of IDH1R132H-reactive T cell clones

On-trial brain tumor tissue is obtained in the scope of the NOA21 trial, allowing for single cell analysis of immune cells isolated from the tumor to understand the mode of action of the IDH1R132H vaccine. To this date, six patient samples were used for FACS-based enrichment of T cells and myeloid cells, of which TCR testing data for three patients (ID1-ID3) is available.

Analysis of the differential gene expression pattern of CD4+ reactive vs. CD4+ non-reactive TILs was performed, in which T cells were classified to be reactive or non-reactive on basis of their CDR3 sequences and in vitro TCR testing results discussed before. Reactive T cell clones were enriched in CD40LG+ T helper cell clusters, which matches previous observations of a CD40LG positive IDH1R132H-reactive clone found in a patient of the NOA16 trial (Platten et al. 2021). CD40LG is known to be temporarily upregulated upon activation (Elgueta et al. 2009). Other markers found to be upregulated on reactive CD4+ T cells as compared to non-reactive cells are LINC00892, HLA-DRB5 and TNF Superfamily Member 14 (TNFSF14), which were all reported to be associated with T cell activation (Iaccarino et al. 2022; Skeate et al. 2020; Tippalagama et al. 2021).

In contrast to that, IL7Rα expression was low in CD4+ IDH1R132H-reactive T cells, which is in line with the observation that high IFNγ expression, secreted amongst others by activated T cells, is known to downregulate this receptor (Gocher, Workman, and Vignali 2022). Low IL7Rα expression was also observed in CD8+ T cells reactive against mutation-associated antigens in lung cancer patients, but high in T cell clones reactive against influenza, indicating that TCRs selected for future testing of IDH1R132H reactivity could be excluded from analysis if they express this marker (Caushi et al. 2021).

It is still heavily discussed whether CD4+ T cells can be cytotoxic. Amongst other cancer entities, cytotoxic CD4+ T cells were described in bladder cancer, were cytotoxic CD4+ T cells were positive for "GZMA (granzyme A), GZMB (granzyme B), and NKG7" (Natural Killer Cell Granule Protein 7), as well as PRF1 (perforin), and GNLY (Oh et al. 2020). Matching with that, upregulation of markers such as "GZMA, GZMB, GZMH, PRF1, NKG7 (TIA-1), GNLY, CD40LG, KLRG1, KLRB1, and ITGAL (CD11A)" with downregulation of "CCR7, CD27, CD28, and IL7R" were suggested as markers to define CD4+ cytotoxic T cells in people with advanced age (Hashimoto et al. 2019). At first sight it seems as if cytotoxic CD4+ IDH1R132H-reactive T cells might be present amongst those which were classified as reactive, as TILs expressing these TCRs were positive for CD40LG, GZMA, GNLY, and KLRB1, while being negative for IL7R (**Figure 8**). However, GZMB and NKG7 were higher in non-reactive clones, and most importantly PRF1, as well as KLRG1 and ITGAL were not amongst the top up- or downregulated genes, indicating that IDH1R132H-reactive clones are not cytotoxic CD4+ T cells.

Seeing that GNLY positive CD8+ IDH1R132H-reactive clones were identified in at least one vaccinated patient, it is more likely that the anti-tumor effect observed after vaccination with the IDH1R132H peptide is induced through cytotoxic CD8+ T cells as compared to cytotoxic CD4+ T cells. IDH1R132H-reactive CD4+ T cells more likely exert their functions for anti-tumor immunity as T helper cells, which support the CD8-mediated anti-tumor immunity as discussed in chapter 4.3.5. Further assays are required to indeed confirm cytotoxicity of aforementioned CD8+ IDH1R132H-reactive clones.

Additional single cell sequencing datasets with immune-subsets isolated from the tumors of patients receiving IDH1R132H long peptide vaccinations will be prepared to gain insights into the gene expression program of IDH1R132H-reactive clones within the tumor. Besides generating further TIL single cell sequencing datasets, it is planned to also sequence myeloid cells, B cells and NK cells to gain a deeper understanding on how the individual immune cell subsets interact and to understand their respective role in anti-tumor immunity in patients with IDH1R132H-mutant gliomas. In addition to that, analysis of additional single cell sequencing datasets will allow us to comprehend the mode of

action of avelumab, which is tested in combination with the IDH1R132H long peptide-vaccine in the scope of the NOA21 trial.

4.4 Screening for reactive TCRs in non-brain tumor patients

ESPEC-SUIT was used to expand T cell populations reactive against private tumor neoepitopes of three patients. Two of three patients were pre-vaccinated with long peptide vaccines against the epitopes-of-interest, whereas one patient was not vaccinated, but nevertheless, putatively reactive T cell clones that expanded strongly in ESPEC from peripheral blood were observed. For POC-005, up to 666 clones could be tested for reactivity. Reactivity of these clones will be assessed using high-throughput assays, as described before (chapter 4.2).

For patient POC-001, 17/18 long peptides caused specific T cell expansion in ESPEC. Interestingly background activation was observed for HD-Pep-1782 upon re-stimulation in ELISpot, but no reactivity against this peptide was observed in an ELISpot assay performed at baseline before expansion (data not shown). It could be that clones reactive against this epitope had a high proliferative capacity and were able to expand without peptide stimulation, as some of the clones expanded under stimulation with HD-Pep-1782 are also found expanded in other cultures as based on TCRβ deep sequencing data, which is also reflected in higher spot counts in post-ESPEC IFNγ QC-ELISpot analysis (**Figure 10A**).

Of 28 tested clones from patient POC-001, 25 clones were shown to be reactive, with two of them being present within the colorectal cancer (TCR ID3) or liver metastasis (TCR ID1) before onset of vaccination, respectively, but none of them being present at baseline in blood (**Figure 10E**). Their recruitment to the tumor indicates that indeed TCRs that could be relevant for anti-tumor immunity were discovered. Reactivity against the corresponding wildtype peptides was not tested and will be important to exclude the possibility of selecting cross-reactive TCRs. It was interesting to observe that TCR-transduced expanded PBMCs with high degree of TNFα and CD107a expression after in vitro co-culture (high functional avidity) were made up of a higher fraction of CD8+ clones transfected with the TCR-of-interest, despite these TCRs being selected from CD4+ clones (**Figure 10C**). Possibly these TCRs have a high affinity to the pMHC class II complex and are therefore less dependent on the CD4 or CD8 co-receptor. TCR ID1 and ID3 showed slight reactivity in CD8+ clones. It would be interesting to test the performance of a TCR with high functional avidity derived from a CD4+ clone in CD8+ T cells.

A high number of TCRs expanded in ESPEC cultures of POC-001 were derived from CD4+ T cell clones and a higher number of long peptides caused positive expansions in ESPEC for patient POC-005 as compared to short peptide pools (**Table 11**). This is in accordance with a previous publication on personalized mRNA vaccines, which reported CD4+ T cell responses against 70-95% of these epitopes being detected upon immunization of three independent mouse models with either long peptides or mRNA encoding for the same epitopes (Kreiter et al. 2015). Vaccination with mRNA excluded possible introduction of bias due to the use of long peptides. It could be that a high number of CD4+ T cell responses were observed due to a higher number of epitopes that can be presented on MHC II as compared to MHC I, as both peptide length and sequence requirements are less strict for MHC II epitopes (Arnold et al. 2002). Using short peptides for screening, as performed for patients POC-004 and POC-005, could increase the number of hits for CD8+ clones. For patient POC-005, only 3 of 145 short peptides elicited a positive response in post-ESPEC QC ELISpot analysis. This is in line with other publications, which reported for example 8 of 230 mutated neoepitopes predicted to bind MHC I to be recognized in co-culture assays with TILs isolated from melanoma (Wickstrom et al. 2019).

Other groups participating in the collaboration used peptide-based expansion assays with subsequent multimer staining and FACS-based enrichment to identify reactive TCRs. Interestingly, there was often a divergence in which T cell clones expanded and which TCRs were detected by different approaches.

This could have similar causes as the inter-assay variations observed in post-ESPEC QC IFNγ ELISpots for patient POC-005, when the same set of peptides and cryopreserved PBMCs from the same timepoint elicited different cultures to be classified as positive in two independent assays, as discussed in chapter 4.2. On the other hand, this could be due to the relatively lower number of TCRs screened by other labs, which only screened seven TCRs of which three were reactive. Screening a high number of TCRs for patients POC-004 and POC-005 might allow better compare both screening approaches.

Overall, this data underlines that ESPEC-SUIT can be used to identify tumor-reactive TCRs from a diverse patient population and that this assay could be suitable to define a subset of TCRs that could be used for TCR-transgenic therapies. One downside of this approach is that several months are required for RNAseq and WES of the tumor sample, bioinformatic analysis for selection of suitable epitopes, ordering of peptides for ESPEC-SUIT, expansion of cells, TCRβ deep sequencing and single cell sequencing of the post-expansion culture. MS analysis can be performed in parallel and takes about one month to complete, as heavy labelled peptides for targeted MS analysis take around 2-4 weeks to be delivered. Subsequent production of the TCR-transgenic cells in a good manufacturing practice (GMP) setting are also expected to take weeks to months, and chances are high that the patients' tumor might have undergone immune editing and acquired new mutations in the meantime. However, the TCR-POC "proof-of-concept" collaboration was not aiming at providing a TCR-transgenic therapy for patients, but was brought to life to showcase that it would be in principle possible to provide such a therapy to patients and to compare different types of analysis and assays available in laboratories of the German Cancer Research Institute in Heidelberg.

One major issue that was faced when following this approach was that it relies heavily on prediction of neoepitopes for TCR screening. With algorithms for analysis of the mutanome and prediction of HLA-binding frequently facing issues in terms of sensitivity, predictive power (especially for MHC II) and lack of understanding of understudied sources of cancer neoantigens, immunogenic neoantigens cannot be reliably predicted yet (Capietto, Hoshyar, and Delamarre 2022). An alternative approach to circumvent these problems are gene expression signatures, as discussed in the next chapter.

4.5 Gene-signature based TCR discovery

To speed up the discovery of tumor-reactive TCRs and to avoid the need for laborious in vitro assays, a large number of publications recently proposed that tumor-reactive TILs can be identified through specific gene expression signatures that are differential to non-reactive bystander cells. So far, none of these analyzes specifically aimed at brain tumors but rather focused on different cancer entities, such as lung cancer (Caushi et al. 2021; Hanada et al. 2022), melanoma (Oliveira et al. 2021; Veatch et al. 2022), gastrointestinal cancer (Zheng et al. 2022) or metastatic cancer (Lowery et al. 2022). Our laboratory previously described a gene signature for a single CD4+ IDH1R132H-reactive TCR in a PsPD tissue, however, this patient received the IDH1R132H vaccination in the scope of the NOA16 trial, which could potentially affect its gene signature (Platten et al. 2021).

TCR discovery through gene signatures has several advantages. Most importantly, the need to pre-define target neoepitopes through complex analysis of WES, RNAseq and immunopeptidomics is abolished. This is advantageous as a large number of putative epitopes are hard to predict, such as those derived from frameshift mutations, gene fusions (e.g. through alternative splicing variants or dysregulation of transposable elements on RNA-level, or through chromosomal re-arrangements or deletions on DNA level), post-translational modifications (e.g. glycosylation, phosphorylation, citrullination), of non-coding genomic regions (e.g. regions that re-gain their protein-coding function in tumor cells, or non-functional proteins translated from long non-coding RNA) and possibly even intracellular pathogens (Kalaora et al. 2021). Moreover, the risk of introducing bias through algorithms

predicting HLA binding of candidate epitopes is reduced, especially for epitopes presented on MHC II alleles, where the accuracy of predictions is still low (Capietto, Hoshyar, and Delamarre 2022).

A major downside to the signature approach is that none of the signatures published so far can be successfully applied to identify TCRs from other tumor entities, despite all of them including CXCL13 as a relevant marker (not shown). For example, CXCL13 was described to be co-expressed on a fraction of tissue resident memory T cells with high PD-1 expression in NSCLC, which are commonly considered to be exhausted, with CXCL13-expression of these cells being suggested to be a sign of functional adaptation to the TME (Oja et al. 2018). CXCL13-expressing cells are found within tertiary lymphoid structures (TLS) in NSCLC and might promote formation of these structures (Oja et al. 2018).

Therefore, our laboratory aimed at identifying a gene signature that can be used to identify tumor-reactive TCRs in brain cancer. For this, I processed tumor tissue of the melanoma brain metastasis of patient BT21 and performed single cell RNA and VDJ sequencing of FACS-enriched TILs. Using an approach for high-throughput generation of TCR-encoding RNA established by Edward Green and Tamara Boschert, Chin Leng Tan and I screened the top 83 TCR clonotypes of the tumor repertoire of patient BT21 for reactivity, identifying a total of 46 reactive TCRs, which were found to be enriched within the tumor as compared to blood (**Figure 11**). Being able to identify reactive TCRs was relatively likely for this melanoma metastasis, as around 40-70% of melanoma patients that received autologous TIL transfer show clinical response (van den Berg et al. 2020; Wickstrom et al. 2019). In addition to that, melanomas carry a high mutational burden as compared to other cancer entities, thereby increasing the chance of observing tumor-reactive TCRs (Chalmers et al. 2017).

The next goal is to decipher which antigens were recognized by those TCRs found to be reactive. Tumor-reactive TCRs from melanoma patients are known to frequently be reactive against cancer-testis antigens, melanoma-associated antigens, but also individual neoepitopes (van den Berg et al. 2020). BT21 is Melan-A positive based on flow cytometric data and 268 functional SNV mutations were identified based on WES and RNAseq data of the tumor of this patient, which are potential target antigens for those TCRs observed to be reactive (not shown, analysis by Edward Green (DKFZ Heidelberg, Germany)). Of note, 262 of these SNVs were present in the tumor cell line, showing that it well reflects the tumor mutanome.

To identify relevant antigens, an approach called T-FINDER (T cell Functional Identification and (Neo)-antigen Discovery of Epitopes and Receptors) is planned to be used, which was established by the laboratory of John Lindner (BioMedX, Heidelberg, Germany), who will carry out this analysis in accordance to their latest publication (available on bioRxiv: Schmid et al. 2023). WES and RNAseq analysis of tumor tissue was used to define the mutanome of BT21, and TMG constructs were established on this basis, which will be transduced into B-LCLs. JURKAT and SKW-3 reporter cell lines (for testing TCRs derived from CD4+ and CD8+ clones, respectively) will be electroporated with a set of TCRs-of-interest. APCs encoding for a variety of TMGs are multiplexed in different combinations and co-cultured with TCR-transduced reporter cells, which allows to decipher which antigens are recognized per TCR. Major benefits of this pipeline are that autologous APCs can be used, thereby preventing problems with incompatibility on the HLA level. On top of that, TMGs allow for intracellular processing of target epitopes, with the positive side effect of being more cost effective as compared to peptide-based assays.

In contrast to the melanoma metastasis BT21, no reactive TCRs were so far identified for primary brain tumors that did not receive anti-tumor vaccinations. However, TCRs selected for testing were chosen based on a gene signature that was defined based on literature research, which differs from gene expression signatures observed for reactive clones of patient BT21. Chin Leng Tan is currently working on re-analyzing previously generated single cell sequencing datasets of primary brain tumors to select

further TCRs for cloning and testing against tumor-derived cell lines based on the BT21 dataset. Lower amounts of potentially tumor-reactive T cells can be expected in these datasets as they lack CXCL13+ T cells, which is in contrast to observations in metastatic brain tumors (Wischnewski et al. 2023). Overall immunogenicity of primary brain tumors seems to be low, which is most likely due to the comparable low number of mutations found in these tissues (Cohen et al. 2003). On top of that, brain tumor microenvironments are very immunosuppressive due to for example little amounts of T cell recruiting cytokines, as well as presence of T cell inhibiting oncometabolites such as 2-HG or tryptophan depletion (Wischnewski et al. 2023; Bunse et al. 2018; Platten et al. 2014). In addition, the BBB and an aberrant vasculature pose an additional hurdle (Leko et al. 2021; Wischnewski et al. 2023).

Despite these limitations, identification of tumor-reactive TCRs in brain tumors should be possible as shown by the laboratory of Steven Rosenberg, who managed to stimulate and isolate a tumor-reactive clone from blood of a glioblastoma patient using peptides and TMGs (Leko et al. 2021). It will be interesting to search for tumor-reactive TCRs in primary brain tumors to show that this tumor could indeed be targeted with TCR-transgenic therapies in the future.

5. Conclusion

T cell immunotherapy is a promising approach to target tumors and can be especially beneficial for patients with brain tumors, which are known to infiltrate into healthy brain tissue, thereby complicating complete surgical resection. This thesis used two approaches to identify and validate neoepitope-specific T cell receptors for glioma immunotherapy, namely ESPEC-SUIT and gene expression signatures.

Having identified a total of 108 reactive TCRs from seven patients against IDH1R132H, 46 TCRs against a melanoma brain metastasis of a non-vaccinated patient (BT21), 25 TCRs against the melanoma lymph node metastasis of patient POC-001 is to my knowledge one of the largest endeavors in TCR discovery. Many published studies only test a few dozen TCRs to validate for example gene expression signatures, e.g. 7 by Caushi et al. (2021) from two patients, of which 5 were reactive, or 31 reactive TCRs from 9 patients by Lowery et al. (2022). It is planned to further extend the TCR dataset by screening additional TCRs from CD4+ and CD8+ T cells for reactivity against IDH1R132H, or patient-individual epitopes expressed by patients of the NOA21 and TCR-POC cohort.

Screening an even higher number of TCRs for reactivity will allow to re-define and improve the process used for selection of TCRs based on post-ESPEC TCRβ deep sequencing data. To meet the need for more high-throughput testing, the TCR testing pipeline will be scaled up using the JURKAT reporter cell line validated in this thesis, possibly introducing CD8 co-receptor alongside the transgenic TCR to improve assay sensitivity. Using a plate reader to quantify GFP expression will save time when acquiring data as compared to using a flow cytometer to quantify GFP fluorescence intensity. Whether these assays are sufficiently sensitive to detect TCRs of intermediate affinity and suitable for screenings against tumor cell lines will be tested with receptors and cell lines generated during this thesis.

A gene expression signature established by Chin Leng Tan on basis of BT21 TCR testing data represents and alternative and antigen-agnostic source for candidate TCR selection on basis of gene expression signatures, in particular for unvaccinated patient cohorts. Here it will be interesting to simplify and generalize TCR selection, e.g. by sorting TILs with certain protein expression patterns, in order to streamline the path from sample collection to validated TCR. The signature will also allow to compare features of tumor-reactive TCRs across patient cohorts, such as NOA21 arm receiving vaccination, checkpoint inhibition or both.

High-throughput TCR testing will also be used to screen additional IDH1R132H-reactive TCRs from CD8+ clones to broaden understanding of the contribution of CD4 and CD8 T cell mediated anti-IDH1R132H vaccine responses and their clinical impact. Single cell sequencing analysis of different immune cell subsets, such as T cells, myeloid cells, B cells and NK cells, from tumor samples in scope of the NOA21 trial will complete the picture of tumor-immune interactions in this patient cohort.

In addition, TCRs derived from CD8+ clones are of therapeutic interest. The fact that some TCRs derived from CD4+ clones in the scope of TCR-POC were reactive in both CD4+ and CD8+ T cells indicates cytotoxic responses might be elicited by expressing CD4-derived TCRs in CD8+ cells. If this was true, either IDH1R132H-reactive TCRs from co-receptor independent CD4+ clones, or TCRs derived from CD8+ clones could be used for TCR-transgenic therapy. This would not only be beneficial for patients with IDH1-mutant brain tumors, but could also be of use for patients with other IDH1R132H-expressing tumor entities, such as AML, thyroid carcinoma, chondrosarcoma or intrahepatic cholangiocarcinoma.

A final piece in the puzzle of IDH1R132H-reactive TCRs will be testing the cytotoxicity of TCRs derived from CD8+ or cytokine secretion of TCRs derived from CD4+ T cells in co-culture assays with tumor cell lines or other target cell lines that endogenously express and naturally process IDH1R132H for MHC presentation. Based on a collection of publications I speculate that the mode of action of IDH1R132H peptide loading on MHC class II molecules might cause it to be presented in two antigenically-different

3D conformations, also referred to isomers. Based on this hypothesis, endogenously processed peptide is presented as a stable isoform, whereas exogenously loaded peptide is presented in a less stable conformation. Possibly, CD4+ derived TCRs with reactivity against wildtype and mutant IDH1 are only reactive to externally loaded peptide, while TCRs with exclusive reactivity to mutant IDH1 should only be reactive against internally processed IDH1R132H.

Screening a higher number of IDH1R132H-reactive TCRs and testing of their HLA restriction could allow to define CDR3 motifs, which could enable further TCR discovery, patient selection and helpful in defining the mode of IDH1R132H peptide presentation on MHC II molecules. The latter could have important consequences for future vaccine strategies, possible favoring RNA-based formulation over peptide-based formulations to ensure endogenous antigen processing and generation of an efficient anti-tumor T cell response.

6. Supplementary

6.1 Gating strategies

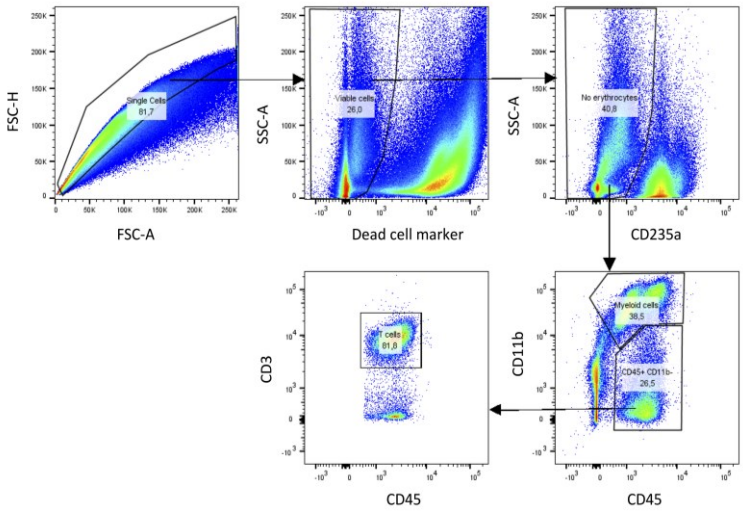

Supplementary figure 1. Gating strategy used for FACS-based enrichment of T cells and myeloid cells from tumor single cell suspensions prior to single cell sequencing.

6.2 HLA typing data

Supplementary table 1. HLA typing data of patients included in this thesis. Depending on the resolution, typing results from DKMS were either reported as G code or as MAC/NMPD (National Marrow Donor Program) code. N.a.= not analyzed.

Patient ID	ID1	ID2	ID3	ID4	ID5	ID6	ID7	ID14	POC-001	POC-004	POC-005	BT21
HLA-A_1	03:01:01G	03:01:01G	02:01:01G	01:01:01G	01:01:01G	02:01:01G	03:01:01G	02:01:01G	68:01:02G	02:01	01:01:01G	24:02:01G
HLA-A_2	24:02:01G	68:02:01G	24:02:01G	29:02:01G	02:01:01G	32:01:01G	03:01:01G	03:01:01G	49:01:01G	03:01	68:02:01G	24:02:01G
HLA-B_1	07:02:01G	07:05:01G	15:18:01G	15:01:01G	08:01:01G	51:01:01G	07:02:01G	35:01:01G	51:01:01G	07:02	08:01:01G	07:02:01G
HLA-B_2	44:02:01G	14:02:01G	18:01:01G	40:01:01G	57:01:01G	44:02:01G	08:01:01G	50:01:01G	07:01:01G	27:05:00	14:02:01G	15:01:01G
HLA-C_1	07:04:01G	08:02:01G	07:01:01G	03:03:01G	06:02:01G	05:01:01G	07:AMATM	04:01:01G	15:BRXNR	01:02	07:DUVSN	03:DUVRJ
HLA-C_2	07:CENAH	15:05:01G	07:04:01G	03:CEJXD	07:01:01G	15:02:01G	07:AUDFC	06:02:01G	11:01:01	07:02	08:02:01G	07:DXFTV
HLA-DRB1_1	15:ADHVT	13:03:01	11:04:01G	08:BWPS	03:RPXT	04:02:01	01:JZDV	01:DMFJC	14:54:01	01:01	13:03	11:AWZTN
HLA-DRB1_2	16:01:01	14:CENAU	15:01:01G	13:01:01	07:BMSUC	13:01:01	03:RPXT	07:BMSUC	n.a.	04:01	14:DKMNJ	13:BZXDN
DRB3_1	NNNN	01:BZFC	02:ERVA	02:ERVA	n.a.	02:ERVA	01:BZFC	NNNN	n.a.	n.a.	01:DZXZX	02:DWDNB
DRB3_2	NNNN	02:ERVA	NNNN	NNNN	n.a.	NNNN	NNNN	NNNN	n.a.	n.a.	02:DWDNC	02:DWDNB
DRB4_1	NNNN	NNNN	NNNN	NNNN	n.a.	01:03:01	NNNN	01:DJJXS	n.a.	n.a.	NNNN	NNNN
DRB4_2	NNNN	NNNN	NNNN	NNNN	n.a.	NNNN	NNNN	NNNN	n.a.	n.a.	NNNN	NNNN
DRB5_1	01:HUJ	NNNN	01:HUJ	NNNN	n.a.	NNNN	NNNN	NNNN	n.a.	n.a.	NNNN	NNNN
DRB5_2	02:XA	NNNN	NNNN	NNNN	n.a.	NNNN	NNNN	NNNN	n.a.	n.a.	NNNN	NNNN
DQA1_1	01:02	01:CAVSX	01:CAVSY	01:03:01	n.a.	01:03:01	01:CAVSX	01:DMFHW	n.a.	n.a.	01:DZWSF	01:DZWSR
DQA1_2	01:CAVSY	05:BZCGW	05:BZCGW	04:01:01	n.a.	03:01:01	05:01	02:AM	03:BMSUA	n.a.	05:EADGP	05:EADGP
HLA-DQB1_1	05:CETHW	03:CEMZB	03:CEMZB	04:CETHX	02:BJHMX	n.a.	n.a.	02:DKCVG	05:BYMRT	05:01	03:DZVMJ	03:DZVMJ
HLA-DQB1_2	06:CAVTF	05:BYMRT	06:CAVTF	06:CAVTH	03:03:02	n.a.	n.a.	05:DJGUF	01:AETTG	03:01	05:DJUVT	06:DWDEX
DPA1_1	01:CESVC	01:CESVC	01:CESVC	01:CESVC	04:BYVXE	01:CESVC	01:CESVC	01:DNXSD	02:AJXDJ	n.a.	01:DZWSD	01:DZWSD
DPA1_2	01:CESVC	02:CJAX	01:CESVC	01:CESVC	16:BYMRW	01:CESVC	01:CESVC	01:DNXSD	n.a.	n.a.	01:DZWSD	02:01:02G
HLA-DPB1_1	02:CEMZH	04:BYVXE	04:BYMSJ	03:CEMZC	n.a.	n.a.	n.a.	02:DCGFB	n.a.	04:01P	02:DZVNC	01:DMJGW
HLA-DPB1_2	04:BYMSJ	14:BYMSZ	04:BYMSJ	04:BYVXE	n.a.	n.a.	n.a.	04:DMAFX	n.a.	23:01P	04:DZVMH	02:DZVNE

6.3 Peptides used for ESPEC cultures in TCR-POC

Supplementary table 2. Peptides used for ESPEC cultures of patient POC-001.

Peptide ID	Peptide sequence	Gene
HD-Pep-1773	GDAEAVKGIGSSKVLKSGPQDHV	LGMN
HD-Pep-1774	SEIEARIAATTANGQPRRRSIQD	MAP3K7-A
HD-Pep-1775	NILDVPEIVISANGQPRRRSIQD	MAP3K7-B
HD-Pep-1776	ESLMHYQPFSFSKNASVPTITAK	MEP1A
HD-Pep-1777	NPCAEGWMDWAVSKISGWTQALP	NDRG1
HD-Pep-1778	ESDLDKVFHLPITTFIGGQESAL	OGDH
HD-Pep-1779	FPLSSPFRQVVQPRVEGKPVNPP	TRAPPC9
HD-Pep-1780	WDSETGENDSFTGKGHTNQVSRM	WDR1
HD-Pep-1781	HQVTLLDFGASREFTDHYIEVVKAAAD	ADCK4
HD-Pep-1782	RVQVLPDAVLYYILPRKVLQMDFLVHPA	APC
HD-Pep-1783	PAYLNSLNNFLLRLTCQNTMLPDMASSCIAILIQECKTKNKPQSAV	ABCA12
HD-Pep-1784	GNPRDLRVSDPMTSTMKLSWSGA	COL12A1
HD-Pep-1785	EQRFTCYMEHSRNHGTHPVPSGK	MICB
HD-Pep-1786	EVDTLSTLSLSNAQHWTQAKEKG	SETBP1
HD-Pep-1787	KCLEENNGVDKHVTRFVLPVGAT	SLC1A3
HD-Pep-1788	AIFAPNPSLMLCLDVQSEKSEGN	WDR44
HD-Pep-1789	WSPSAARLVSSHSGWFPRIPQAQ	NRP2
HD-Pep-1790	PGPRDAQAHPGHPRAVPTQCDVP	GAA

Supplementary table 3. Peptides used for ESPEC cultures of patient POC-004.

Peptide ID	Peptide sequence	Gene
E4853	TVYPPSSTAK	CMV
E4854	KLGGALQAK	CMV
E4856	TPRVTGGGAM	CMV
E4858	RPHERNGFTVL	CMV
E4859	CRVLCCYVL	CMV
E4846	CLGGLLTMV	EBV
E4847	FLYALALLL	EBV
E4852	RVRAYTYSK	EBV
E4857	RPPIFIRLL	EBV
E4851	RLRAEAQVK	EBV
E4850	ILRGSVAHK	Flu
E4855	LPFDKTTVM	Flu
E4917	SRFSRQLRS	fusion12
E4918	SRFSRQLR	fusion12
E4919	FSRFSRQLRSF	fusion12
E4920	FSRFSRQL	fusion12

E4921	FSRQLRSFLK	fusion12
E4781	RFSRQLRSF	fusion12
E4782	FSRQLRSFL	fusion12
E4783	RSFLKRQCL	fusion12
E4784	SVKGFSRFSR	fusion12
E4922	RRIRHQFEKS	fusion13
E4923	RRIRHQFEKSP	fusion13
E4924	VIEDLADAL	fusion13
E4785	RHQFEKSPYL	fusion13
E4786	KSPYLYQNEF	fusion13
E4787	QFEKSPYLY	fusion13
E4788	HQFEKSPYLY	fusion13
E4789	ALRRIRHQF	fusion13
E4790	IRHQFEKSPYL	fusion13
E4791	SPYLYQNEF	fusion13
E4792	RIRHQFEK	fusion13
E4793	IRHQFEKSPY	fusion13
E4794	AVIEDLADA	fusion13
E4795	AVIEDLADAL	fusion13
E4925	RIRYSNEDNK	fusion14
E4926	IRYSNEDNKKL	fusion14
E4927	IRYSNEDNK	fusion14
E4928	IRYSNEDNKK	fusion14
E4929	QRIRYSNEDNK	fusion14
E4796	RIRYSNEDNKK	fusion14
E4797	YSNEDNKKL	fusion14
E4930	AFDVREREV	fusion18
E4931	VLPGAKPIKI	fusion2
E4798	KPIKICIL	fusion2
E4799	VLPGAKPIK	fusion2
E4800	AKPIKICIL	fusion2
E4801	KTTAADFLRWK	fusion20
E4802	AVIEGKYSA	fusion20
E4803	AVIEGKYSAYL	fusion20
E4804	GLAVIEGKYSA	fusion20
E4805	SAYLKTTAA	fusion20
E4806	TAADFLRWK	fusion20
E4807	ISFGLAVIEGK	fusion20
E4808	AVIEGKYSAY	fusion20
E4932	ARFMSPMVFFP	fusion24
E4933	MVFFPETYL	fusion24
E4934	KARFMSPMVFF	fusion24
E4935	EKARFMSPMVF	fusion24
E4936	ARFMSPMV	fusion24
E4809	KARFMSPMVF	fusion24

E4810	TAFRKTVFL	fusion24
E4811	VFFPETYL	fusion24
E4812	RFMSPMVF	fusion24
E4813	SPMVFFPET	fusion24
E4814	TYLWMTAFRK	fusion24
E4815	SPMVFFPETY	fusion24
E4816	TYLWMTAF	fusion24
E4817	FFPETYLW	fusion24
E4818	FMSPMVFFP	fusion24
E4819	AVIEKARFM	fusion24
E4820	GISFGLAVIEK	fusion24
E4937	RRKTYTVK	fusion25
E4938	GKRRKTYTVK	fusion25
E4821	FLQATHVQPDL	fusion25
E4939	ACRRIRASQLL	fusion26
E4940	SFTDTVRSM	fusion26
E4941	FTDTVRSM	fusion26
E4942	RREERGACR	fusion26
E4943	RREERGACRR	fusion26
E4944	CRRIRASQLLL	fusion26
E4945	CRRIRASQLL	fusion26
E4822	IRASQLLL	fusion26
E4823	RIRASQLL	fusion26
E4824	HSTWMGIPK	fusion26
E4825	RRIRASQL	fusion26
E4826	MGIPKGEFF	fusion26
E4827	STWMGIPK	fusion26
E4946	STSPLGSFSF	fusion36
E4828	KSYCNHRITK	fusion36
E4829	SLNHISKSY	fusion36
E4830	SPLGSFSF	fusion36
E4831	GSFSFSLNH	fusion36
E4832	SPLGSFSFSLN	fusion36
E4833	SPETVLQST	fusion36
E4834	SKSYCNHRITK	fusion36
E4835	TVLQSTSPL	fusion36
E4836	TSPLGSFSFSL	fusion36
E4837	TSPLGSFSF	fusion36
E4947	HDFRPEQSLTK	fusion40
E4838	QLCGILILA	fusion6
E4839	ALHQLCGILIL	fusion6
E4840	HQLCGILIL	fusion6
E4948	LMPLRLNIDQL	fusion8
E4841	RLNIDQLQSLK	fusion8
E4842	LRLNIDQLQSL	fusion8

E4843	NIDQLQSLK	fusion8
E4844	YFYKVIQV	fusion9
E4845	CPCQNNTEM	MEGF8
E4848	YLQPRTFLL	SARS
E4849	RLQSLQTYV	SARS

Supplementary table 4. Peptides used for ESPEC cultures of patient POC-005.

Peptide ID	Peptide sequence	Gene
HD-Pep-3053	CLLDILDTAGREEYSAMRDQY	NRAS
HD-Pep-3054	NCGASTIRLLISLRAKHTQEN	CCT3
HD-Pep-3055	LRELRQRLEDVQLRGQTDLPP	WWC3
HD-Pep-3056	TDSDIIAKMKSTFVERDRKRE	SNRPA
HD-Pep-3057	TVAISDAAQLSHDYCTTPGGT	EIF4EBP2
HD-Pep-3058	FLGGSIVKGGLVQVLEDEELK	SELENBP1
HD-Pep-3059	EVMQLTYLPTFPLLADCIIPI	NRD1
HD-Pep-3060	YQKMPAFLHEKEQHHLERLRK	TRIM51
HD-Pep-3061	AVTGSLSENDSLRFKPHPSNM	NGDN
HD-Pep-3062	GMGAPLVSVADVARTVAQLWN	OSGEP
HD-Pep-3063	GTRLEALFRFFVIWHLTREIQ	DOPEY2
HD-Pep-3064	GIRVLGIAFSFARDHPVFCAL	SUPT6H
HD-Pep-3065	YIHLENLLARFYFDPREAYPD	SMU1
HD-Pep-3066	SALTDLGGLDSVWLFVVVGGV	TSPAN17
HD-Pep-3067	WLALFLSLKAFYRLHQLRSWG	INO80
HD-Pep-3068	VQSEIFPLETSAFAIKEQGFR	GMPS
HD-Pep-3069	AVDDVPFSIPVASEIADLSNI	WDR12
HD-Pep-3070	GIDRYPRKVTTAMGKKKIAKR	RPL27
HD-Pep-3071	AQAIIDTTDDLTATESASSSV	MAGEC1
HD-Pep-3072	AAASPLSTPTFAQAAGIEPCT	CD320
HD-Pep-3073	AQQGEYSEAILILRAALKLEP	FKBP8
HD-Pep-3074	ESTMYPKAVQNLCGWRIRSLA	RCC2
HD-Pep-3075	LLSRIPSSKEINKMKERAIQT	KIAA0368
HD-Pep-3076	KVRTNDRKELEEVRVQYTGRD	MGAT1
HD-Pep-3077	NIHLNLDRRTEYLKGYTLVEY	RBM8A
HD-Pep-3078	KAWALLQKRILKTHQALD	COASY
HD-Pep-3079	LGAFLNHWRNKFHCGFSITVG	TOMM40L
HD-Pep-3080	PSLIPLFVFIETGATGATLYL	NDUFA4
HD-Pep-3081	TGDKLTDRDIVVLQRGGTGFA	NOSIP
HD-Pep-3082	LQQREAATKSFRTSVQPTFTA	UBR4
HD-Pep-3083	GAETGDPRMKLKQVSRDLGLA	SLC38A10
HD-Pep-3084	VGPGPTAAAADEERQRKLQEY	CKAP2L
HD-Pep-3085	IIERFIFVMPSVEAPPPSLHA	SRCAP
HD-Pep-3086	SNPSGSLVTPFLVTSSLTDPR	MEF2D

HD-Pep-3087	VNTLLANDPTFLRKNLSIQRY	MTOR
HD-Pep-3088	DINVITGILKNYLRELPTPLI	SYDE1
HD-Pep-3089	EVVDSLKIESSTSATTHEARP	PPRC1
HD-Pep-3090	ASEWFLIANRFYKVSAASSFF	SLC22A15
HD-Pep-3091	REVQLKPKHQSYKLGRQWPEL	FRMD8
HD-Pep-3092	HCMRLIGFSEKALALMKARVK	ACAD10
HD-Pep-3093	YVCAAFLIKWKKEILDEEDFQ	TBC1D22B
HD-Pep-3094	QSIDKTAGKIRYSDTRRWPQDGRHEHPNDRK	Fusion 1
HD-Pep-3095	IARFQKMRGMQEQFLFYHNLLDLPE	Fusion 4
HD-Pep-3096	DLLLQRGPQYSEHPTFTSQYRIQGKLE	pp65 (363-373)
HD-Pep-3097	EQTHSKAGLLVSDGGPNLYNIRNLH	PB1 (591-599)
HD-Pep-3098	NRVASRKCRAKFKQLLQHYREVAS	BZLF-1 (190-197)
HD-Pep-3099	TAQAWNAGFLRGRAYGLDLLRTEGE	EBNA3A (193-201)
HD-Pep-3100	AKARAKKDELRRKMMYMCYRNIEFF	IE1 (199-207)
HD-Pep-3101	QSIDKTAGKIRYSDTRRWPQDGR	Fusion 1
Peptide_001	ILDTAGREEY	NRAS
Peptide_002	DTAGREEYSA	NRAS
Peptide_003	YPRKVTTAM	RPL27
Peptide_005	DRYPRKVTTA	RPL27
Peptide_006	RYPRKVTTAM	RPL27
Peptide_007	DRYPRKVTTAM	RPL27
Peptide_008	YPRKVTTAMG	RPL27
Peptide_009	YPRKVTTA	RPL27
Peptide_010	STIRLLISL	CCT3
Peptide_011	TIRLLISL	CCT3
Peptide_012	IIDTTDDL	MAGEC1
Peptide_013	TPTFAQAAGI	CD320
Peptide_014	STPTFAQAA	CD320
Peptide_015	STPTFAQAAGI	CD320
Peptide_016	LSTPTFAQA	CD320
Peptide_017	ELRQRLEDV	WWC3
Peptide_018	ELRQRLEDVQL	WWC3
Peptide_019	YSEAILIL	FKBP8
Peptide_020	EAILILRAA	FKBP8
Peptide_021	ILILRAAL	FKBP8
Peptide_022	EAILILRAAL	FKBP8
Peptide_023	AILILRAAL	FKBP8
Peptide_024	YPKAVQNL	RCC2
Peptide_025	TMYPKAVQNL	RCC2
Peptide_026	MYPKAVQNL	RCC2
Peptide_027	STMYPKAVQNL	RCC2
Peptide_028	IAKMKSTF	SNRPA
Peptide_029	IAKMKSTFV	SNRPA
Peptide_030	IIAKMKSTFV	SNRPA
Peptide_031	ISDAAQLSHDY	EIF4EBP2

Peptide_032	ISDAAQLSH	EIF4EBP2
Peptide_033	IVKGGLVQV	SELENBP1
Peptide_034	SIVKGGLVQV	SELENBP1
Peptide_035	TYLPTFPLL	NRD1
Peptide_036	LTYLPTFPL	NRD1
Peptide_037	LTYLPTFPLL	NRD1
Peptide_038	QLTYLPTFPL	NRD1
Peptide_039	MQLTYLPTFPL	NRD1
Peptide_040	FLHEKEQHHL	TRIM51
Peptide_041	LSENDSLRF	NGDN
Peptide_042	SRIPSSKEI	KIAA0368
Peptide_043	ELEEVRVQY	MGAT1
Peptide_044	RRTEYLKGY	RBM8A
Peptide_045	NLDRRTEYL	RBM8A
Peptide_047	RRTEYLKGYTL	RBM8A
Peptide_048	ALLQKRIL	COASY
Peptide_049	RILKTHQAL	COASY
Peptide_050	WALLQKRIL	COASY
Peptide_051	KRILKTHQAL	COASY
Peptide_052	LLQKRILKT	COASY
Peptide_053	WRNKFHCGF	TOMM40L
Peptide_054	SVADVARTV	OSGEP
Peptide_056	DVARTVAQL	OSGEP
Peptide_057	VADVARTV	OSGEP
Peptide_058	VADVARTVA	OSGEP
Peptide_059	SVADVARTVA	OSGEP
Peptide_060	VSVADVARTV	OSGEP
Peptide_061	VADVARTVAQL	OSGEP
Peptide_062	ETGATGATL	NDUFA4
Peptide_063	LTDRDIVVL	NOSIP
Peptide_064	FRFFVIWHL	DOPEY2
Peptide_066	EALFRFFVI	DOPEY2
Peptide_067	TRLEALFRFF	DOPEY2
Peptide_068	EALFRFFVI	DOPEY2
Peptide_070	FRTSVQPTF	UBR4
Peptide_071	SFRTSVQPTF	UBR4
Peptide_072	EAATKSFRTSV	UBR4
Peptide_073	EAATKSFRT	UBR4
Peptide_074	ATKSFRTSV	UBR4
Peptide_076	DPRMKLKQV	SLC38A10
Peptide_077	ETGDPRMKL	SLC38A10
Peptide_078	RMKLKQVSRDL	SLC38A10
Peptide_079	FSFARDHPV	SUPT6H
Peptide_082	AADEERQRKL	CKAP2L
Peptide_083	FYFDPREAY	SMU1

Peptide_084	HLENLLARFY	SMU1
Peptide_085	NLLARFYF	SMU1
Peptide_086	DSVWLFVVV	TSPAN17
Peptide_087	LTDLGGLDSV	TSPAN17
Peptide_089	KAFYRLHQL	INO80
Peptide_092	SLKAFYRLHQL	INO80
Peptide_093	SLKAFYRL	INO80
Peptide_094	FLSLKAFYRL	INO80
Peptide_095	SVEAPPPSL	SRCAP
Peptide_096	FIFVMPSVEA	SRCAP
Peptide_097	EIFPLETSA	GMPS
Peptide_098	EIFPLETSAFA	GMPS
Peptide_099	TPFLVTSSL	MEF2D
Peptide_101	VTPFLVTSSL	MEF2D
Peptide_102	FSIPVASEI	WDR12
Peptide_105	AVDDVPFSIPV	WDR12
Peptide_106	DVPFSIPVA	WDR12
Peptide_107	FSIPVASEIA	WDR12
Peptide_108	FLRKNLSI	MTOR
Peptide_109	TFLRKNLSI	MTOR
Peptide_110	ILKNYLREL	SYDE1
Peptide_112	NVITGILKNYL	SYDE1
Peptide_113	STSATTHEA	PPRC1
Peptide_114	NRFYKVSAA	SLC22A15
Peptide_116	LIANRFYKV	SLC22A15
Peptide_118	QLKPKHQSYKL	FRMD8
Peptide_119	KPKHQSYKL	FRMD8
Peptide_120	QLKPKHQSY	FRMD8
Peptide_121	LKPKHQSYKL	FRMD8
Peptide_122	FSEKALAL	ACAD10
Peptide_124	FSEKALALM	ACAD10
Peptide_126	LIKWKKEIL	TBC1D22B
Peptide_127	FLIKWKKEIL	TBC1D22B
Peptide_128	LIKWKKEI	TBC1D22B
Peptide_129	FLIKWKKEI	TBC1D22B
Peptide_130	LRPFDLVILF	FLNA
Peptide_131	LRPFDLVIL	FLNA
Peptide_132	FYCGKTLLF	JKAMP
Peptide_133	GRHYWEIEV	TRIM27
Peptide_134	HIGYFPNKQV	GCH1
Peptide_135	FPNKQVLGL	GCH1
Peptide_136	GYFPNKQVL	GCH1
Peptide_137	SRPATEAEL	HDAC6
Peptide_138	LTSRPATEA	HDAC6
Peptide_139	AAYWKRVGY	ADAMTSL4

Peptide_140	YWKRVGYSA	ADAMTSL4
Peptide_141	SAVLAPGILV	MET
Peptide_142	SIDKTAGKIRY	fusion1
Peptide_143	IRYSDTRRW	fusion1
Peptide_144	KTAGKIRY	fusion1
Peptide_145	IDKTAGKIRY	fusion1
Peptide_146	HPNDRKGKCSF	fusion1
Peptide_147	DRKGKCSF	fusion1
Peptide_149	DRKGKCSFA	fusion1
Peptide_150	RRWPQDGRH	fusion1
Peptide_151	RRWPQDGRHEH	fusion1
Peptide_152	EQFLFYHNL	fusion7
Peptide_153	GMQEQFLFY	fusion7
Peptide_154	MRGMQEQFL	fusion7
Peptide_155	FLFYHNLL	fusion7
Peptide_156	RGMQEQFLFY	fusion7
Peptide_157	MQEQFLFY	fusion7
Peptide_158	MRGMQEQFLFY	fusion7
Peptide_159	EQFLFYHNL	fusion7
Peptide_161	FQKMRGMQEQF	fusion7
Peptide_162	MRGMQEQFL	fusion7
Peptide_163	MRGMQEQFLF	fusion7
Peptide_164	GMQEQFLFY	fusion7
Peptide_165	MRGMQEQFLFY	fusion7
Peptide_166	LLDLPECCSL	fusion7

7. References

Adler, L. N., W. Jiang, K. Bhamidipati, M. Millican, C. Macaubas, S. C. Hung, and E. D. Mellins. 2017. 'The Other Function: Class II-Restricted Antigen Presentation by B Cells', *Front Immunol*, 8: 319.

Al-Khallaf, H. 2017. 'Isocitrate dehydrogenases in physiology and cancer: biochemical and molecular insight', *Cell Biosci*, 7: 37.

Alam, M. S. 2018. 'Proximity Ligation Assay (PLA)', *Curr Protoc Immunol*, 123: e58.

Aldape, K., K. M. Brindle, L. Chesler, R. Chopra, A. Gajjar, M. R. Gilbert, N. Gottardo, D. H. Gutmann, D. Hargrave, E. C. Holland, D. T. W. Jones, J. A. Joyce, P. Kearns, M. W. Kieran, I. K. Mellinghoff, M. Merchant, S. M. Pfister, S. M. Pollard, V. Ramaswamy, J. N. Rich, G. W. Robinson, D. H. Rowitch, J. H. Sampson, M. D. Taylor, P. Workman, and R. J. Gilbertson. 2019. 'Challenges to curing primary brain tumours', *Nat Rev Clin Oncol*, 16: 509-20.

Alspach, E., D. M. Lussier, A. P. Miceli, I. Kizhvatov, M. DuPage, A. M. Luoma, W. Meng, C. F. Lichti, E. Esaulova, A. N. Vomund, D. Runci, J. P. Ward, M. M. Gubin, R. F. V. Medrano, C. D. Arthur, J. M. White, K. C. F. Sheehan, A. Chen, K. W. Wucherpfennig, T. Jacks, E. R. Unanue, M. N. Artyomov, and R. D. Schreiber. 2019. 'MHC-II neoantigens shape tumour immunity and response to immunotherapy', *Nature*, 574: 696-701.

Andersen, R., M. C. W. Westergaard, J. W. Kjeldsen, A. Muller, N. W. Pedersen, S. R. Hadrup, O. Met, B. Seliger, B. Kromann-Andersen, T. Hasselager, M. Donia, and I. M. Svane. 2018. 'T-cell Responses in the Microenvironment of Primary Renal Cell Carcinoma-Implications for Adoptive Cell Therapy', *Cancer Immunol Res*, 6: 222-35.

Andreatta, M., B. Alvarez, and M. Nielsen. 2017. 'GibbsCluster: unsupervised clustering and alignment of peptide sequences', *Nucleic Acids Res*, 45: W458-W63.

Arnold, P. Y., N. L. La Gruta, T. Miller, K. M. Vignali, P. S. Adams, D. L. Woodland, and D. A. Vignali. 2002. 'The majority of immunogenic epitopes generate CD4+ T cells that are dependent on MHC class II-bound peptide-flanking residues', *J Immunol*, 169: 739-49.

Aslan, K., V. Turco, J. Blobner, J. K. Sonner, A. R. Liuzzi, N. G. Nunez, D. De Feo, P. Kickingereder, M. Fischer, E. Green, A. Sadik, M. Friedrich, K. Sanghvi, M. Kilian, F. Cichon, L. Wolf, K. Jahne, A. von Landenberg, L. Bunse, F. Sahm, D. Schrimpf, J. Meyer, A. Alexander, G. Brugnara, R. Roth, K. Pfleiderer, B. Niesler, A. von Deimling, C. Opitz, M. O. Breckwoldt, S. Heiland, M. Bendszus, W. Wick, B. Becher, and M. Platten. 2020. 'Heterogeneity of response to immune checkpoint blockade in hypermutated experimental gliomas', *Nat Commun*, 11: 931.

Aspelund, A., S. Antila, S. T. Proulx, T. V. Karlsen, S. Karaman, M. Detmar, H. Wiig, and K. Alitalo. 2015. 'A dural lymphatic vascular system that drains brain interstitial fluid and macromolecules', *J Exp Med*, 212: 991-9.

Axelrod, M. L., R. S. Cook, D. B. Johnson, and J. M. Balko. 2019. 'Biological Consequences of MHC-II Expression by Tumor Cells in Cancer', *Clin Cancer Res*, 25: 2392-402.

Beeson, C., and H. M. McConnell. 1994. 'Kinetic intermediates in the reactions between peptides and proteins of major histocompatibility complex class II', *Proc Natl Acad Sci U S A*, 91: 8842-5.

Ben-Avi, R., R. Farhi, A. Ben-Nun, M. Gorodner, E. Greenberg, G. Markel, J. Schachter, O. Itzhaki, and M. J. Besser. 2018. 'Establishment of adoptive cell therapy with tumor infiltrating lymphocytes for non-small cell lung cancer patients', *Cancer Immunol Immunother*, 67: 1221-30.

Betts, M. R., and R. A. Koup. 2004. 'Detection of T-cell degranulation: CD107a and b', *Methods Cell Biol*, 75: 497-512.

Boschert, Tamara, Kristina Kromer, Taga Lerner, Katharina Lindner, Gordon Haltenhof, Chin Leng Tan, Kristine Jähne, Isabel Poschke, Lukas Bunse, Niklas Grassl, Iris Mildenberger, Katharina Sahm, Michael Platten, John M Lindner, and Edward W Green. 2023. 'Neoepitope-specific vaccination of a patient with diffuse midline glioma targeting H3K27M induces polyclonal B and T cell responses across diverse HLA alleles', *bioRxiv*: 2023.04.28.538672.

Bouwmeester, R., R. Gabriels, N. Hulstaert, L. Martens, and S. Degroeve. 2021. 'DeepLC can predict retention times for peptides that carry as-yet unseen modifications', *Nat Methods*, 18: 1363-69.

Bradbury, M. W., and R. J. Westrop. 1983. 'Factors influencing exit of substances from cerebrospinal fluid into deep cervical lymph of the rabbit', *J Physiol*, 339: 519-34.

Brossart, P. 2020. 'The Role of Antigen Spreading in the Efficacy of Immunotherapies', *Clin Cancer Res*, 26: 4442-47.

Bruderer, R., O. M. Bernhardt, T. Gandhi, S. M. Miladinovic, L. Y. Cheng, S. Messner, T. Ehrenberger, V. Zanotelli, Y. Butscheid, C. Escher, O. Vitek, O. Rinner, and L. Reiter. 2015. 'Extending the limits of quantitative proteome profiling with data-independent acquisition and application to acetaminophen-treated three-dimensional liver microtissues', *Mol Cell Proteomics*, 14: 1400-10.

Bui, H. H., J. Sidney, K. Dinh, S. Southwood, M. J. Newman, and A. Sette. 2006. 'Predicting population coverage of T-cell epitope-based diagnostics and vaccines', *BMC Bioinformatics*, 7: 153.

Bunse, L., S. Pusch, T. Bunse, F. Sahm, K. Sanghvi, M. Friedrich, D. Alansary, J. K. Sonner, E. Green, K. Deumelandt, M. Kilian, C. Neftel, S. Uhlig, T. Kessler, A. von Landenberg, A. S. Berghoff, K. Marsh, M. Steadman, D. Zhu, B. Nicolay, B. Wiestler, M. O. Breckwoldt, R. Al-Ali, S. Karcher-Bausch, M. Bozza, I. Oezen, M. Kramer, J. Meyer, A. Habel, J. Eisel, G. Poschet, M. Weller, M. Preusser, M. Nadji-Ohl, N. Thon, M. C. Burger, P. N. Harter, M. Ratliff, R. Harbottle, A. Benner, D. Schrimpf, J. Okun, C. Herold-Mende, S. Turcan, S. Kaulfuss, H. Hess-Stumpp, K. Bieback, D. P. Cahill, K. H. Plate, D. Hanggi, M. Dorsch, M. L. Suva, B. A. Niemeyer, A. von Deimling, W. Wick, and M. Platten. 2018. 'Suppression of antitumor T cell immunity by the oncometabolite (R)-2-hydroxyglutarate', *Nat Med*, 24: 1192-203.

Bunse, L., A. K. Rupp, I. Poschke, T. Bunse, K. Lindner, A. Wick, J. Blobner, M. Misch, G. Tabatabai, M. Glas, O. Schnell, J. Gempt, M. Denk, G. Reifenberger, M. Bendszus, P. Wuchter, J. P. Steinbach, W. Wick, and M. Platten. 2022. 'AMPLIFY-NEOVAC: a randomized, 3-arm multicenter phase I trial to assess safety, tolerability and immunogenicity of IDH1-vac combined with an immune checkpoint inhibitor targeting programmed death-ligand 1 in isocitrate dehydrogenase 1 mutant gliomas', *Neurol Res Pract*, 4: 20.

Bunse, L., T. Schumacher, F. Sahm, S. Pusch, I. Oezen, K. Rauschenbach, M. Gonzalez, G. Solecki, M. Osswald, D. Capper, B. Wiestler, F. Winkler, C. Herold-Mende, A. von Deimling, W. Wick, and M. Platten. 2015. 'Proximity ligation assay evaluates IDH1R132H presentation in gliomas', *J Clin Invest*, 125: 593-606.

Capietto, A. H., R. Hoshyar, and L. Delamarre. 2022. 'Sources of Cancer Neoantigens beyond Single-Nucleotide Variants', *International Journal of Molecular Sciences*, 23.

Caushi, J. X., J. Zhang, Z. Ji, A. Vaghasia, B. Zhang, E. H. Hsiue, B. J. Mog, W. Hou, S. Justesen, R. Blosser, A. Tam, V. Anagnostou, T. R. Cottrell, H. Guo, H. Y. Chan, D. Singh, S. Thapa, A. G. Dykema, P. Burman, B. Choudhury, L. Aparicio, L. S. Cheung, M. Lanis, Z. Belcaid, M. El Asmar, P. B. Illei, R. Wang, J. Meyers, K. Schuebel, A. Gupta, A. Skaist, S. Wheelan, J. Naidoo, K. A. Marrone, M. Brock, J. Ha, E. L. Bush, B. J. Park, M. Bott, D. R. Jones, J. E. Reuss, V. E. Velculescu, J. E. Chaft, K. W. Kinzler, S. Zhou, B. Vogelstein, J. M. Taube, M. D. Hellmann, J. R. Brahmer, T. Merghoub, P. M. Forde, S. Yegnasubramanian, H. Ji, D. M. Pardoll, and K. N. Smith. 2021. 'Transcriptional programs of neoantigen-specific TIL in anti-PD-1-treated lung cancers', *Nature*, 596: 126-32.

Chalmers, Z. R., C. F. Connelly, D. Fabrizio, L. Gay, S. M. Ali, R. Ennis, A. Schrock, B. Campbell, A. Shlien, J. Chmielecki, F. Huang, Y. He, J. Sun, U. Tabori, M. Kennedy, D. S. Lieber, S. Roels, J. White, G. A. Otto, J. S. Ross, L. Garraway, V. A. Miller, P. J. Stephens, and G. M. Frampton. 2017. 'Analysis of 100,000 human cancer genomes reveals the landscape of tumor mutational burden', *Genome Med*, 9: 34.

Chang, J. 2021. 'MHC multimer: A Molecular Toolbox for Immunologists', *Mol Cells*, 44: 328-34.

Cheng, J., K. Bendjama, K. Rittner, and B. Malone. 2021. 'BERTMHC: improved MHC-peptide class II interaction prediction with transformer and multiple instance learning', *Bioinformatics*, 37: 4172-79.

Chong, C., F. Marino, H. Pak, J. Racle, R. T. Daniel, M. Muller, D. Gfeller, G. Coukos, and M. Bassani-Sternberg. 2018. 'High-throughput and Sensitive Immunopeptidomics Platform Reveals

Profound Interferongamma-Mediated Remodeling of the Human Leukocyte Antigen (HLA) Ligandome', *Mol Cell Proteomics*, 17: 533-48.

Cohen, A. L., S. L. Holmen, and H. Colman. 2013. 'IDH1 and IDH2 mutations in gliomas', *Curr Neurol Neurosci Rep*, 13: 345.

Cohen, C. J., G. Denkberg, A. Lev, M. Epel, and Y. Reiter. 2003. 'Recombinant antibodies with MHC-restricted, peptide-specific, T-cell receptor-like specificity: new tools to study antigen presentation and TCR-peptide-MHC interactions', *J Mol Recognit*, 16: 324-32.

Consogno, G., S. Manici, V. Facchinetti, A. Bachi, J. Hammer, B. M. Conti-Fine, C. Rugarli, C. Traversari, and M. P. Protti. 2003. 'Identification of immunodominant regions among promiscuous HLA-DR-restricted CD4+ T-cell epitopes on the tumor antigen MAGE-3', *Blood*, 101: 1038-44.

Danilova, L., V. Anagnostou, J. X. Caushi, J. W. Sidhom, H. Guo, H. Y. Chan, P. Suri, A. Tam, J. Zhang, M. E. Asmar, K. A. Marrone, J. Naidoo, J. R. Brahmer, P. M. Forde, A. S. Baras, L. Cope, V. E. Velculescu, D. M. Pardoll, F. Housseau, and K. N. Smith. 2018. 'The Mutation-Associated Neoantigen Functional Expansion of Specific T Cells (MANAFEST) Assay: A Sensitive Platform for Monitoring Antitumor Immunity', *Cancer Immunol Res*, 6: 888-99.

de la Fuente, M. I., H. Colman, M. Rosenthal, B. A. Van Tine, D. Levacic, T. Walbert, H. K. Gan, M. Vieito, M. M. Milhem, K. Lipford, S. Forsyth, S. M. Guichard, Y. Mikhailov, A. Sedkov, J. Brevard, P. F. Kelly, H. Mohamed, and V. Monga. 2023. 'Olutasidenib (FT-2102) in patients with relapsed or refractory IDH1-mutant glioma: A multicenter, open-label, phase Ib/II trial', *Neuro Oncol*, 25: 146-56.

Desgranges, C., M. F. Lavoue, J. Patet, and G. de-The. 1979. 'In vitro transforming activity of Epstein-Barr virus (EBV). II. Differences between M81 and B95-8 EBV strains', *Biomedicine*, 30: 102-8.

Dijkstra, K. K., C. M. Cattaneo, F. Weeber, M. Chalabi, J. van de Haar, L. F. Fanchi, M. Slagter, D. L. van der Velden, S. Kaing, S. Kelderman, N. van Rooij, M. E. van Leerdam, A. Depla, E. F. Smit, K. J. Hartemink, R. de Groot, M. C. Wolkers, N. Sachs, P. Snaebjornsson, K. Monkhorst, J. Haanen, H. Clevers, T. N. Schumacher, and E. E. Voest. 2018. 'Generation of Tumor-Reactive T Cells by Co-culture of Peripheral Blood Lymphocytes and Tumor Organoids', *Cell*, 174: 1586-98 e12.

Dong, Y., X. Li, L. Zhang, Q. Zhu, C. Chen, J. Bao, and Y. Chen. 2019. 'CD4(+) T cell exhaustion revealed by high PD-1 and LAG-3 expression and the loss of helper T cell function in chronic hepatitis B', *BMC Immunol*, 20: 27.

Eisen, H. N., Y. Sykulev, and T. J. Tsomides. 1996. 'Antigen-specific T-cell receptors and their reactions with complexes formed by peptides with major histocompatibility complex proteins', *Adv Protein Chem*, 49: 1-56.

Elgueta, R., M. J. Benson, V. C. de Vries, A. Wasiuk, Y. Guo, and R. J. Noelle. 2009. 'Molecular mechanism and function of CD40/CD40L engagement in the immune system', *Immunol Rev*, 229: 152-72.

Ellingson, B. M., P. Y. Wen, and T. F. Cloughesy. 2017. 'Modified Criteria for Radiographic Response Assessment in Glioblastoma Clinical Trials', *Neurotherapeutics*, 14: 307-20.

Gessulat, S., T. Schmidt, D. P. Zolg, P. Samaras, K. Schnatbaum, J. Zerweck, T. Knaute, J. Rechenberger, B. Delanghe, A. Huhmer, U. Reimer, H. C. Ehrlich, S. Aiche, B. Kuster, and M. Wilhelm. 2019. 'Prosit: proteome-wide prediction of peptide tandem mass spectra by deep learning', *Nat Methods*, 16: 509-18.

Gocher, A. M., C. J. Workman, and D. A. A. Vignali. 2022. 'Interferon-gamma: teammate or opponent in the tumour microenvironment?', *Nat Rev Immunol*, 22: 158-72.

Han, S., Y. Liu, S. J. Cai, M. Qian, J. Ding, M. Larion, M. R. Gilbert, and C. Yang. 2020. 'IDH mutation in glioma: molecular mechanisms and potential therapeutic targets', *Br J Cancer*, 122: 1580-89.

Hanada, K. I., C. Zhao, R. Gil-Hoyos, J. J. Gartner, C. Chow-Parmer, F. J. Lowery, S. Krishna, T. D. Prickett, S. Kivitz, M. R. Parkhurst, N. Wong, Z. Rae, M. C. Kelly, S. L. Goff, P. F. Robbins, S. A. Rosenberg, and J. C. Yang. 2022. 'A phenotypic signature that identifies neoantigen-reactive T cells in fresh human lung cancers', *Cancer Cell*, 40: 479-93 e6.

Hao, Y., S. Hao, E. Andersen-Nissen, W. M. Mauck, 3rd, S. Zheng, A. Butler, M. J. Lee, A. J. Wilk, C. Darby, M. Zager, P. Hoffman, M. Stoeckius, E. Papalexi, E. P. Mimitou, J. Jain, A. Srivastava, T. Stuart, L.

M. Fleming, B. Yeung, A. J. Rogers, J. M. McElrath, C. A. Blish, R. Gottardo, P. Smibert, and R. Satija. 2021. 'Integrated analysis of multimodal single-cell data', *Cell*, 184: 3573-87 e29.

Hashimoto, K., T. Kouno, T. Ikawa, N. Hayatsu, Y. Miyajima, H. Yabukami, T. Terooatea, T. Sasaki, T. Suzuki, M. Valentine, G. Pascarella, Y. Okazaki, H. Suzuki, J. W. Shin, A. Minoda, I. Taniuchi, H. Okano, Y. Arai, N. Hirose, and P. Carninci. 2019. 'Single-cell transcriptomics reveals expansion of cytotoxic CD4 T cells in supercentenarians', *Proc Natl Acad Sci U S A*, 116: 24242-51.

Hassan, C., M. G. Kester, G. Oudgenoeg, A. H. de Ru, G. M. Janssen, J. W. Drijfhout, R. M. Spaapen, C. R. Jimenez, M. H. Heemskerk, J. H. Falkenburg, and P. A. van Veelen. 2014. 'Accurate quantitation of MHC-bound peptides by application of isotopically labeled peptide MHC complexes', *J Proteomics*, 109: 240-4.

Heijmans, C. M. C., N. G. de Groot, and R. E. Bontrop. 2020. 'Comparative genetics of the major histocompatibility complex in humans and nonhuman primates', *Int J Immunogenet*, 47: 243-60.

Ho, N. I., L. G. M. Huis In 't Veld, T. K. Raaijmakers, and G. J. Adema. 2018. 'Adjuvants Enhancing Cross-Presentation by Dendritic Cells: The Key to More Effective Vaccines?', *Front Immunol*, 9: 2874.

Horbinski, C., T. Berger, R. J. Packer, and P. Y. Wen. 2022. 'Clinical implications of the 2021 edition of the WHO classification of central nervous system tumours', *Nat Rev Neurol*, 18: 515-29.

Horowitz, A., R. H. Behrens, L. Okell, A. R. Fooks, and E. M. Riley. 2010. 'NK cells as effectors of acquired immune responses: effector CD4+ T cell-dependent activation of NK cells following vaccination', *J Immunol*, 185: 2808-18.

Hu, Y., G. R. Petroni, W. C. Olson, A. Czarkowski, M. E. Smolkin, W. W. Grosh, K. A. Chianese-Bullock, and C. L. Slingluff, Jr. 2014. 'Immunologic hierarchy, class II MHC promiscuity, and epitope spreading of a melanoma helper peptide vaccine', *Cancer Immunol Immunother*, 63: 779-86.

Iaccarino, I., F. Mourtada, S. Reinke, P. Patil, G. Doose, G. Monaco, S. Hoffmann, R. Siebert, and W. Klapper. 2022. 'LINC00892 Is an lncRNA Induced by T Cell Activation and Expressed by Follicular Lymphoma-Resident T Helper Cells', *Noncoding RNA*, 8.

Jardim, D. L., A. Goodman, D. de Melo Gagliato, and R. Kurzrock. 2021. 'The Challenges of Tumor Mutational Burden as an Immunotherapy Biomarker', *Cancer Cell*, 39: 154-73.

Jessen, N. A., A. S. Munk, I. Lundgaard, and M. Nedergaard. 2015. 'The Glymphatic System: A Beginner's Guide', *Neurochem Res*, 40: 2583-99.

Jiang, S., L. W. Wang, M. J. Walsh, S. J. Trudeau, C. Gerdt, B. Zhao, and B. E. Gewurz. 2018. 'CRISPR/Cas9-Mediated Genome Editing in Epstein-Barr Virus-Transformed Lymphoblastoid B-Cell Lines', *Curr Protoc Mol Biol*, 121: 31 12 1-31 12 23.

Joffre, O. P., E. Segura, A. Savina, and S. Amigorena. 2012. 'Cross-presentation by dendritic cells', *Nat Rev Immunol*, 12: 557-69.

June, C. H. 2007. 'Adoptive T cell therapy for cancer in the clinic', *J Clin Invest*, 117: 1466-76.

Justesen, S., M. Harndahl, K. Lamberth, L. L. Nielsen, and S. Buus. 2009. 'Functional recombinant MHC class II molecules and high-throughput peptide-binding assays', *Immunome Res*, 5: 2.

Jutz, S., A. Hennig, W. Paster, O. Asrak, D. Dijanovic, F. Kellner, W. F. Pickl, J. B. Huppa, J. Leitner, and P. Steinberger. 2017. 'A cellular platform for the evaluation of immune checkpoint molecules', *Oncotarget*, 8: 64892-906.

Jutz, S., J. Leitner, K. Schmetterer, I. Doel-Perez, O. Majdic, K. Grabmeier-Pfistershammer, W. Paster, J. B. Huppa, and P. Steinberger. 2016. 'Assessment of costimulation and coinhibition in a triple parameter T cell reporter line: Simultaneous measurement of NF-kappaB, NFAT and AP-1', *J Immunol Methods*, 430: 10-20.

Kalaora, S., A. Nagler, D. Nejman, M. Alon, C. Barbolin, E. Barnea, S. L. C. Ketelaars, K. Cheng, K. Vervier, N. Shental, Y. Bussi, R. Rotkopf, R. Levy, G. Benedek, S. Trabish, T. Dadosh, S. Levin-Zaidman, L. T. Geller, K. Wang, P. Greenberg, G. Yagel, A. Peri, G. Fuks, N. Bhardwaj, A. Reuben, L. Hermida, S. B. Johnson, J. R. Galloway-Pena, W. C. Shropshire, C. Bernatchez, C. Haymaker, R. Arora, L. Roitman, R. Eilam, A. Weinberger, M. Lotan-Pompan, M. Lotem, A. Admon, Y. Levin, T. D. Lawley, D. J. Adams, M. P. Levesque, M. J. Besser, J. Schachter, O. Golani, E. Segal, N. Geva-Zatorsky, E.

Ruppin, P. Kvistborg, S. N. Peterson, J. A. Wargo, R. Straussman, and Y. Samuels. 2021. 'Identification of bacteria-derived HLA-bound peptides in melanoma', *Nature*, 592: 138-43.

Kayki-Mutlu, G., Z. S. Aksoyalp, L. Wojnowski, and M. C. Michel. 2023. 'A year in pharmacology: new drugs approved by the US Food and Drug Administration in 2022', *Naunyn Schmiedebergs Arch Pharmacol*: 1-14.

Khan, U., and H. Ghazanfar. 2018. 'T Lymphocytes and Autoimmunity', *Int Rev Cell Mol Biol*, 341: 125-68.

Kilian, M., T. Bunse, W. Wick, M. Platten, and L. Bunse. 2021. 'Genetically Modified Cellular Therapies for Malignant Gliomas', *International Journal of Molecular Sciences*, 22.

Kilian, M., R. Sheinin, C. L. Tan, M. Friedrich, C. Kramer, A. Kaminitz, K. Sanghvi, K. Lindner, Y. C. Chih, F. Cichon, B. Richter, S. Jung, K. Jahne, M. Ratliff, R. M. Prins, N. Etminan, A. von Deimling, W. Wick, A. Madi, L. Bunse, and M. Platten. 2023. 'MHC class II-restricted antigen presentation is required to prevent dysfunction of cytotoxic T cells by blood-borne myeloids in brain tumors', *Cancer Cell*, 41: 235-51 e9.

Kissick, H. T., M. G. Sanda, L. K. Dunn, and M. S. Arredouani. 2014. 'Immunization with a peptide containing MHC class I and II epitopes derived from the tumor antigen SIM2 induces an effective CD4 and CD8 T-cell response', *PLoS One*, 9: e93231.

Kleiveland, C. R. 2015. 'Peripheral Blood Mononuclear Cells.' in K. Verhoeckx, P. Cotter, I. Lopez-Exposito, C. Kleiveland, T. Lea, A. Mackie, T. Requena, D. Swiatecka and H. Wichers (eds.), *The Impact of Food Bioactives on Health: in vitro and ex vivo models* (Cham (CH)).

Kreiter, S., M. Vormehr, N. van de Roemer, M. Diken, M. Lower, J. Diekmann, S. Boegel, B. Schrors, F. Vascotto, J. C. Castle, A. D. Tadmor, S. P. Schoenberger, C. Huber, O. Tureci, and U. Sahin. 2015. 'Mutant MHC class II epitopes drive therapeutic immune responses to cancer', *Nature*, 520: 692-6.

Krensky, A. M., and C. Clayberger. 2009. 'Biology and clinical relevance of granulysin', *Tissue Antigens*, 73: 193-8.

Krug, L. M., T. Dao, A. B. Brown, P. Maslak, W. Travis, S. Bekele, T. Korontsvit, V. Zakhaleva, J. Wolchok, J. Yuan, H. Li, L. Tyson, and D. A. Scheinberg. 2010. 'WT1 peptide vaccinations induce CD4 and CD8 T cell immune responses in patients with mesothelioma and non-small cell lung cancer', *Cancer Immunol Immunother*, 59: 1467-79.

Kula, T., M. H. Dezfulian, C. I. Wang, N. S. Abdelfattah, Z. C. Hartman, K. W. Wucherpfennig, H. K. Lyerly, and S. J. Elledge. 2019. 'T-Scan: A Genome-wide Method for the Systematic Discovery of T Cell Epitopes', *Cell*, 178: 1016-28 e13.

Lantz, O., and L. Teyton. 2022. 'Identification of T cell antigens in the 21st century, as difficult as ever', *Semin Immunol*, 60: 101659.

Lee, H. J., Y. A. Kim, C. K. Sim, S. H. Heo, I. H. Song, H. S. Park, S. Y. Park, W. S. Bang, I. A. Park, M. Lee, J. H. Lee, Y. S. Cho, S. Chang, J. Jung, J. Kim, S. B. Lee, S. Y. Kim, M. S. Lee, and G. Gong. 2017. 'Expansion of tumor-infiltrating lymphocytes and their potential for application as adoptive cell transfer therapy in human breast cancer', *Oncotarget*, 8: 113345-59.

Lee, J., J. H. Sheen, O. Lim, Y. Lee, J. Ryu, D. Shin, Y. Y. Kim, and M. Kim. 2020. 'Abrogation of HLA surface expression using CRISPR/Cas9 genome editing: a step toward universal T cell therapy', *Sci Rep*, 10: 17753.

Lee, K. A., A. M. Thomas, L. A. Bolte, J. R. Bjork, L. K. de Ruijter, F. Armanini, F. Asnicar, A. Blanco-Miguez, R. Board, N. Calbet-Llopart, L. Derosa, N. Dhomen, K. Brooks, M. Harland, M. Harries, E. R. Leeming, P. Lorigan, P. Manghi, R. Marais, J. Newton-Bishop, L. Nezi, F. Pinto, M. Potrony, S. Puig, P. Serra-Bellver, H. M. Shaw, S. Tamburini, S. Valpione, A. Vijay, L. Waldron, L. Zitvogel, M. Zolfo, E. G. E. de Vries, P. Nathan, R. S. N. Fehrmann, V. Bataille, G. A. P. Hospers, T. D. Spector, R. K. Weersma, and N. Segata. 2022. 'Cross-cohort gut microbiome associations with immune checkpoint inhibitor response in advanced melanoma', *Nat Med*, 28: 535-44.

Leko, V., G. Cafri, R. Yossef, B. Paria, V. Hill, D. Gurusamy, Z. Zheng, J. J. Gartner, T. D. Prickett, S. L. Goff, P. Robbins, Y. C. Lu, and S. A. Rosenberg. 2021. 'Identification of neoantigen-reactive T lymphocytes in the peripheral blood of a patient with glioblastoma', *J Immunother Cancer*, 9.

Li, S., J. Wilamowski, S. Teraguchi, F. J. van Eerden, J. Rozewicki, A. Davila, Z. Xu, K. Katoh, and D. M. Standley. 2019. 'Structural Modeling of Lymphocyte Receptors and Their Antigens', *Methods Mol Biol*, 2048: 207-29.

Li, Yijian, Jingyu Qi, Yang Liu, Yuyu Zheng, Haibin Zhu, Yupeng Zang, Xiangyu Guan, Sichong Xie, Hongyan Zhao, Yunyun Fu, Haitao Xiang, Weicong Zhang, Huanyi Chen, Huan Liu, Yuntong Zhao, Yu Feng, Fanyu Bu, Yanling Liang, Yang Li, Qumiao Xu, Ying He, Li Sun, Longqi Liu, Ying Gu, Xun Xu, Yong Hou, Xuan Dong, and Ya Liu. 2023. 'High-throughput screening of functional neo-antigens and their specific TCRs via the Jurkat reporter system combined with droplet microfluidics', *bioRxiv*: 2023.02.20.529171.

Liao, W., C. Du, and J. Wang. 2020. 'The cGAS-STING Pathway in Hematopoiesis and Its Physiopathological Significance', *Front Immunol*, 11: 573915.

Liu, Z., and P. A. Roche. 2015. 'Macropinocytosis in phagocytes: regulation of MHC class-II-restricted antigen presentation in dendritic cells', *Front Physiol*, 6: 1.

Louis, D. N., A. Perry, P. Wesseling, D. J. Brat, I. A. Cree, D. Figarella-Branger, C. Hawkins, H. K. Ng, S. M. Pfister, G. Reifenberger, R. Soffietti, A. von Deimling, and D. W. Ellison. 2021. 'The 2021 WHO Classification of Tumors of the Central Nervous System: a summary', *Neuro Oncol*, 23: 1231-51.

Louveau, A., I. Smirnov, T. J. Keyes, J. D. Eccles, S. J. Rouhani, J. D. Peske, N. C. Derecki, D. Castle, J. W. Mandell, K. S. Lee, T. H. Harris, and J. Kipnis. 2015. 'Structural and functional features of central nervous system lymphatic vessels', *Nature*, 523: 337-41.

Lowery, F. J., S. Krishna, R. Yossef, N. B. Parikh, P. D. Chatani, N. Zacharakis, M. R. Parkhurst, N. Levin, S. Sindiri, A. Sachs, K. J. Hitscherich, Z. Yu, N. R. Vale, Y. C. Lu, Z. Zheng, L. Jia, J. J. Gartner, V. K. Hill, A. R. Copeland, S. K. Nah, R. V. Masi, B. Gasmi, S. Kivitz, B. C. Paria, M. Florentin, S. P. Kim, K. I. Hanada, Y. F. Li, L. T. Ngo, S. Ray, M. L. Shindorf, S. T. Levi, R. Shepherd, C. Toy, A. Y. Parikh, T. D. Prickett, M. C. Kelly, R. Beyer, S. L. Goff, J. C. Yang, P. F. Robbins, and S. A. Rosenberg. 2022. 'Molecular signatures of antitumor neoantigen-reactive T cells from metastatic human cancers', *Science*, 375: 877-84.

Lu, Y. C., Z. Zheng, F. J. Lowery, J. J. Gartner, T. D. Prickett, P. F. Robbins, and S. A. Rosenberg. 2021. 'Direct identification of neoantigen-specific TCRs from tumor specimens by high-throughput single-cell sequencing', *J Immunother Cancer*, 9.

Ma, Y., Q. Wang, Q. Dong, L. Zhan, and J. Zhang. 2019. 'How to differentiate pseudoprogression from true progression in cancer patients treated with immunotherapy', *Am J Cancer Res*, 9: 1546-53.

Majzner, R. G., S. Ramakrishna, K. W. Yeom, S. Patel, H. Chinnasamy, L. M. Schultz, R. M. Richards, L. Jiang, V. Barsan, R. Mancusi, A. C. Geraghty, Z. Good, A. Y. Mochizuki, S. M. Gillespie, A. M. S. Toland, J. Mahdi, A. Reschke, E. H. Nie, I. J. Chau, M. C. Rotiroti, C. W. Mount, C. Baggott, S. Mavroukakis, E. Egeler, J. Moon, C. Erickson, S. Green, M. Kunicki, M. Fujimoto, Z. Ehlinger, W. Reynolds, S. Kurra, K. E. Warren, S. Prabhu, H. Vogel, L. Rasmussen, T. T. Cornell, S. Partap, P. G. Fisher, C. J. Campen, M. G. Filbin, G. Grant, B. Sahaf, K. L. Davis, S. A. Feldman, C. L. Mackall, and M. Monje. 2022. 'GD2-CAR T cell therapy for H3K27M-mutated diffuse midline gliomas', *Nature*, 603: 934-41.

Mann, S. E., Z. Zhou, L. G. Landry, A. M. Anderson, A. K. Alkanani, J. Fischer, M. Peakman, R. Mallone, K. Campbell, A. W. Michels, and M. Nakayama. 2020. 'Multiplex T Cell Stimulation Assay Utilizing a T Cell Activation Reporter-Based Detection System', *Front Immunol*, 11: 633.

Marzella, D. F., F. M. Parizi, D. van Tilborg, N. Renaud, D. Sybrandi, R. Buzatu, D. T. Rademaker, P. A. C. t Hoen, and L. C. Xue. 2022. 'PANDORA: A Fast, Anchor-Restrained Modelling Protocol for Peptide: MHC Complexes', *Front Immunol*, 13: 878762.

Medawar, P. B. 1948. 'Immunity to homologous grafted skin; the fate of skin homografts transplanted to the brain, to subcutaneous tissue, and to the anterior chamber of the eye', *Br J Exp Pathol*, 29: 58-69.

Mehta, G. U., P. Malekzadeh, T. Shelton, D. E. White, J. A. Butman, J. C. Yang, U. S. Kammula, S. L. Goff, S. A. Rosenberg, and R. M. Sherry. 2018. 'Outcomes of Adoptive Cell Transfer With Tumor-infiltrating Lymphocytes for Metastatic Melanoma Patients With and Without Brain Metastases', *J Immunother*, 41: 241-47.

Melero, I., A. Rouzaut, G. T. Motz, and G. Coukos. 2014. 'T-cell and NK-cell infiltration into solid tumors: a key limiting factor for efficacious cancer immunotherapy', *Cancer Discov*, 4: 522-6.

Miggelbrink, A. M., J. D. Jackson, S. J. Lorrey, E. S. Srinivasan, J. Waibl-Polania, D. S. Wilkinson, and P. E. Fecci. 2021. 'CD4 T-Cell Exhaustion: Does It Exist and What Are Its Roles in Cancer?', *Clin Cancer Res*, 27: 5742-52.

Mikhaylov, V., and A. J. Levine. 2023. 'Accurate modeling of peptide-MHC structures with AlphaFold', *bioRxiv*.

Minervina, A. A., M. V. Pogorelyy, E. A. Komech, V. K. Karnaukhov, P. Bacher, E. Rosati, A. Franke, D. M. Chudakov, I. Z. Mamedov, Y. B. Lebedev, T. Mora, and A. M. Walczak. 2020. 'Primary and secondary anti-viral response captured by the dynamics and phenotype of individual T cell clones', *Elife*, 9.

Morch, A. M., S. Balint, A. M. Santos, S. J. Davis, and M. L. Dustin. 2020. 'Coreceptors and TCR Signaling - the Strong and the Weak of It', *Front Cell Dev Biol*, 8: 597627.

Morgan, R. A., N. Chinnasamy, D. Abate-Daga, A. Gros, P. F. Robbins, Z. Zheng, M. E. Dudley, S. A. Feldman, J. C. Yang, R. M. Sherry, G. Q. Phan, M. S. Hughes, U. S. Kammula, A. D. Miller, C. J. Hessman, A. A. Stewart, N. P. Restifo, M. M. Quezado, M. Alimchandani, A. Z. Rosenberg, A. Nath, T. Wang, B. Bielekova, S. C. Wuest, N. Akula, F. J. McMahon, S. Wilde, B. Mosetter, D. J. Schendel, C. M. Laurencot, and S. A. Rosenberg. 2013. 'Cancer regression and neurological toxicity following anti-MAGE-A3 TCR gene therapy', *J Immunother*, 36: 133-51.

Morgan, R. A., M. E. Dudley, J. R. Wunderlich, M. S. Hughes, J. C. Yang, R. M. Sherry, R. E. Royal, S. L. Topalian, U. S. Kammula, N. P. Restifo, Z. Zheng, A. Nahvi, C. R. de Vries, L. J. Rogers-Freezer, S. A. Mavroukakis, and S. A. Rosenberg. 2006. 'Cancer regression in patients after transfer of genetically engineered lymphocytes', *Science*, 314: 126-9.

Muller, T. R., C. Schuler, M. Hammel, A. Kohler, S. Jutz, J. Leitner, K. Schober, D. H. Busch, and P. Steinberger. 2020. 'A T-cell reporter platform for high-throughput and reliable investigation of TCR function and biology', *Clin Transl Immunology*, 9: e1216.

Ni, J., O. Holsken, M. Miller, Q. Hammer, M. Luetke-Eversloh, C. Romagnani, and A. Cerwenka. 2016. 'Adoptively transferred natural killer cells maintain long-term antitumor activity by epigenetic imprinting and CD4(+) T cell help', *Oncoimmunology*, 5: e1219009.

O'Rourke, D. M., M. P. Nasrallah, A. Desai, J. J. Melenhorst, K. Mansfield, J. J. D. Morrissette, M. Martinez-Lage, S. Brem, E. Maloney, A. Shen, R. Isaacs, S. Mohan, G. Plesa, S. F. Lacey, J. M. Navenot, Z. Zheng, B. L. Levine, H. Okada, C. H. June, J. L. Brogdon, and M. V. Maus. 2017. 'A single dose of peripherally infused EGFRvIII-directed CAR T cells mediates antigen loss and induces adaptive resistance in patients with recurrent glioblastoma', *Sci Transl Med*, 9.

Oh, D. Y., S. S. Kwek, S. S. Raju, T. Li, E. McCarthy, E. Chow, D. Aran, A. Ilano, C. S. Pai, C. Rancan, K. Allaire, A. Burra, Y. Sun, M. H. Spitzer, S. Mangul, S. Porten, M. V. Meng, T. W. Friedlander, C. J. Ye, and L. Fong. 2020. 'Intratumoral CD4(+) T Cells Mediate Anti-tumor Cytotoxicity in Human Bladder Cancer', *Cell*, 181: 1612-25 e13.

Oja, A. E., B. Piet, D. van der Zwan, H. Blaauwgeers, M. Mensink, S. de Kivit, J. Borst, M. A. Nolte, R. A. W. van Lier, R. Stark, and P. Hombrink. 2018. 'Functional Heterogeneity of CD4(+) Tumor-Infiltrating Lymphocytes With a Resident Memory Phenotype in NSCLC', *Front Immunol*, 9: 2654.

Oliveira, G., K. Stromhaug, S. Klaeger, T. Kula, D. T. Frederick, P. M. Le, J. Forman, T. Huang, S. Li, W. Zhang, Q. Xu, N. Cieri, K. R. Clauser, S. A. Shukla, D. Neuberg, S. Justesen, G. MacBeath, S. A. Carr, E. F. Fritsch, N. Hacohen, M. Sade-Feldman, K. J. Livak, G. M. Boland, P. A. Ott, D. B. Keskin, and C. J. Wu. 2021. 'Phenotype, specificity and avidity of antitumour CD8(+) T cells in melanoma', *Nature*, 596: 119-25.

Owens, T., I. Bechmann, and B. Engelhardt. 2008. 'Perivascular spaces and the two steps to neuroinflammation', *J Neuropathol Exp Neurol*, 67: 1113-21.

Panina-Bordignon, P., A. Tan, A. Termijtelen, S. Demotz, G. Corradin, and A. Lanzavecchia. 1989. 'Universally immunogenic T cell epitopes: promiscuous binding to human MHC class II and promiscuous recognition by T cells', *Eur J Immunol*, 19: 2237-42.

Pellegatta, S., L. Valletta, C. Corbetta, M. Patane, I. Zucca, F. Riccardi Sirtori, M. G. Bruzzone, G. Fogliatto, A. Isacchi, B. Pollo, and G. Finocchiaro. 2015. 'Effective immuno-targeting of the IDH1 mutation R132H in a murine model of intracranial glioma', *Acta Neuropathol Commun*, 3: 4.

Peterson, D. A., R. J. DiPaolo, O. Kanagawa, and E. R. Unanue. 1999. 'Quantitative analysis of the T cell repertoire that escapes negative selection', *Immunity*, 11: 453-62.

Pino, L. K., B. C. Searle, J. G. Bollinger, B. Nunn, B. MacLean, and M. J. MacCoss. 2020. 'The Skyline ecosystem: Informatics for quantitative mass spectrometry proteomics', *Mass Spectrom Rev*, 39: 229-44.

Platten, M., L. Bunse, A. Wick, T. Bunse, L. Le Cornet, I. Harting, F. Sahm, K. Sanghvi, C. L. Tan, I. Poschke, E. Green, S. Justesen, G. A. Behrens, M. O. Breckwoldt, A. Freitag, L. M. Rother, A. Schmitt, O. Schnell, J. Hense, M. Misch, D. Krex, S. Stevanovic, G. Tabatabai, J. P. Steinbach, M. Bendszus, A. von Deimling, M. Schmitt, and W. Wick. 2021. 'A vaccine targeting mutant IDH1 in newly diagnosed glioma', *Nature*, 592: 463-68.

Platten, M., N. von Knebel Doeberitz, I. Oezen, W. Wick, and K. Ochs. 2014. 'Cancer Immunotherapy by Targeting IDO1/TDO and Their Downstream Effectors', *Front Immunol*, 5: 673.

Poschke, I. C., J. C. Hassel, A. Rodriguez-Ehrenfried, K. A. M. Lindner, I. Heras-Murillo, L. M. Appel, J. Lehmann, T. Lovgren, S. L. Wickstrom, C. Lauenstein, J. Roth, A. K. Konig, Jbag Haanen, J. van den Berg, R. Kiessling, F. Bergmann, M. Flossdorf, O. Strobel, and R. Offringa. 2020. 'The Outcome of Ex Vivo TIL Expansion Is Highly Influenced by Spatial Heterogeneity of the Tumor T-Cell Repertoire and Differences in Intrinsic In Vitro Growth Capacity between T-Cell Clones', *Clin Cancer Res*, 26: 4289-301.

Posti, J. P., M. Bori, T. Kauko, M. Sankinen, J. Nordberg, M. Rahi, J. Frantzen, V. Vuorinen, and J. O. Sipila. 2015. 'Presenting symptoms of glioma in adults', *Acta Neurol Scand*, 131: 88-93.

Pu, Z., S. B. Lovitch, E. K. Bikoff, and E. R. Unanue. 2004. 'T cells distinguish MHC-peptide complexes formed in separate vesicles and edited by H2-DM', *Immunity*, 20: 467-76.

Quezada, S. A., T. R. Simpson, K. S. Peggs, T. Merghoub, J. Vider, X. Fan, R. Blasberg, H. Yagita, P. Muranski, P. A. Antony, N. P. Restifo, and J. P. Allison. 2010. 'Tumor-reactive CD4(+) T cells develop cytotoxic activity and eradicate large established melanoma after transfer into lymphopenic hosts', *J Exp Med*, 207: 637-50.

Rabinowitz, J. D., K. Tate, C. Lee, C. Beeson, and H. M. McConnell. 1997. 'Specific T cell recognition of kinetic isomers in the binding of peptide to class II major histocompatibility complex', *Proc Natl Acad Sci U S A*, 94: 8702-7.

Racle, J., P. Guillaume, J. Schmidt, J. Michaux, A. Larabi, K. Lau, M. A. S. Perez, G. Croce, R. Genolet, G. Coukos, V. Zoete, F. Pojer, M. Bassani-Sternberg, A. Harari, and D. Gfeller. 2023. 'Machine learning predictions of MHC-II specificities reveal alternative binding mode of class II epitopes', *Immunity*.

Reynisson, B., B. Alvarez, S. Paul, B. Peters, and M. Nielsen. 2020. 'NetMHCpan-4.1 and NetMHCIIpan-4.0: improved predictions of MHC antigen presentation by concurrent motif deconvolution and integration of MS MHC eluted ligand data', *Nucleic Acids Res*, 48: W449-W54.

Rosenberg, S. A., and M. E. Dudley. 2009. 'Adoptive cell therapy for the treatment of patients with metastatic melanoma', *Curr Opin Immunol*, 21: 233-40.

Rosskopf, S., J. Leitner, W. Paster, L. T. Morton, R. S. Hagedoorn, P. Steinberger, and M. H. M. Heemskerk. 2018. 'A Jurkat 76 based triple parameter reporter system to evaluate TCR functions and adoptive T cell strategies', *Oncotarget*, 9: 17608-19.

Sampson, J. H., M. D. Gunn, P. E. Fecci, and D. M. Ashley. 2020. 'Brain immunology and immunotherapy in brain tumours', *Nat Rev Cancer*, 20: 12-25.

Schaettler, M. O., R. Desai, A. Z. Wang, A. J. Livingstone, D. K. Kobayashi, A. T. Coxon, J. A. Bowman-Kirigin, C. J. Liu, M. Li, D. E. Bender, M. J. White, D. M. Kranz, T. M. Johanns, and G. P. Dunn. 2023. 'TCR-engineered adoptive cell therapy effectively treats intracranial murine glioblastoma', *J Immunother Cancer*, 11.

Schlager, C., H. Korner, M. Krueger, S. Vidoli, M. Haberl, D. Mielke, E. Brylla, T. Issekutz, C. Cabanas, P. J. Nelson, T. Ziemssen, V. Rohde, I. Bechmann, D. Lodygin, F. Odoardi, and A. Flugel. 2016.

'Effector T-cell trafficking between the leptomeninges and the cerebrospinal fluid', *Nature*, 530: 349-53.

Schmid, Theresa, Miray Cetin, Veronica Pinamonti, Ana Mellado Fuentes, Kristina Kromer, Taga Lerner, Jing Zhang, Tamara Boschert, Yonatan Herzig, Christopher Ehlert, Laura Fisch, Valeriia Dragan, Arlette Kouwenhoven, Bertrand Van Schoubroeck, Hans Wils, Carl Van Hove, Michael Platten, Edward Green, Frederik Stevenaert, Nathan J. Felix, and John M. Lindner. 2023. 'T-FINDER: A highly sensitive, pan-HLA platform for functional T cell receptor and ligand discovery', *bioRxiv*: 2023.05.16.540992.

Schmitt, L., J. J. Boniface, M. M. Davis, and H. M. McConnell. 1999. 'Conformational isomers of a class II MHC-peptide complex in solution', *J Mol Biol*, 286: 207-18.

Schoenberger, S. P., R. E. Toes, E. I. van der Voort, R. Offringa, and C. J. Melief. 1998. 'T-cell help for cytotoxic T lymphocytes is mediated by CD40-CD40L interactions', *Nature*, 393: 480-3.

Schumacher, T., L. Bunse, S. Pusch, F. Sahm, B. Wiestler, J. Quandt, O. Menn, M. Osswald, I. Oezen, M. Ott, M. Keil, J. Balss, K. Rauschenbach, A. K. Grabowska, I. Vogler, J. Diekmann, N. Trautwein, S. B. Eichmuller, J. Okun, S. Stevanovic, A. B. Riemer, U. Sahin, M. A. Friese, P. Beckhove, A. von Deimling, W. Wick, and M. Platten. 2014. 'A vaccine targeting mutant IDH1 induces antitumour immunity', *Nature*, 512: 324-7.

Schumacher, T., L. Bunse, W. Wick, and M. Platten. 2014. 'Mutant IDH1: An immunotherapeutic target in tumors', *Oncoimmunology*, 3: e974392.

Seliger, B., F. Ruiz-Cabello, and F. Garrido. 2008. 'IFN inducibility of major histocompatibility antigens in tumors', *Adv Cancer Res*, 101: 249-76.

Sevenich, L. 2019. 'Turning "Cold" Into "Hot" Tumors-Opportunities and Challenges for Radio-Immunotherapy Against Primary and Metastatic Brain Cancers', *Front Oncol*, 9: 163.

Shafer, P., L. M. Kelly, and V. Hoyos. 2022. 'Cancer Therapy With TCR-Engineered T Cells: Current Strategies, Challenges, and Prospects', *Front Immunol*, 13: 835762.

Shklovskaya, E., and H. Rizos. 2021. 'MHC Class I Deficiency in Solid Tumors and Therapeutic Strategies to Overcome It', *International Journal of Molecular Sciences*, 22.

Skeate, J. G., M. E. Otsmaa, R. Prins, D. J. Fernandez, D. M. Da Silva, and W. M. Kast. 2020. 'TNFSF14: LIGHTing the Way for Effective Cancer Immunotherapy', *Front Immunol*, 11: 922.

Slifka, M. K., and J. L. Whitton. 2001. 'Functional avidity maturation of CD8(+) T cells without selection of higher affinity TCR', *Nat Immunol*, 2: 711-7.

Speetjens, F. M., P. J. Kuppen, M. J. Welters, F. Essahsah, A. M. Voet van den Brink, M. G. Lantrua, A. R. Valentijn, J. Oostendorp, L. M. Fathers, H. W. Nijman, J. W. Drijfhout, C. J. van de Velde, C. J. Melief, and S. H. van der Burg. 2009. 'Induction of p53-specific immunity by a p53 synthetic long peptide vaccine in patients treated for metastatic colorectal cancer', *Clin Cancer Res*, 15: 1086-95.

Speiser, D. E., O. Chijioke, K. Schaeuble, and C. Munz. 2023. 'CD4(+) T cells in cancer', *Nat Cancer*, 4: 317-29.

Stevanovic, S., L. M. Draper, M. M. Langhan, T. E. Campbell, M. L. Kwong, J. R. Wunderlich, M. E. Dudley, J. C. Yang, R. M. Sherry, U. S. Kammula, N. P. Restifo, S. A. Rosenberg, and C. S. Hinrichs. 2015. 'Complete regression of metastatic cervical cancer after treatment with human papillomavirus-targeted tumor-infiltrating T cells', *J Clin Oncol*, 33: 1543-50.

Stopfer, L. E., A. S. Gajadhar, B. Patel, S. Gallien, D. T. Frederick, G. M. Boland, R. J. Sullivan, and F. M. White. 2021. 'Absolute quantification of tumor antigens using embedded MHC-I isotopologue calibrants', *Proc Natl Acad Sci U S A*, 118.

Suzuki, S., A. Shigenari, S. Ito, J. K. Kulski, and T. Shiina. 2021. 'Identification of three novel HLA-DRA alleles by next-generation sequencing', *HLA*, 98: 560-62.

Tippalagama, R., A. Singhania, P. Dubelko, C. S. Lindestam Arlehamn, A. Crinklaw, M. Pomaznoy, G. Seumois, A. D. deSilva, S. Premawansa, D. Vidanagama, B. Gunasena, N. D. S. Goonawardhana, D. Ariyaratne, T. J. Scriba, R. H. Gilman, M. Saito, R. Taplitz, P. Vijayanand, A. Sette, B. Peters, and J. G. Burel. 2021. 'HLA-DR Marks Recently Divided Antigen-Specific Effector CD4 T Cells in Active Tuberculosis Patients', *J Immunol*, 207: 523-33.

Tsimberidou, A. M., K. Van Morris, H. H. Vo, S. Eck, Y. F. Lin, J. M. Rivas, and B. S. Andersson. 2021. 'T-cell receptor-based therapy: an innovative therapeutic approach for solid tumors', *J Hematol Oncol*, 14: 102.

Unanue, E. R., V. Turk, and J. Neefjes. 2016. 'Variations in MHC Class II Antigen Processing and Presentation in Health and Disease', *Annu Rev Immunol*, 34: 265-97.

Uyttenhove, C., L. Pilotte, I. Theate, V. Stroobant, D. Colau, N. Parmentier, T. Boon, and B. J. Van den Eynde. 2003. 'Evidence for a tumoral immune resistance mechanism based on tryptophan degradation by indoleamine 2,3-dioxygenase', *Nat Med*, 9: 1269-74.

van den Berg, J. H., B. Heemskerk, N. van Rooij, R. Gomez-Eerland, S. Michels, M. van Zon, R. de Boer, N. A. M. Bakker, A. Jorritsma-Smit, M. M. van Buuren, P. Kvistborg, H. Spits, R. Schotte, H. Mallo, M. Karger, J. A. van der Hage, Mwjm Wouters, L. M. Pronk, M. H. Geukes Foppen, C. U. Blank, J. H. Beijnen, B. Nuijen, T. N. Schumacher, and Jbag Haanen. 2020. 'Tumor infiltrating lymphocytes (TIL) therapy in metastatic melanoma: boosting of neoantigen-specific T cell reactivity and long-term follow-up', *J Immunother Cancer*, 8.

van Lith, M., R. M. McEwen-Smith, and A. M. Benham. 2010. 'HLA-DP, HLA-DQ, and HLA-DR have different requirements for invariant chain and HLA-DM', *J Biol Chem*, 285: 40800-8.

Veatch, J. R., S. M. Lee, C. Shasha, N. Singhi, J. L. Szeto, A. S. Moshiri, T. S. Kim, K. Smythe, P. Kong, M. Fitzgibbon, B. Jesernig, S. Bhatia, S. S. Tykodi, E. T. Hall, D. R. Byrd, J. A. Thompson, V. G. Pillarisetty, T. Duhen, A. McGarry Houghton, E. Newell, R. Gottardo, and S. R. Riddell. 2022. 'Neoantigen-specific CD4(+) T cells in human melanoma have diverse differentiation states and correlate with CD8(+) T cell, macrophage, and B cell function', *Cancer Cell*, 40: 393-409 e9.

Vest Hansen, N., L. Ostergaard Pedersen, A. Stryhn, and S. Buus. 2001. 'Phage display of peptide / major histocompatibility class I complexes', *Eur J Immunol*, 31: 32-8.

Viner, N. J., C. A. Nelson, B. Deck, and E. R. Unanue. 1996. 'Complexes generated by the binding of free peptides to class II MHC molecules are antigenically diverse compared with those generated by intracellular processing', *J Immunol*, 156: 2365-8.

Vreeland, T. J., G. T. Clifton, G. S. Herbert, D. F. Hale, D. O. Jackson, J. S. Berry, and G. E. Peoples. 2016. 'Gaining ground on a cure through synergy: combining checkpoint inhibitors with cancer vaccines', *Expert Rev Clin Immunol*, 12: 1347-57.

Wainwright, D. A., I. V. Balyasnikova, A. L. Chang, A. U. Ahmed, K. S. Moon, B. Auffinger, A. L. Tobias, Y. Han, and M. S. Lesniak. 2012. 'IDO expression in brain tumors increases the recruitment of regulatory T cells and negatively impacts survival', *Clin Cancer Res*, 18: 6110-21.

Weller, M., M. van den Bent, M. Preusser, E. Le Rhun, J. C. Tonn, G. Minniti, M. Bendszus, C. Balana, O. Chinot, L. Dirven, P. French, M. E. Hegi, A. S. Jakola, M. Platten, P. Roth, R. Ruda, S. Short, M. Smits, M. J. B. Taphoorn, A. von Deimling, M. Westphal, R. Soffietti, G. Reifenberger, and W. Wick. 2021. 'EANO guidelines on the diagnosis and treatment of diffuse gliomas of adulthood', *Nat Rev Clin Oncol*, 18: 170-86.

Weller, M., W. Wick, K. Aldape, M. Brada, M. Berger, S. M. Pfister, R. Nishikawa, M. Rosenthal, P. Y. Wen, R. Stupp, and G. Reifenberger. 2015. 'Glioma', *Nat Rev Dis Primers*, 1: 15017.

Wickstrom, S. L., T. Lovgren, M. Volkmar, B. Reinhold, J. S. Duke-Cohan, L. Hartmann, J. Rebmann, A. Mueller, J. Melief, R. Maas, M. Ligtenberg, J. Hansson, R. Offringa, B. Seliger, I. Poschke, E. L. Reinherz, and R. Kiessling. 2019. 'Cancer Neoepitopes for Immunotherapy: Discordance Between Tumor-Infiltrating T Cell Reactivity and Tumor MHC Peptidome Display', *Front Immunol*, 10: 2766.

Wischnewski, V., R. R. Maas, P. G. Aruffo, K. Soukup, G. Galletti, M. Kornete, S. Galland, N. Fournier, J. Lilja, P. Wirapati, J. Lourenco, A. Scarpa, R. T. Daniel, A. F. Hottinger, J. P. Brouland, A. Losurdo, E. Voulaz, M. Alloisio, M. E. Hegi, E. Lugli, and J. A. Joyce. 2023. 'Phenotypic diversity of T cells in human primary and metastatic brain tumors revealed by multiomic interrogation', *Nat Cancer*.

Wojciechowska-Durczynska, K., K. Wieczorek-Szukala, B. Stefanski, A. Zygmunt, J. Stepniak, M. Karbownik-Lewinska, and A. Lewinski. 2021. 'Percentage of Myeloid Dendritic Cells in Peripheral

Venous Blood Is Negatively Related to Incidence of Graves' Orbitopathy', *Mediators Inflamm*, 2021: 8896055.

Yan, H., D. W. Parsons, G. Jin, R. McLendon, B. A. Rasheed, W. Yuan, I. Kos, I. Batinic-Haberle, S. Jones, G. J. Riggins, H. Friedman, A. Friedman, D. Reardon, J. Herndon, K. W. Kinzler, V. E. Velculescu, B. Vogelstein, and D. D. Bigner. 2009. 'IDH1 and IDH2 mutations in gliomas', *N Engl J Med*, 360: 765-73.

Yang, H., D. Ye, K. L. Guan, and Y. Xiong. 2012. 'IDH1 and IDH2 mutations in tumorigenesis: mechanistic insights and clinical perspectives', *Clin Cancer Res*, 18: 5562-71.

Yang, K., Z. Wu, H. Zhang, N. Zhang, W. Wu, Z. Wang, Z. Dai, X. Zhang, L. Zhang, Y. Peng, W. Ye, W. Zeng, Z. Liu, and Q. Cheng. 2022. 'Glioma targeted therapy: insight into future of molecular approaches', *Mol Cancer*, 21: 39.

Zheng, C., J. N. Fass, Y. P. Shih, A. J. Gunderson, N. Sanjuan Silva, H. Huang, B. M. Bernard, V. Rajamanickam, J. Slagel, C. B. Bifulco, B. Piening, P. H. A. Newell, P. D. Hansen, and E. Tran. 2022. 'Transcriptomic profiles of neoantigen-reactive T cells in human gastrointestinal cancers', *Cancer Cell*, 40: 410-23 e7.

Zheng, G. X., J. M. Terry, P. Belgrader, P. Ryvkin, Z. W. Bent, R. Wilson, S. B. Ziraldo, T. D. Wheeler, G. P. McDermott, J. Zhu, M. T. Gregory, J. Shuga, L. Montesclaros, J. G. Underwood, D. A. Masquelier, S. Y. Nishimura, M. Schnall-Levin, P. W. Wyatt, C. M. Hindson, R. Bharadwaj, A. Wong, K. D. Ness, L. W. Beppu, H. J. Deeg, C. McFarland, K. R. Loeb, W. J. Valente, N. G. Ericson, E. A. Stevens, J. P. Radich, T. S. Mikkelsen, B. J. Hindson, and J. H. Bielas. 2017. 'Massively parallel digital transcriptional profiling of single cells', *Nat Commun*, 8: 14049.

Zhou, Y., C. M. Weyman, H. Liu, A. Almasan, and A. Zhou. 2008. 'IFN-gamma induces apoptosis in HL-60 cells through decreased Bcl-2 and increased Bak expression', *J Interferon Cytokine Res*, 28: 65-72.